Chem Soc Rev

REVIEW ARTICLE

View Article Online
View Journal | View Issue

Cite this: *Chem. Soc. Rev.*, 2014, **43**, 7378

Single-molecule electronics: from chemical design to functional devices

Lanlan Sun,[a] Yuri A. Diaz-Fernandez,†[a] Tina A. Gschneidtner,[a] Fredrik Westerlund,[a] Samuel Lara-Avila[b] and Kasper Moth-Poulsen*[a]

Received 29th April 2014

DOI: 10.1039/c4cs00143e

www.rsc.org/csr

The use of single molecules in electronics represents the next limit of miniaturisation of electronic devices, which would enable us to continue the trend of aggressive downscaling of silicon-based electronic devices. More significantly, the fabrication, understanding and control of fully functional circuits at the single-molecule level could also open up the possibility of using molecules as devices with novel, not-foreseen functionalities beyond complementary metal-oxide semiconductor technology (CMOS). This review aims at highlighting the chemical design and synthesis of single molecule devices as well as their electrical and structural characterization, including a historical overview and the developments during the last 5 years. We discuss experimental techniques for fabrication of single-molecule junctions, the potential application of single-molecule junctions as molecular switches, and general physical phenomena in single-molecule electronic devices.

1. Introduction and background

The developments in micro-fabrication and field effect transistors are key enabling technologies for today's information society. It is hard to imagine superfast and omnipresent electronic devices, information technology, the internet and mobile communication technologies without access to continuously cheaper and smaller microprocessors. The giant leaps in performance from the first computing machines to today's

[a] *Department of Chemical and Biological Engineering, Chalmers University of Technology, SE-412 96 Göteborg, Sweden. E-mail: kasper.moth-poulsen@chalmers.se*
[b] *Department of Micro and Nanotechnology, MC2, Chalmers University of Technology, SE-412 96 Göteborg, Sweden*
† Present address: Open Innovation Hub for Antimicrobial Surfaces, Surface Science Research Centre, Department of Chemistry, University of Liverpool, Liverpool L69 3BX, UK.

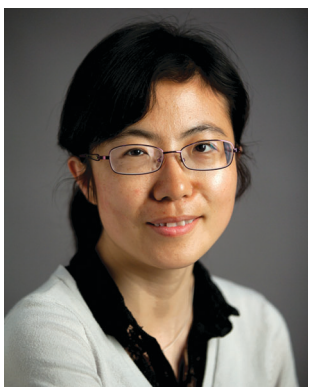

Lanlan Sun

Dr Lanlan Sun is a postdoctor in the Department of Chemical and Biological Engineering, Chalmers University of Technology. She received her PhD degree from State Key Laboratory of Electroanalytical Chemistry, Changchun Institute of Applied Chemistry, China, in 2009. Her current research interests are single molecule devices fabricated by chemical assembly of gold nanoparticle dimers.

Yuri A. Diaz-Fernandez

Yuri A. Diaz Fernandez (YDF) received his BSc and MSc degrees from the Nuclear Science Institute of Havana (Cuba), and his PhD degree from the University of Pavia (Italy). YDF has several years of experience in Nanotechnology, Surface Science, Chemistry of Materials, and Colloidal Chemistry. During his research career, YDF has gained expertise in the design and synthesis of supramolecular systems and self-assembled nanostructured materials for different applications, including antibacterial surfaces, chemical catalysis, and molecular sensing. Currently YDF is working as Science Innovator in the Open Innovation Hub for Antimicrobial Surfaces, at the Surface Science Center of University of Liverpool (UK).

mobile devices are to a large extent realized *via* miniaturization of the active components.

Further miniaturization of electronic devices remains an enormous challenge. Conventional top-down lithography has reached the limit where reliable and reproducible fabrication of sub-20 nm features is cumbersome and economically unfeasible. In this sense, it is remarkable that chemically identical molecules, with sizes on the order of 1 nm, can be synthesized in molar amounts and yet perform a variety of electronic tasks including current limiting, rectification and switching, reminiscent of their solid-state device counterpart. Experimental findings in electron transport through single molecules put forth the idea that beyond silicon CMOS technology, the next limit of miniaturization of electronic components is the realization of single-molecule electronics.[1]

Since the first theoretical proposal by Aviram and Ratner in the 1970's,[2] it took almost 20 years of technological development to realize the first experiment resembling transport through single molecules.[3] Since then, 20 more years after, the techniques to investigate transport through single molecules appear to have stagnated and the experimental methods developed in the 1990's are still in widespread use. Nonetheless, along this time several technical and theoretical developments have helped us to understand electron transport through single molecules. For example, fundamentally new concepts for device function beyond CMOS-like logics have emerged examples include spintronics, quantum interference, electromechanics and thermoelectronic devices studied at the single molecule level. Nonetheless, many challenges need to be overcome before single-molecule electronics can be a reality. One of the main challenges involves the realisation of a technology for mass production of single molecule devices. Chemistry has been the key element in the design and synthesis of functional molecules, and it is one of the most promising ways to bridge the state-of the-art lithography techniques (resolution ~20–50 nm) and molecular-scale dimensions (~1 nm) *via e.g.* chemically driven self-assembly techniques. Several recent review articles have focused on specific experimental aspects of molecular electronics.[4–14] In this review

Tina A. Gschneidtner

Tina Gschneidtner (TG) received her Dipl. NanoSc in 2011 from the University of Kassel in Germany. She was an exchange student in 2009 at the University of California at Berkeley (Prof. C. Chang) and is currently a doctoral student at Chalmers University of Technology with KMP. TG is working on synthetic organic chemistry, plasmonic and catalytic nanoparticles, and light-directed surface functionalization.

Fredrik Westerlund

Fredrik Westerlund (FW) received his MSc (2001) and PhD (2006) from Chalmers University of Technology (Sweden). He was a postdoctoral fellow at the University of Copenhagen (2007–2009), with Profs Bjørnholm and Laursen, and Gothenburg University (2009–2010), with Prof. Tegenfeldt. In 2010 FW was recruited to Chalmers University of Technology as an Assistant Professor. His research is focused on single DNA molecule techniques.

Samuel Lara-Avila

Samuel Lara-Avila graduated as Mechatronics Engineer in 2005 (ITESM, Mexico), received his MSc in 2007 (KU Leuven, Belgium and Chalmers University of Technology, Sweden) and PhD degree in 2012 from Chalmers University of Technology (Sweden). After completing his PhD studies, he joined the Quantum Device Physics Laboratory at Chalmers University of Technology as Assistant Professor. His research interests include electron transport through low dimensional-systems such as single-molecules and graphene, directed assembly of nanoparticles and light–matter interactions.

Kasper Moth-Poulsen

Kasper Moth-Poulsen (KMP) received his BSc (2000), Cand. Scient. (2003) and PhD (2007) degrees in Chemistry from University of Copenhagen (Denmark). He was a postdoctoral fellow at the University of Copenhagen (2007–2009), with Prof. Bjørnholm, and then at University of California at Berkeley (2009–2010) with Profs Segalman and Vollhardt. In 2011 KMP was recruited to Chalmers University of Technology (Sweden) as an assistant professor and since 2014 as Associate professor. His research is focused on synthetic chemistry, single molecule electronics, nanoparticle synthesis, energy storage and self-assembly.

we aim at giving a broad overview of this field, with a focus on vital issues such as self-assembly of nanogaps, molecular systems, and physical phenomena. To narrow the scope of the paper, we focus our discussions on systems with a single or a few molecules in each functional device, however we have not been strict with this definition and have included some examples of devices with small ensembles of molecules as well. To put the recent research progress into historical perspective, we include some historical references as well as introductions to the most commonly employed experimental methods. We discuss the most relevant physical phenomena observed in single molecule devices throughout the years and then we focus on single molecule switches that we consider the most promising way to materialize the implementation of single molecule devices.

2. Experimental methods to address single-molecule electron transport

One of the main challenges in single-molecule electronic devices is to fabricate electrodes with a single molecule in between them. Ideally, these electrodes would allow reliable and reproducible characterization of single molecule devices at room temperature. A variety of techniques have been developed to construct metal–molecule–metal junctions, including mechanical break junctions,[15] electrochemical deposition,[16] electromigration,[17] electron beam lithography,[18] shadow mask evaporation,[19] scanning probe techniques,[3,20] on-wire lithography[21,22] and molecular rulers.[23,24] The focus here is a discussion of fabrication methods of single-molecule junctions, for example, scanning probe microscopy (SPM), mechanical break junctions (MCBJs), electromigration break junctions (EBJs), and self-assembly of nanostructures. The first three methods have been widely used for experimental single-molecule electronics, while the self-assembly method is an emerging, yet very promising route towards (mass) production of single-molecule devices.

2.1. Scanning probe microscopy (SPM)

The great advantage of SPM-based techniques is that they enable the direct observation of the system (molecule) under investigation, while simultaneously allowing realization of other types of studies such as electron transport.[25–30] SPM includes a range of microscopy techniques that are considered as an evolution of scanning tunneling microscopy (STM). Two SPM techniques, STM and conducting probe atomic force microscopy (C-AFM), have been widely used to investigate single-molecule electronic systems by forming a metal–molecule–metal junction between the metallic tip and the substrate (Fig. 1). In order to form the molecular junction, the tip/substrate can be either immersed in the target molecule solution during experiments or decorated with molecules before measurements. Using STM experiments, Weiss *et al.* probed the conductivity of molecular wire self-assembled monolayers on Au.[3] The molecular wires acted as a conducting link from the gold substrate through a ''non-conducting'' layer to the top of the STM tip.

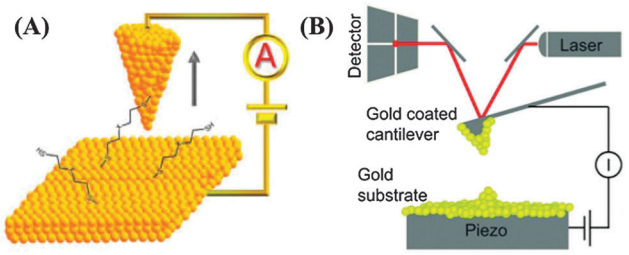

Fig. 1 (A) Schematic representation of the STM break junction. Reprinted with permission from E. Wierzbinski, X. Yin, K. Werling and D. H. Waldeck, *J. Phys. Chem. B*, 2012, **117**, 4431–4441. Copyright 2013 American Chemical Society.[31] (B) A modified conductive atomic force microscope (C-AFM): the junction is formed between the Cr–Au coated cantilever and an Au-coated substrate, and the separation is controlled by a piezo. Reprinted with permission from M. Frei, S. V. Aradhya, M. Koentopp, M. S. Hybertsen and L. Venkataraman, *Nano Lett.*, 2011, **11**, 1518–1523. Copyright 2011 American Chemical Society.[32]

The electron transport mechanisms of STM and C-AFM are somewhat different. In STM, the current is due to tunneling, since the metallic tip and a conducting substrate are in very close proximity but not in actual physical contact. In C-AFM, on the other hand, an external circuit is used to apply current between the metallic tip and a conducting substrate, which are in direct contact. A detailed introduction to the use of STM and AFM in chemistry in single molecule electronics can be found in ref. 30 and 33–36.

A further development is SPM-based break junctions, where the charge transport properties of a single molecule, or a small number of molecules, is studied by repeatedly crashing the SPM tip into and out of contact with the substrate electrode surface containing the target molecules.[34,35] Many efforts have been made to develop the SPM break junction technique. Haiss *et al.* introduced a simple method to measure single alkanedithiol molecule conductivities, using the spontaneous formation of molecular wires between the STM tip and the Au substrate.[36] In a recent review, Niu *et al.* presented recent SPM studies of phthalocyanine, a candidate for molecular electronics highlighting the power of SPM techniques for the ability to both image and probe the properties of single molecule electronic systems.[29,37,39,41–47,53–63]

2.2. Mechanically controlled break junctions (MCBJs)

MCBJs are a powerful technique for characterizing conductance through single-molecular devices. MCBJs allow automated cyclic formation/breaking of metal–single molecule–metal junctions, which enables collecting statistics (conductance histograms) in an experimentally reasonable time for different geometric realizations of a molecule/metal interface.[8] This technique has allowed the understanding of, for example, why independent experiments, aiming at measuring the conductance of the same molecule, might yield different results. MCBJs were firstly introduced by Moreland *et al.*[38] and Muller *et al.*[39] and then further developed by Reed *et al.*[15,40] to fabricate electrodes with a gap of a few nanometers. As shown in Fig. 2, a notched metal wire glued onto a bendable substrate is elongated and finally fractured, when the substrate is bent by moving

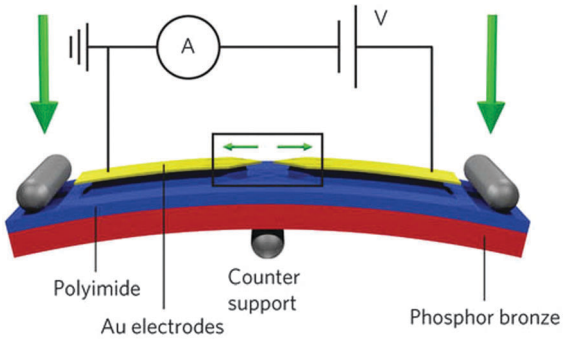

Fig. 2 Schematic illustration of a MCBJ, which shows the layout of the MCBJ set-up. Reprinted by permission from Nature Nanotechnology (M. L. Perrin, C. J. O. Verzijl, C. A. Martin, A. J. Shaikh, R. Eelkema, H. van EschJan, J. M. van Ruitenbeek, J. M. Thijssen, H. S. J. van der Zant and D. Dulic, *Nat. Nanotechnol.*, 2013, **8**, 282–287), Copyright (2013).[41]

a piezo-controlled pushing rod. Two sharp electrodes are formed automatically after the wire is broken and then molecules with two terminal anchoring groups can be assembled to link the two electrodes. The molecules can be introduced both before and after the formation of the electrodes. In Reed's study, 1,4-benzenedithiol (BDT) in tetrahydrofuran (THF) was introduced before the breaking, and a monolayer of BDT was formed on the surface of the gold wire.[15] The reproducibility of the minimum conductance at a consistent value implied that the number of active molecules in the junction could be as few as one. Experimental details and comparisons of the different experimental platforms used for MCBJ-break junctions for molecular electronics are discussed in ref. 8.

The unambiguous identification of a single molecule contacted in the junction is still a challenge, but significant progress has been made to establish that a single molecule forms the contact.[42–47] For these purposes, the MCBJ technique has been combined with other experimental methods, such as STM imaging,[48] Raman spectroscopy,[49] inelastic electron tunneling spectroscopy,[50,51] and inelastic noise spectroscopy.[52] Both inelastic electron tunneling spectroscopy and inelastic noise spectroscopy are useful molecular signature techniques. For inelastic noise spectroscopy, the molecular-vibration-induced current noise is useful for single-molecule identification. In particular, Ruitenbeek *et al.* studied the conductance of a single hydrogen molecule by using MCBJs to fabricate pure metallic Pt contacts of atomic size.[43] They demonstrated that a single hydrogen molecule could form a stable bridge between Pt electrodes. Ruitenbeek *et al.* then carried out shot noise measurements on the Pt–D_2–Pt junction formed by the MCBJ technique, and the observed quantum suppression indicated that the junction was indeed formed by just a single molecule.[45,79–83]

2.3. Electromigration break junctions (EBJs)

EBJs incorporate the possibility of having an electrostatic gate to a single-molecule junction by forming nanoscale contacts for single molecules on top of an oxidized conducting substrate, which acts as a gate. The first report of fabricating metallic electrodes with nanoscale separation by electromigration was by Park *et al.* in 1999.[17] When applying an electric field onto a metallic nanowire defined by electron-beam lithography, the metal atoms migrate, which results in the breakage of the nanowire. By carefully controlling the current, two stable metallic electrodes can be formed with 1–2 nm separation. This separation is a good match with the length scale of typical molecules employed in single-molecule nanodevices. The assembly of molecules into the junctions is similar to that in STM junctions and MCBJs, where the molecules are deposited onto the electrode surface before or after the breaking. The breaking process can be controlled in real-time by monitoring the current–voltage curve until only a tunnelling signal is observed.[17,53]

Above all, the EBJ is an advantageous method to fabricate a three-electrode molecular device, as shown in Fig. 3.[53–55] The third gate is already present under the wire before electrobreaking (or it can be the underlying conducting, oxidized silicon substrate).[56,57] When compared with the MCBJ method, the drawback of the EBJ technique lies in the difficulty of obtaining a large number of metal–molecule geometries with the same junction. Therefore, it is not simple to measure large numbers of single-molecule junctions, and many devices are needed to study the statistical behaviour of the molecules.[56,58] To increase device yield, Johnson *et al.* used a feedback-controlled electromigration process to fabricate a large number of nanogaps simultaneously in a single-step process.[59] For a detailed discussion on the feedback-EBJ we refer to recent reviews.[4,6,10,91–96] A general challenge for MCBJs and EBJs is the lack of direct evidence (observation) of single-molecule junction formation. To circumvent this problem, and in order to improve the control the EBJ process, *in situ* STM, AFM imaging and transmission electron microscopy (TEM) have been employed during nanogap formation by electromigration.[60–64] Although the electromigration-induced wire breaking approach can create a 1–2 nm gap to bridge the target molecules, identification of the molecule in the gap is still a key issue for these single-molecule devices. In this context, Raman spectroscopy and inelastic electron tunneling spectroscopy (IETS) have been applied to complement the electronic transport of the single-molecule device.[65–67] For example, Natelson *et al.* examined paramercaptoaniline (PMA) between electromigration-created

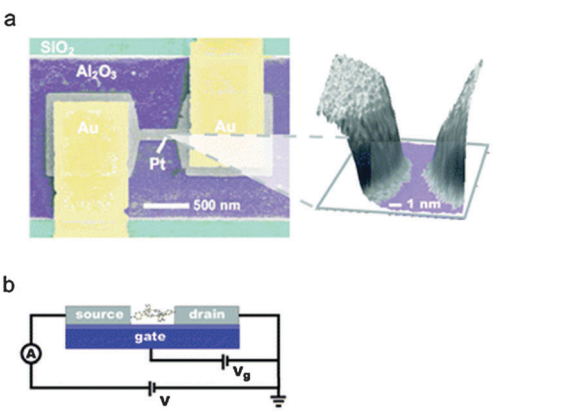

Fig. 3 (a) Colorized SEM image of the single-molecule device based on the Pt nanogap. (b) Schematic representation of the EBJ device.[75]

nanogaps using Raman spectroscopy.[65] Before electromigration, no Raman peak for PMA was observed; after electromigration, surface enhanced Raman peaks for PMA were detected in the obtained gaps. IETS can also be used to identify molecules bridged in the electromigrated nanogap, which supplies a full line spectrum and assigned vibrational spectra of the individual molecules.[68–70] As described in the MCBJ section, Raman spectra and inelastic electron tunneling spectroscopy can supply a large amount of information about the configuration of the molecule in the EBJ produced gaps.[71–74]

2.4. Self-assembly of nanostructures

The methods mentioned above are all based on a top-down fabrication strategy, where nanogaps are firstly constructed by using standard semiconductor nanofabrication technologies, and then in a second step the active molecules are introduced into the nanogaps. Another, much less explored, yet interesting approach is the bottom-up assembly of metallic electrodes from the molecule utilizing solution based self-assembly methods.[76,77] The general idea is to pre-fabricate on a chip metallic contacts using photo- or e-beam lithography, with dimensions which will be limited by lithographic resolution (~250 nm for deep UV and ~30–50 for e-beam) and then exploit self-assembly of chemically synthesized metal–molecule–metal structures to bridge lithographically pre-fabricated electrodes.[78]

The first challenge is the synthesis of metal–molecule–metal nanostructures. In this context, Dadosh *et al.* have developed a method that can yield gold nanoparticle dimers linked by single molecules *via* a self-assembly process.[24] Nanoparticle dimers (Au–molecule–Au) were fabricated by mixing a solution of dithiol molecules with a gold nanoparticle solution. In this method, it is possible to identify if a single molecule is in the nanogap, because trimers, tetramers, and aggregates will be formed when more than one molecule binds to a certain nanoparticle. In the method of Dadosh *et al.*, dimers of 30 nm-diameter gold nanoparticles were deposited onto electrodes with a 40–50 nm separation, and single-molecule conductance was measured. For a summary of synthesis of nanoparticle dimers we refer to our recent review.[77] With similar nanoparticle–molecule–nanoparticle bridge structures, Parsons *et al.* investigated the conduction mechanisms and stability of single OPE (oligo(*p*-phenylene ethylenes)) molecules.[79]

Furthermore, Jain *et al.* reported a strategy to fabricate 1–2 nm nanogaps *via* seed-mediated growth of end-to-end linked gold nanorods (AuNRs).[80] Mayor *et al.* demonstrated that the interparticle distance of gold nanoparticle dimers could be controllable by an atomic alteration in the structure of the linker molecule.[81] Bar-Joseph *et al.* presented a single electron device by placing a self-assembled metallic nanoparticle dimer in between e-beam lithography defined electrodes.[82] Maruccio *et al.* fabricated devices based on bisferrocene molecule–gold nanoparticles, and studied their transport properties.[83] The device was built on a solid support fabricated by a combination of optical lithography and chemical etching, and it showed similar behaviour to devices fabricated by conventional methods (Fig. 4). Firstly, the gold nanoparticles were assembled in the solution, linked by bisferrocene molecules. Secondly, the nanoparticle dimers were directed onto the electrodes by self-assembly. The bisferrocene molecules act not only as the linker molecule between the nanoparticles, but also as the functional molecular electronic component. This method demonstrates the potential of combining top down lithography with bottom self-assembly in the fabrication of a single-molecule device. Naaman *et al.* fabricated a hybrid device made from gold nanoparticles linked by alkyldithiol molecules with different lengths and investigated the dependence of conduction on the molecule length.[84] For further reviews on the use of self-assembly in single-molecule electronic devices, we refer to ref. 7 and 76.

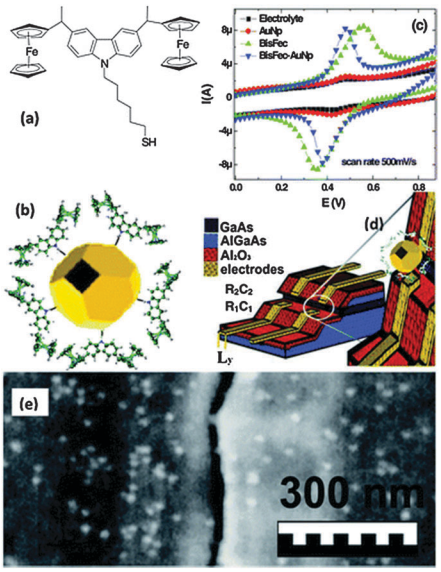

Fig. 4 Nanodevices based on bisferrocene–gold nanoparticle hybrids. (a) Structure of the bisferrocene molecules used in the device. (b) Schematic representation of the linkage of bisferrocene molecules to the surface of gold nanoparticles. (c) Cyclic voltammograms demonstrating the formation of bisferrocene–AuNPs hybrids. (d) Schematic view of the nanogap electrodes and (e) SEM image of the measured nanojunctions.[83]

Chemical growth of metallic nanostructures can also be used as a building block for the construction of nanogaps.[85,86] Bjørnholm *et al.* combined a top-down and bottom-up approach to construct the nanogaps by directed *in situ* growth of AuNR-based nanostructures inside PMMA nanochannels prefabricated by top-down e-beam lithography.[87] The PMMA nanochannels provide an additional handle for positioning the AuNRs, and nanoscale gaps between the electrode and the nanorods can be obtained. When the AuNRs are long enough to bridge the electrodes, 1–5 nm nanogaps are formed at the interface between *in situ* grown AuNRs and the pre-patterned gold electrode. Alivisatos *et al.* used a controlled assembly of gold nanoparticles into defined locations on a chip and within a circuit by utilizing capillary interactions.[88] Wolf *et al.* recently reported the oriented assembly of short gold nanorods (below 100 nm of length) from colloidal suspensions by a capillary assembly process on surfaces.[89] In their method, the gold nanorods can be aligned on the single particle level, and oriented nanorod dimers are obtained with narrow inter-particle gaps. Rey *et al.* reported a

directed capillary method to assemble AuNRs into chains between two electrodes.[90] The gap between each AuNR is about 5–7 nm, which may be caused by the CTAB bilayer on the surface of the AuNRs. The thickness of one CTAB bilayer is about 3.2 nm,[91] thus the interlayer between two AuNRs is about 6 nm. These AuNR based nanogaps can serve as a platform to fabricate structures for nanodevices.

In addition to AuNRs, carbon nanotubes (CNTs) have also attracted a lot of interest as building blocks for nanogaps, because CNTs are one-dimensional conductors or semiconductors and have a diameter similar to the size of the target molecules.[92–96] Typically, following metal deposition and a lift-off process, nanogaps of CNTs can be obtained. Besides CNTs, graphene and many nanowires, including nanowires made from organic and inorganic materials, can also be used to fabricate the nanogap.[97–99]

The on-wire lithography method has been widely used to fabricate nanogaps. Firstly, multisegmented Au–Ag nanowires are fabricated by electron beam evaporation. Secondly, the Ag segment can be removed using high temperature or chemical etching techniques, and the thickness of Ag determines the size of the nanogap.[21,22,100,101] Recently, Mirkin *et al.* developed the on-wire lithography technique to fabricate gold nanorod dimers with a 2 nm gap.[102–105] One of the main advantages of the on-wire lithography method is that the gap size can be controllably tuned during the nanowire synthesis process.

In addition to bifunctional small organic molecules, biomolecules have also been used as single-molecule electronic components. Since thiolated DNA was used for the first time to link gold nanoparticle dimers in 1996, DNA has attracted substantial interest for self-assembly of nanoparticles.[106,107] Significant progress in DNA-directed assembly of nanoparticles has been reported in recent years,[108–110] especially for DNA-linked nanoparticle dimers.[111–116] In these studies, the gaps formed between two nanoparticles are tunable and depend on the length and the number of linker DNA molecules.[113–117] Another advantage of using DNA is that the assembly is reversible: by cycling the temperature of the DNA–nanoparticle solution above and below the melting temperature of the DNA, the nanoparticles can be linked or dissociated.[106,118] Bidault *et al.* reported reversible switching of inter-particle distances in DNA bridged gold nanoparticle dimers.[119] The distance between gold nanoparticles could be switched from 5 nm to 15 nm, by hybridizing or removing a single DNA strand. A recent report revealed that a 1 nm gap can be generated by DNA-tailored nanoparticles.[120] The detailed electric properties of DNA molecules have raised some debate. Kasumov *et al.* reported that DNA between rhenium/carbon metallic contacts is possibly superconductive at low temperatures.[121] Dekker *et al.* found that DNA with a length of about 10 nm is a semiconductor, while DNA with ~100 nm long strands is an insulator.[122] The measurements were carried out using conducting AFM and STM, in which collections of DNA molecules were measured. The conductivity of a single DNA strand was measured later by Guo *et al.*, where single DNA molecules terminated with amines were connected to electrodes.[123] The well-matched DNA in the gap exhibited a resistance on the order of 1 MΩ. A base mismatch in the DNA double helix decreased the conductivity about 300 fold compared with a well-matched one.

2.5. Data collection and analysis

The unequivocal identification of a single molecule between metallic electrodes is a challenge common to all experimental techniques employed to fabricate single-molecule devices. Measurements of current–voltage characteristics readily provide information about electrical resistance of the device under study, but the measured resistance is prone to large variations upon nanoscopic changes in the metal–molecule contact geometry. As a consequence, significant discrepancies in the measured electrical resistance of a single molecule can be found from experiment to experiment even when the same molecules and contacts are employed. The analysis of single molecule conductance simply from its current–voltage (*I–V*) characteristics is therefore fundamentally incomplete.

A way to quantify the resistance of a metal–single molecule–metal junction in a meaningful way is by using the so-called conductance histogram method, a statistical analysis introduced by Krans *et al.*[124] for studying metallic quantum point contacts and first implemented for electrical measurements on molecules by Xu & Tao (Fig. 5).[34] This method consists of recording the electrical conductance of a metal–molecule–metal junction a (statistically) significant number of times (typically >1000). In practice, the large amount of molecular junction realizations needed to collect data is formed by repeatedly moving two metallic contacts into and out of contact, and thus the STM-break junction technique and MCBJ techniques are better suited for recording conductance histograms. In an STM experiment,

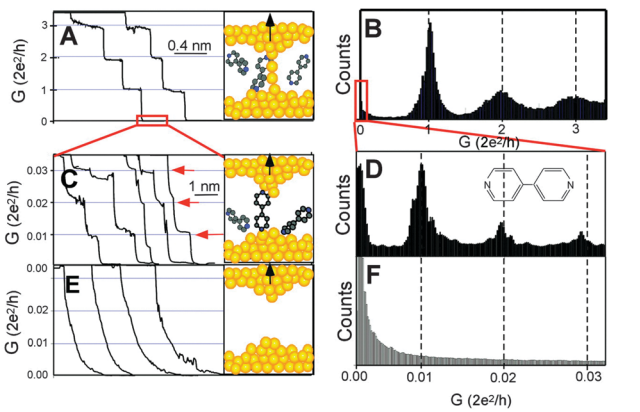

Fig. 5 Use of conductance histograms to investigate single-molecule electrical conductance. (A) The electrical conductance of a gold contact formed between the STM tip and the substrate decreases in quantized units of $G_0 = 2e^2/h$ as the tip is retracted. (B) Corresponding conductance histogram shows peaks near 1, 2 and $3G_0$ due to conductance quantization. (C) The tip–substrate contact is broken, new conductance steps appear if molecules are present in the solution. These conductance steps arise from the formation of a molecular junction between the tip and the substrate electrodes. (D) Conductance histogram of the molecular junction depicted in (C) shows peaks near 0.01, 0.02, and $0.03G_0$ that are ascribed to one, two, and three molecules, respectively. (E and F) As a control experiment, no such steps or peaks are observed in the absence of molecules. Reprinted with permission from ref. 34.

a finite bias voltage between the tip and the substrate, and the current is measured as the STM tip is pushed into/retracted from the substrate. The conductance of the molecule appears when the tip is pulled away from contact with the substrate. In this low conductance regime (tunneling), a new sequence of peaks appears in conductance histograms that reveal the most likely conductance of the molecule under study. Since its introduction, the conductance histogram technique has been used to characterize the electric conductance of a variety of molecules.[35,125,126] More importantly, it has served as a powerful tool to understand electron transport mechanisms through single molecules,[125] and the role of the chemical anchoring group used to bind molecules to metal electrodes.[126] As an example, it has been shown that butane linked to gold electrodes *via* dimethyl phosphines (PMe_2) displays lower contact resistance compared to the same molecule linked to gold by amine groups (NH_2) or methyl sulfides.[126]

The potential of the conductance histogram method to study not only electronic transport through single-molecules but also fine details of metal–molecule contacts was immediately identified and the technique was further refined to extract information about molecule–metal mechanics. Building on previous studies from the same group, Nuckolls *et al.* performed a systematic STM-break junction study involving alkane molecules linked to gold electrodes *via* amine (NH_2), methyl sulfide (SMe), and dimethyl phosphine (PMe_2) groups, where conductance histograms were recorded as a function of junction elongation (Fig. 6).[127] It was found that the conductance *versus* displacement traces showed plateaux during elongation, which provided a signature of junction formation; the plateau length probed the amount of elongation a junction can sustain without breaking. The modified conductance histogram method allowed us to find that (a) longer molecules have a higher probability of forming a single-molecule junction, (b) under stress, anchoring groups can hop from one available Au site to another or even distorting the Au structure by dragging Au atoms out of the surface and (c) confirm that the stronger Au–PMe_2 bond – compared with the Au–NH_2 – displays lower contact resistance and has higher probability of forming a molecular junction.

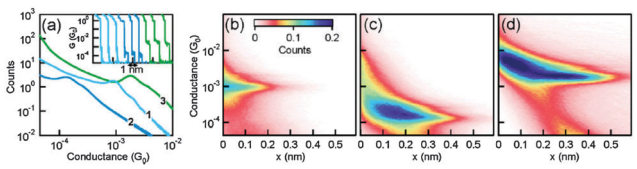

Fig. 6 (a) Conductance histograms on the linear scale of 1,4-butanediamine (M1), 1,6-hexanediamine (M2) and 1,4-bis (dimethylphosphino) butane (M3). The inset displays conductance traces that show a molecular step for each molecule (offset horizontally for clarity). (b–d) 2D histograms of molecules M1, M2, and M3 showing that longer molecules with the same linking group (*i.e.* M1 and M2) have higher probabilities of forming a molecular junction (the stretching length for the conductance peak increases from 2.5 Å for M1 to 4.5 Å for M2) and that dimethyl phosphine anchoring groups have a higher probability of forming a junction than amino groups (*i.e.* M1 compared to M3) while displaying lower contact resistance. Reproduced with permission of Nuckolls *et al.* Formation and evolution of single-molecule junctions. *Phys. Rev. Lett.*, 2009, **102**, 126803.[127]

Similar experiments aiming at understanding the effects of the anchoring group on transport and mechanics of single molecule junctions have been conducted by comparing amino and thiol terminated *n*-alkanes (n = 2–6, 8).[128] In this work, the effect of amino groups observed in ref. 127 was reproduced. Additionally, it was found that thiol groups provide lower contact resistance compared to amino groups in longer molecules ($N > 5$), and also that these groups are more efficient in disturbing gold contacts (*i.e.* they lead to significantly higher Au atom re-arrangement). This latter observation was deduced from the fact that the maximum stretching length for molecular junctions of alkane–dithiols can reach values almost the double of the molecular length. In a recent work, the same group studied further the null impact of amino anchoring groups on re-arrangement of gold atoms in the contacts.[129] The binding stability of amino terminated oligo(phenylenethynylene) to gold electrodes was determined by recording conductance histograms as a function of junction elongation at different stretching speeds. Contrary to *e.g.* thiol terminated molecules in their previous report, it was found that the elongation of single-molecule junctions (amino-terminated) needed to break the junction is lower than molecular length irrespective of stretching speed, confirming that amino groups do not lead to rearrangement of gold atoms in the contacts.

The electrical stability of a single molecule device is linked to the nanoscopic mechanical stability in a number of metal–molecule junctions. In this direction, Frei *et al.*[32] have developed a technique to correlate conductance measurements and binding force in metal–single molecule junctions. Using a modified C-AFM setup, conductance and force histograms were studied for the case of Au point contacts, and gold linked to benzene, butane and hexamine *via* amine anchoring groups as well as the case of gold–bipyridine junctions. The Au point contact is used as a calibration measurement by comparing their measured value to literature reports. Authors show that 1,4-benzenediamine binds most weakly to Au atoms, while the pyridine–gold bond exhibits the largest breaking force among all the molecules under study. Since all the anchoring groups contain a nitrogen atom, the stronger Au–N bond formed in Au–bipyridine was shown *via* DFT calculations to be a consequence of the electronic structure of the molecular backbone altering the N–Au bond strengths in all molecules.

Despite the enormous experimental challenges to fabricate identical single-molecule devices in a reproducible way, the development of clever techniques for data collection and analysis have enabled the study and understanding of electron transport through single molecules across different experimental realizations. A research line in single-molecule electronics is thus the development of techniques that allow unleashing the full potential of available fabrication techniques such as those described in this section.

3. Molecular systems for single-molecule electronics

The molecular unit in a single-molecule device can be divided into the anchoring groups, the link between the metallic

contacts and the molecular kernel. The overall performance of a single-molecule electronic device is determined by the electrode/molecule interface (anchor) and the internal electronic structure of the molecular kernel. Thus, chemical design and synthesis are of paramount importance for single-molecule electronic devices. In this section we present some of the different designed motifs used to control the electronic properties and assembly of molecules into single-molecule electronic devices. Further, we discuss how chemical design of the molecules influences the transport properties. This discussion is continued in further detail in Section 4 (on physical phenomena in single-molecule junctions) and 5 (on molecular switches).

Electron transport through molecules in nanoscale junctions is sensitive to very small changes in atomic configuration. One example is the possible arrangement of thiols on a gold surface which is discussed by Häkkinen *et al.* in a recent review.[130] Moreover, several studies have shown the influences of different types of chemical anchoring groups on the molecule and the metal surface in the junction.[34,131–136] Not only the specific anchoring group, but also variations in the type of electrode material,[137–139] different molecular geometries[140,141] and conformations[142] heavily influence measurable properties of the metal–molecule–metal junction. Fig. 7 shows artist impression of a $Mn(Terpy)_2$ molecule bound in an asymmetric fashion to two electrodes. Structural differences in molecular wires, including their anchoring groups, length, conformation and alignment with the Fermi level of the electrodes, will be discussed in this section.

3.1. Anchoring groups

The anchoring group, responsible for the direct contact between metal and the molecular kernel, needs to be considered in terms of its mechanical stability and also regarding its electronic transparency (weak or strong coupling).

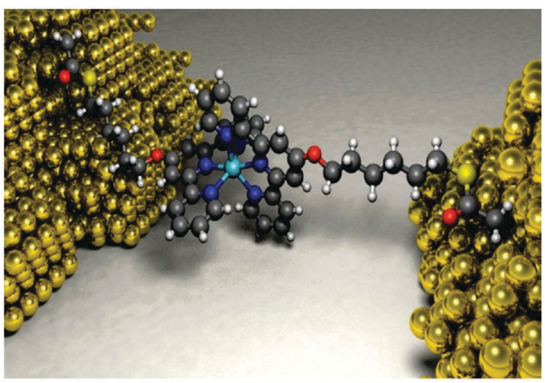

Fig. 7 Schematic of a single-molecule device in which a $[Mn(terpy\text{-}O\text{-}(CH_2)_6\text{-}SAc)_2]^{2+}$ molecule is bound in between two gold electrodes. The asymmetric geometry illustrates a likely realization of the device which gives rise to asymmetric coupling to the source and drain electrodes and the difference in gate-coupling to the two ligand moieties that is implied by the transport data.[143] Reprinted with permission from E. A. Osorio, K. Moth-Poulsen, H. S. J. van der Zant, J. Paaske, P. Hedegård, K. Flensberg, J. Bendix and T. Bjørnholm, *Nano Lett.*, 2010, **10**, 105–110. Copyright 2010 American Chemical Society.[31]

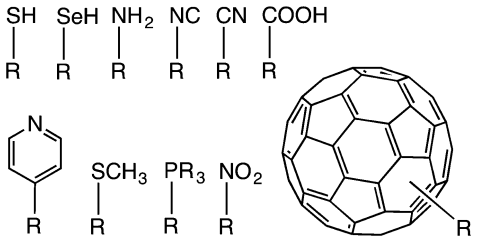

Fig. 8 Typical anchoring groups for single-molecule electronics.

The most explored example of anchoring groups is thiols on gold surfaces (Fig. 8). But in addition to thiol (–SH),[144–148] some functional groups with good affinity for gold are selenium (–SeH),[126,149] amino ($-NH_2$),[131,132,135] isocyano (–NC),[131,150] cyano (–CN),[133,134] pyridyl,[34,151] carboxy acid (–COOH),[135] nitro ($-NO_2$),[134] methylthioether ($-SCH_3$),[126] phosphino[126] and fullerenes (Fig. 8).[152–154]

Thiols were the first explored anchoring groups for charge transport experiments and are still the most widely used. They bind strongly to gold (as well as to silver and copper) and the bond is even stronger than the gold–gold bond itself.[15,155] Amines form a donor–acceptor bond to gold surfaces, preferably with under-coordinated gold,[131] and carboxy acids are believed to bind by ionic and coordinating interactions.[156] Due to different electronic coupling by different types of anchoring groups, the contact resistance varies as Au–S > $Au–NH_2$ > Au–COOH.[135,157] Due to a weaker binding strength of amines and carboxyl groups, a higher bias on the electrode creates instability in the metal–molecule bond. The stability has also been examined for methylphosphines, methylsulfides and primary amines in the order: PMe_2 > SMe > NH_2.[126,127] The junction formation probability and stability of pyridyl, thiol, amine and cyano have been compared and resulted in this sequence: pyridyl > SH > NH_2 > CN.[158]

One challenge with assigning the contact resistance is that the detailed gold–ligand structure might differ significantly from device to device. As an example several different types of coordination geometries exist for the gold–thiol bond such as top-bridge and hollow sites. The relative stability of the different coordination sites might change due to minute changes in local chemistry and/or the forces employed to the system in *e.g.* a MCBJ setup. Small variations in contact resistance have been found to be the main reason for the discrepancies between the reported results from different research groups for the measured conductivities of alkane thiols.[159]

In addition to bond stability, different anchoring groups provide different charge transport mechanisms (transparency) due to their influence on the effective mixing of the HOMO–LUMO (HOMO: highest occupied molecular orbital, LUMO: lowest unoccupied molecular orbital) levels of the molecular kernel and the Fermi energy (E_F) of the metal. Thiols show hole transport through the HOMO, since the HOMO is the closest energy level to the E_F of the gold.[160,161] Amines,[162,163] nitriles[133] and pyridines,[163] on the other hand, are expected to use the LUMO as the transport channel. The position of the HOMO and LUMO relative to the Fermi levels of the electrodes can be

measured experimentally in two terminal devices by a method known as transition voltage spectroscopy (TVS). One recent example of TVS employed in a study on alkane thiols is found in ref. 164. Other recent examples of TVS studies on molecular systems can be found in ref. 159.

Single-molecule electronics usually requires thousands of measurements to describe the specific behaviour of a single molecule in a junction.[140,151] Increasing temperature or adjusting electronic potential at the electrodes to align the E_F of the metal electrode with the HOMO or the LUMO of the molecule might subsequently result in re-arrangement of the atoms at the electrode (*e.g.* Au) or a switching of the anchor between different bonding motifs.[130] To decrease geometric fluctuations of the anchor, multidentate binding motifs have been used by Lee *et al.*[165] They demonstrated that several functional groups bound to the surface could minimize the effect of individual bond fluctuations. Another possibility is to predefine and functionalize the electrodes *via* a selective organic chemistry such as click-chemistry[166] or wrap the electrodes with the molecular backbone of the molecular wire.[167] Conductance measurements with the gold–amine bond reveal quite good reproducibility, due to the defined electronic coupling of the lone pair electrons of the nitrogen to the gold and a high specificity in which NH_2 binds to under-coordinated gold sites.[131] Also, the conductance in a junction keeps a constant value when changing the binding site from one under-coordinated Au to another.[127]

Another system under ambient temperature conditions has been developed by Venkataraman *et al.*, in which a direct Au–C σ-bond is responsible for the contact between the electrode and the molecule.[155,168] The terminated trimethyltin (Me_3Sn–CH_2–π–CH_2–$SnMe_3$) end groups cleave off *in situ* to form a direct C–Au bond. The development of new synthetic routes to promote the formation of covalent sulfur-free bonds between organic molecules and metal surfaces (Fig. 9) opens up new possibilities to control the charge-transport properties at metal–molecule–metal junctions in a reproducible way.[168]

Strong electronic coupling is achieved by the direct covalent σ-bond connection *via* a methylene group and the π-conjugated wire. Compared with a traditional amine–Au contact, the direct covalent connection shows a 100-fold higher conductance. The Au–C bond couples well with the π-system of the molecule, in contrast to an Au–C bond which is connected directly to the molecular wire, without a methylene bond in between.[168] A near-resonant tunnelling is suggested to be responsible for the electron charge transfer. Compared to thiol anchors, Au–C shows a three-order-of-magnitude increase in efficiency for the charge transfer, meaning that devices could be run at lower voltages.[169] Wandlowski *et al.* showed the same approach for alkyne terminated OPE's to create Au–C bonds *via* an *in situ* deprotection of a trimethylsilyl group.[48] Anchoring groups are often covalently bound to the gold electrode, but another possibility is that molecules, such as fullerene (C_{60}, Fig. 8), are adsorbed to the electrode,[51,170,171] where a strong hybridization results in a high conductance.[172] Tao *et al.* reported coupling of single molecules with Au electrodes by electrochemical reduction of a diazonium terminal group which produced direct Au–C covalent bonds *in situ* between the molecule and the Au electrodes.[173]

Danilov *et al.* studied the influence of single methylene groups inserted between the molecular π-systems and the metal electrodes.[137] Fig. 10 depicts the two different molecules incorporated in a junction. A change in the charge transport mechanism from coherent tunnelling to sequential tunnelling (decreased transparency) and Coulomb-blockade behaviour was observed. Due to the insertion of methylene groups, an increase in the resistance in the open state was observed. The directly connected wire shows higher conductance and no gate dependence, which resulted from a strong metal–molecular orbital coupling.[137]

3.2. Molecular backbone

This is the part of the molecular system, which largely defines the electronic functionality of the single-molecule device.

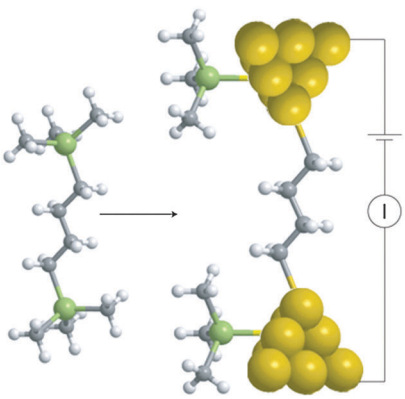

Fig. 9 Junction formation and conductance measurements with 1,4-bis(trimethylstannyl)butane molecules between gold electrodes. (H atoms, white; C atoms, grey; Sn, green). Reprinted by permission from Nature Nanotechnology (Z. L. Cheng, R. Skouta, H. Vazquez, J. R. Widawsky, S. Schneebeli, W. Chen, M. S. Hybertsen, R. Breslow and L. Venkataraman, *Nat. Nanotechnol.*, 2011, **6**, 353–357), Copyright (2011).[168]

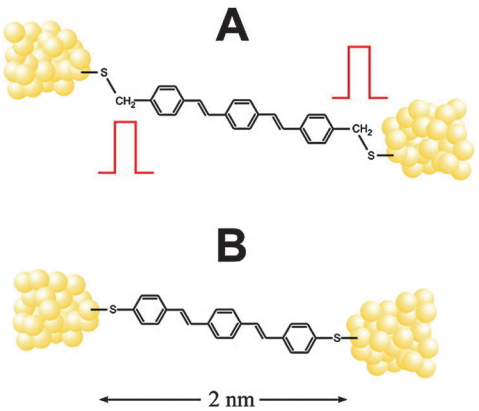

Fig. 10 Schematic representation of molecules A and B placed in electrode gaps. Derivative A has an extra methylene (–CH_2–) group inserted between sulfur and the π-conjugated moiety, providing a tunneling barrier (red). Reprinted with permission from A. Danilov, S. Kubatkin, S. Kafanov, P. Hedegård, N. Stuhr-Hansen, K. Moth-Poulsen and T. Bjørnholm, *Nano Lett.*, 2007, **8**, 1–5. Copyright 2007 American Chemical Society.[137]

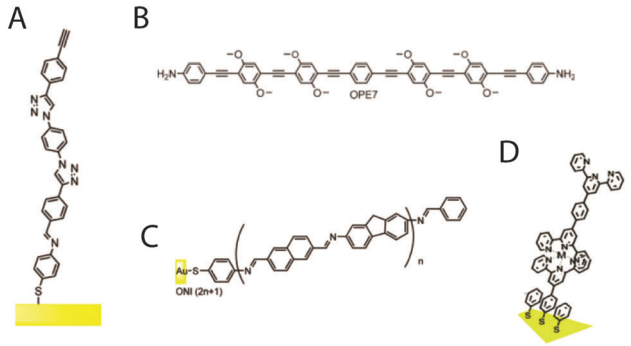

Fig. 11 (A) Oligophenylenetriazole (OPT) synthesized by click chemistry, (B) oligo(*p*-phenylene ethylenes): OPE7, (C) oligofluoreneimine (ONI) and (D) a metal containing molecular wire as examples for typical molecules for single-molecule electronics.[174]

That is, for a given electronic structure of the molecular kernel, the single-molecule device function might turn out to be that of a resistor, a diode, a transistor, *etc.* Molecular switches, a thoroughly studied system, are reviewed in Section 4. For this part we limit the discussion to molecular wires, in which charge transfer occurs through the π-conjugated part of the molecule. Electrons can move freely in the delocalized orbitals over "long" distances. Typical molecular wires[174] (Fig. 11) are oligomers such as oligo(*p*-phenylene ethylenes) (OPE's),[175,176] oligo(*p*-phenylene vinylene) (OPV's),[19,177] oligophenyleneimine (OPI),[178,211,212]oligothiophenes,[179] oligofluoreneimine (ONI's),[180] oligophenylenetriazole (OPT's),[181] oligoanilines,[182] oligoynes,[183] or oligoaryleneethylene (OAE).[184] Another class of molecules are short alkyls such as alkanedithiols,[20,185,186] alkydiamines[131] or phenyldithiols,[35] which have been widely studied as well. Other types of "molecular" systems include metal complexes such as terpyridines incorporating metal ions.[187,188]

At the macroscopic length scale, the conductance of a molecular wire decreases linearly with its length. A junction conductance for short molecules (<3 nm) decays exponentially with the length of the molecule.[142,189,190] Conductance data can be measured using conducting probe AFM (C-AFM) on single molecules or in break junctions (*via* STM or MCBJs).[190]

Charge transfer in saturated and short conjugated molecules occurs due to non-resonant tunnelling,[174] meaning that the electron has no real retention time on the wire. The energy of the tunnelling electron does not have to match the molecular orbital energies well. One example is alkanes, which are poorly conducting[20,34,151] because of a large HOMO–LUMO gap. The conductance decreases with the length of the molecule and with an increasing HOMO–LUMO gap.[135]

Frisbie *et al.* explained a transition from a short range tunnelling charge transport mechanism to a long range "hopping" mechanism by measuring how the electrical resistance varies with temperature and with the length of the molecular wire (from 1 to 7 nm).[101,178,212] This study revealed the theoretically predicted change in direct-current transport from coherent tunnelling to incoherent charge hopping in molecular junctions, as the oligophenyleneimine (OPI) molecular system

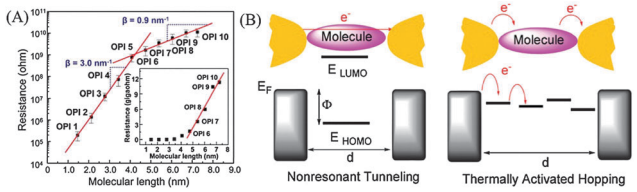

Fig. 12 (A) Electrical resistance of conjugated oligophenylimine (OPI) molecular wires.[178] From [S. H. Choi, B. Kim and C. D. Frisbie, *Science*, 2008, **320**, 1482–1486]. Reprinted with permission from AAAS. (B) Schematic energy diagram for different transport mechanisms, nonresonant tunneling and multistep hopping through molecular wires between metal electrodes.[188]

extends more than 4 nm (Fig. 12)[178] Frisbie *et al.* further showed that a break in the conjugation by introducing a non-conjugating molecule in the wire reduced the conductivity of the molecular wire dramatically. This effect is not observed in short wires, most probably due to the fact that tunnelling is the dominant transport mechanism.[151] The change in the charge transfer mechanism from hopping to tunneling has been shown in other molecular systems as well.[180,181,187] Lu *et al.* observed a transition of the charge transport mechanism from tunnelling to hopping at around 2.75 nm for amine terminated OPEs.[191] The hopping conduction seems to be less length dependent, but more temperature dependent than transport in the tunnelling regime.[180,189]

The molecular conformation of molecular wires also plays an important role in conductance measurements of a metal–molecule–metal junction. Steigerwald *et al.* have shown that an increasing twist degree of freedom of the bonds in the wire results in a decrease in the degree of π-conjugation and therefore a decrease in the junction conductance.[131] Fig. 13 shows schematically a change in the twist angle, and the resulting change of the conjugation path. The highest conductance is measured with molecule 2, which has the lowest twist angle. Another example of variations in the torsion angle in biphenyl was reported by Wandlowski *et al.*[192] They changed the torsion angle of 4,4′-biphenyldithiol and monitored the Raman spectra *in situ*. The intensity of the C=C stretch in Raman spectra depends on the degree of conjugation between the two phenyl rings.

Venkataraman *et al.* showed that some molecules, like bipyridine, could assemble in a metal junction in different geometries, which have an effect on the junction conductance.[162] Conductance histograms of bipyridine-based molecular wires show a double-peak feature, due to their two different

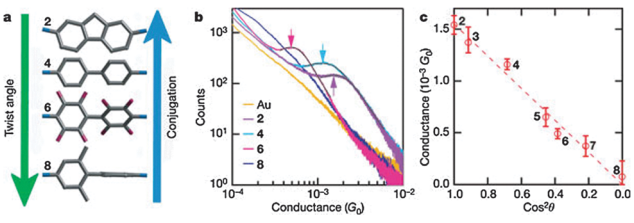

Fig. 13 Dependence of single-molecule junction conductions on molecular conformation. Reprinted by permission from Nature Nanotechnology (L. Venkataraman, J. E. Klare, C. Nuckolls, M. S. Hybertsen and M. L. Steigerwald, *Nature*, 2006, **442**, 904–907), Copyright (2006).[142]

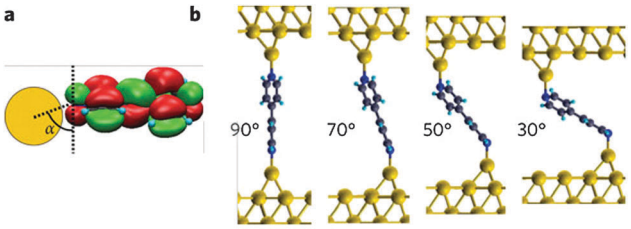

Fig. 14 Mechanically controlled binary conductance. Reprinted by permission from Nature Nanotechnology (S. Y. Quek, M. Kamenetska, M. L. Steigerwald, H. J. Choi, S. G. Louie, M. S. Hybertsen, J. B. Neaton and L. Venkataraman, *Nat. Nanotechnol.*, 2009, **4**, 230–234), Copyright (2009).[162]

binding geometries.[140,162] As a consequence, it is possible to mechanically switch between two defined conductance states by changing the distance in a mechanically controlled break junction. Fig. 14a shows a schematic coupling between the gold s-orbitals (orange) and the bipyridine LUMO (π*), which is the orbital expected to be responsible for the charge transmission. The π* is expected to be perpendicular to the nitrogen lone pair, therefore a high tilting angle α between the nitrogen–gold bond and the π-system allows strong coupling and high conductance. Fig. 14b shows schematically the case of high conductance. These pull–push break junctions have been used to explore the influence of geometry on junction conductance, proven with a library of pyridine-based molecular wires.[140]

Hummelen *et al.* studied the difference in conductance between linear conjugated, broken conjugated and cross-conjugated wires.[190] In cross-conjugated wires, two subsequent single bonds connect π-conjugated systems. These are linearly conjugated to a double bond, a sp^2 hybridized carbon, called the vinylidenic double bond, as in *e.g.* anthraquinone. Hummelen *et al.* found that cross-conjugated wires show a very low conductivity,[193,194] and even lower conductivity than molecular wires with a broken conjugation, see Fig. 15.[190] This effect is correlated with the destructive quantum interference effect[195,196] of cross-conjugated wires (Fig. 15, red molecules).[194,197–199]

3.3. Electrode material

As discussed above, the formation of efficient and reproducible molecule–metal electrode coupling is one key factor for the integration of molecules into circuits in the future.[169] To date, due to its noble metal character, gold has been the electrode material of choice. Future developments could be focused on other materials, such as silicon or carbon. Nanoscale junctions of Si have been fabricated, but the Si–C bond is not as mobile as the S–Au bond, which makes it more difficult to make a well defined SAM.[200] Another approach is using carbon-based electrodes. Graphene and other 2D materials can be grown without defects at the wafer scale, and since graphene is a 2D material, this might pose some advantages when considering the number of contact geometries compared to electrodes made of 3D materials. Guo *et al.*[97,138] functionalized graphene with molecular wires *in situ* by covalent bonds.[138] The junction was fabricated by dash-line lithography, the nanogaps were then cut out by oxygen plasma ion etching. This etching produced carboxyl acid-terminated graphene, which was further functionalized with groups such as amine terminated molecular wires (Fig. 16). Van der Zant *et al.* created graphene electrodes by feedback-controlled electro-burning. The molecular system was introduced in a second step, and the coupling between molecule and graphene was established by π–π stacking (Fig. 17).[96]

Molecular electronics experiments have also been done with other electrode materials in which similar anchoring groups and the same molecular wires can be used. Zhou *et al.* used an electrochemical jump-to-contact scanning tunnelling microscope break junction (ECSTM-BJ) to create gold and copper clusters.[139] They used different bipyridyl molecules and compared the conductance between Au and Cu electrodes, where the Cu electrodes showed a lower conductance. The different electronic coupling efficiencies between the metal and the wire were suggested as the cause of this effect. In another study, Danilov *et al.* compared devices with gold (Au) and lead (Pb) electrode material and found that the low bias regime in the Pb electrode case showed similar molecular charging energies, but different open state gate voltages compared to the gold electrode. For example, the −2.6 V gate

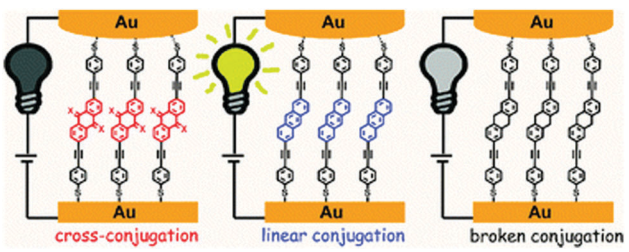

Fig. 15 Schematic of OPEs in a conductive probe AFM junction. With three different molecules: cross conjugated (red), linear (blue) and broken (black) conjugated.[190]

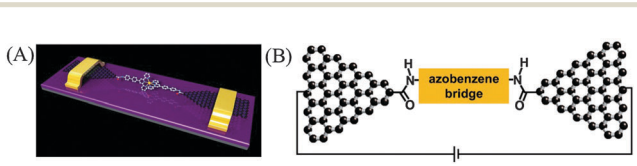

Fig. 16 (A) Depiction of a single-molecule device based on graphene.[97] (B) Schematic of a grapheme–azobenzene junction.[138] Reprinted by permission from John Wiley and Sons, copyright (2012) and (2013).

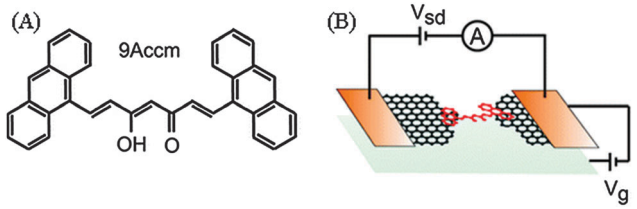

Fig. 17 Anthracene terminated curcuminoid wire (A) brought into a graphene nanogap (B). Reprinted with permission from F. Prins, A. Barreiro, J. W. Ruitenberg, J. S. Seldenthuis, N. Aliaga-Alcalde, L. M. K. Vandersypen and H. S. J. van der Zant, *Nano Lett.*, 2011, **11**, 4607–4611. Copyright 2011 American Chemical Society.[96]

voltage separates the same open state at +0.8 V on the gold electrode.[137] This effect was attributed to the differences in the Fermi level of Au and Pb. In addition, Kaun *et al.* found that the conductance of alkanedithiol junctions could be increased by changing the electrode orientations [100] and [111] using first principles calculations.[201] Their work indicates that Au(100) electrodes provide the high conductance, while Au(111) electrodes provide the low conductance in alkanedithiol single-molecule junctions, which is an interesting observation when considering the spread of different electrode metal facets one can envision observing in the actual device. The effects of different electrode materials, including Au, Ru, and carbon nanotubes, on electronic transport of molecular electronic devices have been studied theoretically by Kim *et al.*[202]

In all examples here, it can be concluded that the molecular structure, including the anchoring group, the molecular wire architecture, length, conformation, and alignment of the Fermi level with the HOMO–LUMO gap are key factors for the junction conductance and open for a wealth of opportunities for chemical design of molecules with tailored properties for single-molecule devices.[310,311]

4. Physical phenomena in single-molecule electronics

Beyond their novelty as electronic devices, metal–molecule–metal junctions are a unique test bed for performing electronic transport studies at the nanoscale. These systems offer a plethora of rich physics, ranging from electrical rectification to quantum mechanical interference at the molecular level. In this section we highlight the experimental work describing physical phenomena observed in single molecules, since the first proposal of unimolecular electronic devices.[2]

4.1. Rectification

A rectifier, also called a diode, is a two-terminal in which current flow is allowed for a given polarity of the voltage applied across its terminals (forward bias), but blocked when the polarity is inverted (reverse bias). An ideal rectifier is thus a voltage-controlled switch.

Rectification is an almost ubiquitous phenomenon in semiconductor technology. A simple metal–semiconductor interface exhibits rectification as a consequence of the mismatch in the Fermi level of the metal and either the conduction or the valence band of the semiconductor. When a metal and an n-type semiconductor are brought into contact and thermal equilibrium (*i.e.* equalization of Fermi levels) is reached, an energy barrier (so-called Schottky barrier) is formed. Rectification occurs because in order for electrons to go from the conduction band of the semiconductor into the metal, this barrier has to be overcome by, for example, applying an external voltage equal to the barrier height. Inversion of the polarity of the voltage (reverse bias) leads to an increase of the barrier, which in principle impedes electron flow, but in practice it leads to a very small saturation current. Larger rectification (ON/OFF ratio) can be achieved by replacing the metal with a p-doped material; in this case the barrier height increases and the saturation current decreases orders of magnitude.

In analogy with a p–n diode, Aviram and Ratner proposed a single molecule consisting of electron rich/donor (n-type) and electron poor/acceptor (p-type) units, separated by a sigma bond that behaves as tunnelling barrier (Fig. 18a).[2] In these asymmetric molecules, rectification occurs if the acceptor/donor levels are carefully chosen. If this is the case, a forward bias (on state) corresponds to a negative voltage applied to metal 1 (cathode) with respect to metal 2 (anode). In the forward bias (Fig. 18b) electrons tunnel from the cathode to the anode in a three step process: (1) from the cathode (metal) to the LUMO of the acceptor level, (2) from the LUMO of the acceptor level to the HOMO of the donor level and (3) from the HOMO of the donor level out into the anode (metal). For reverse polarity the downhill tunneling of electrons from the cathode to the anode is no longer possible (Fig. 18c).

Experimentally, STM became the first technological platform capable of contacting single molecules adsorbed on metallic surfaces. Following the theoretical proposal, studies of rectification in single molecules were obscured by employing dissimilar contact metals (different workfunction), which in principle could by themselves display rectification due to asymmetric tunnelling current. The first experiment reported rectification in a monolayer of hemiquinone (acceptor–donor pair) attached to the surface of Au/Ag (anode) on mica using a Pt tip (cathode).[203] A similar study reported rectification in phthalocyanines chemically bonded to the surface of highly-oriented pyrolytic graphite (HOPG) by wet chemistry.[204] In both cases rectification was explained to be a consequence of the presence of molecules, although a simple mismatch in tip–substrate work functions was not ruled out. To address the case of molecular rectification with symmetric metallic contacts,

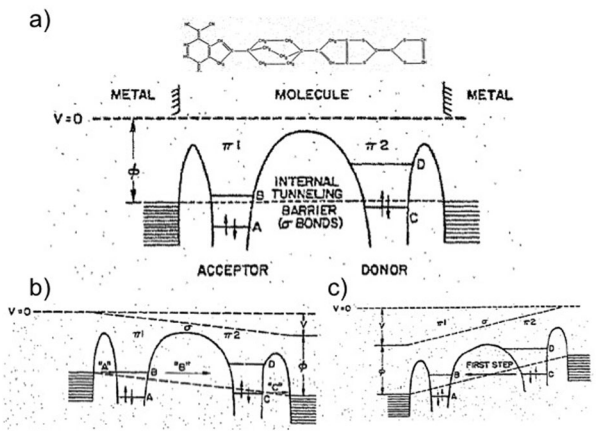

Fig. 18 Aviram–Ratner single-molecule rectifier based on acceptor tetracyanoquinodimethane (TCNQ) and donor tetrathiolfulvalene (TTF) separated by a triple methylene bridge. (A) Structure and energy diagram of the molecule in contact with cathode and anode electrodes. (B) Energy diagram in forward bias (ON state) and (C), reverse bias (OFF state). Reprinted from Aviram and M. A. Ratner, *Chem. Phys. Lett.*, 1974, **29**, 277–283, with permission from Elsevier.[2]

a gold substrate and an STM tip were used to study SAMs in sterically hindered donor–π–acceptor (D–π–A) moieties (instead of D–σ–A).[205] In the studied molecules ($C_{16}H_{33}$–Q3CNQ), the donor and the acceptor are twisted out of the plane to avoid donor and acceptor overlap of molecular orbitals. Remarkably, the planarity of the molecule (dihedral angle between the donor and the acceptor) could be controlled chemically, and this was achieved by sequential exposure of the molecule to HCl (to twist molecule) and NH_3 (to restore planarity). The gold substrate and the tip were chemically functionalized with sulfur and decanethiolate link chains to achieve symmetric contacts to the molecule. As a result, rectification in molecules with twisted moieties was observed, while those that are planar or have a weak donor–acceptor combination exhibited no rectification. Rectification (50–150 ON/OFF ratio) was thus attributed to the molecule asymmetry itself, since rectification disappears when the molecules are planar and molecule contact to the anode/cathode is symmetric. Another example where rectification occurred in the absence of a sigma bond was the case of (asymmetric) dipyrimidinyl–diphenyl covalently attached to the gold electrodes with thiol groups (Fig. 19A). As a control experiment, the symmetric version of the molecule (tetraphenyl) showed no rectification. At zero bias, the hole wave function is strongly localized at the biphenyl end of the molecule near the surface. This is the consequence of the original electronic structure, which reflects the underlying chemical differences between the dipyrimidinyl and diphenyl blocks. Upon application of bias, the lack of symmetry of the molecule wave function results in an enhanced probability of hole transfer from the anode to the molecule.[206]

Using a MCBJ set-up,[15,43,44,207,208] rectification was reported for the first time in a variety of Aviram–Ratner type molecules consisting of two weakly coupled electronic π-systems,[209] covalently attached to electrodes using sulfur–gold bonds. The authors observed asymmetric *IV* curves for asymmetric molecules and symmetric for symmetric molecules, emphasizing the effects of the molecular system. In addition to rectification, this work reported the observation of steps in the *IV* curve that were attributed to the internal electronic structure of the molecule. The origin of this is that, in the presence of an electric field, the energy levels of the π systems are shifted relative to each other. Whenever an unoccupied level passes by an occupied one, an additional transport channel opens up and the current increases in discrete amounts. In addition, it was found that the current through the junction was also affected by the polarizability of the molecule, since the height of the *IV* steps depended on the bias magnitude and polarity.

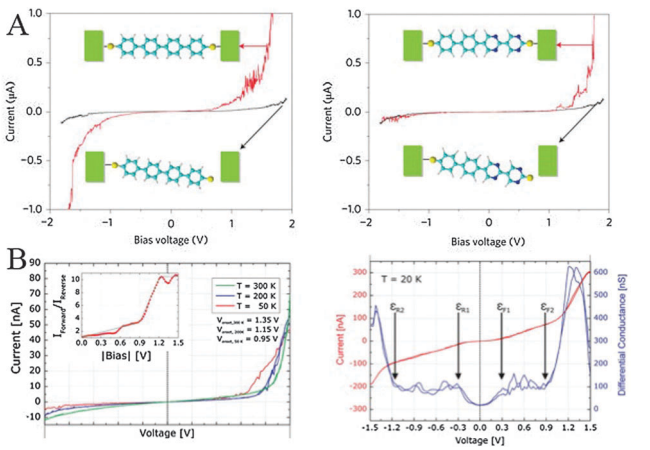

Fig. 19 Rectification in dipyrimidinyl and diphenyl blocks measured in STM (A) configuration and MCBJs (B). In both (independent) experiments rectification was observed only for symmetric molecules (left in a, b). (A) Reprinted by permission from Nature Nanotechnology (I. Diez-Perez, J. Hihath, Y. Lee, L. Yu, L. Adamska, M. A. Kozhushner, I. I. Oleynik and N. Tao, *Nat. Chem.*, 2009, **1**, 635–641), Copyright (2009).[206] (B) Reprinted with permission from E. Lörtscher, B. Gotsmann, Y. Lee, L. Yu, C. Rettner and H. Riel, *ACS Nano*, 2012, **6**, 4931–4939. Copyright 2013 American Chemical Society.[46]

In general, since rectification is a property inherent to material interfaces, the current focus on single-molecule rectification is to avoid experimental artefacts by controlling the molecule–metal contacts and comparing experimental data to theoretical simulations. There are only a few cases where measurements on the same molecule using a different experimental realization agree, notably C_{60} coupled to silver electrodes in a lithographically defined nanogap and STM,[210–213] and more recently diblock dipyrimidinyldiphenyl studied in a MCBJ and STM setup (Fig. 19).[46,206] For C_{60}, though *IV* curves were not quantitatively reproduced (due to the different metal–molecule contacts), a great similarity was observed in the tunneling LDOS by looking at d*I*/d*V*(*V*) plot. For the case of diblock dipyrimidinyl diphenyl, the current–voltage characteristics in a MCBJ set-up exhibited a temperature-independent rectification of up to a factor of 10 in the temperature range between 300 and 50 K, greater to what was reported using STM. As an outlook, the challenges in the single-molecule device are to demonstrate the high rectification ratio (*e.g.* by molecular design) and to develop technologies to improve the reproducibility, room temperature stability and integration of single-molecule rectifiers.

4.2. Vibrational effects

Molecules are flexible entities that can undergo deformations when they exchange energy with the environment. For example, in optical spectroscopy experiments, molecules display sharp absorption for certain wavelengths. When the energy scale of the incoming light is of the order of eVs (UV-visible), absorption lines correspond to transitions between molecular electronic levels. Absorption at lower energy scales (~100 meV's, infrared) reveals vibrations in molecular bonds (*e.g.* stretching) and at even lower energy scales (~meV's, microwave), absorption corresponds to motion in molecular degrees of freedom such as translations and rotations. The total absorption spectrum from the UV-vis to the microwave can be thought of as the fingerprint of a molecule and this is used to identify molecular species in macroscopic samples.

In electron transport experiments, the typical energy scale is in the range of a few hundred milli-electronvolts, which means in principle electrons can excite motion, rotation and vibrations in molecules. For this to be possible, the time the electron

spends in the molecule should be comparable to the time the electron needs to interact with a vibrational level. It turns out that features observed in *IV* due to molecular modes can be compared with optical spectroscopy (*e.g.* Raman or IR) and can be used to identify molecules present in between metallic electrodes.

The excitation of vibrations in molecules due to electrons, inelastic electron tunneling spectroscopy (IETS), was investigated by Jaklevic and Lambe.[215] In their seminal experiment, IETS was used to identify OH groups contained in an insulating barrier between metallic electrodes. In IETS experiments the total current has two components (Fig. 20a): (1) due to elastic electron tunnelling, which increases steadily as a function of voltage and (2) due to inelastic electron tunnelling, which causes discrete steps in current every time the applied voltage matches a characteristic vibrational mode with energy $h\nu$ and increases steadily thereafter. The current due to inelastic tunnelling is only a minimal fraction of the total current and can thus be better observed as antisymmetric (around zero bias) peaks in the $d^2I/dV^2(V)$ plot (Fig. 20b). An analogy to aid in the understanding of tunnelling spectroscopy is presented in Fig. 20c.[216] A water tank has two openings separated by a height h and therefore two components of the water flow: (1) a steadily increasing flow in the bottom channel and (2) a flow through the top channel, which has a threshold pressure ρgh (with ρ the density of water and g the gravitational constant), and steadily increases thereafter. The total water flow F has a kink when the input pressure matches Pi = ρgh. This kink might be difficult to observe in the $F(P)$ plot, but it would be easier to see it in $dF/dP(P)$ and even easier in $d^2F/dP^2(P)$: a flow opening at height h is revealed by a peak at pressure $P = \rho gh$. In IETS, the pressure threshold corresponds to a voltage threshold every time the input voltage matches the energy scale of a vibrationally or a rotationally excited molecular level.

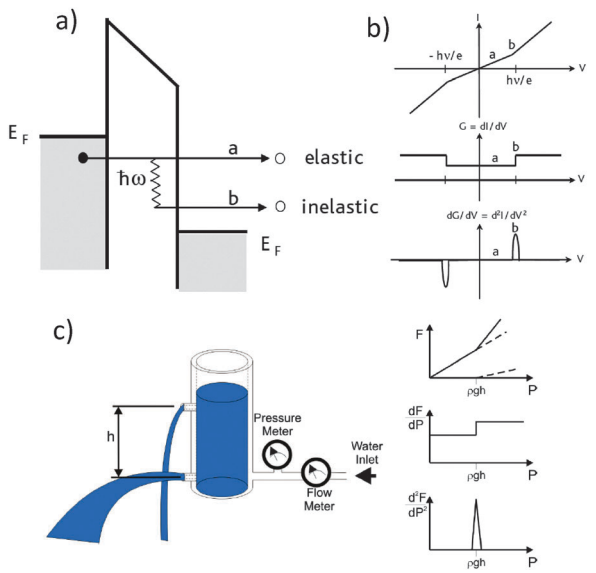

Fig. 20 Study of vibrational effects in molecules by inelastic electron tunnelling spectroscopy (IETS).[362] (a) In addition to elastic tunnelling current through a molecule, an additional inelastic current channel opens every time the applied voltage matches a characteristic vibrational mode with energy $h\nu$.[214] (b) The small current due to inelastic tunnelling is better observed as symmetric (antisymmetric) steps (peaks) around zero bias in the (dI/dV) $d^2I/dV^2(V)$ plot. (c) An analogy to IETS in a water tank with two openings separated by a height h. Water flow (current) has two components: (1) a flow in the bottom channel which increases with input pressure $P(V)$ and (2) a flow through the top channel which has a threshold pressure ρgh. The total water flow F has a kink when the input pressure matches Pi = ρgh.

Over the years, IETS has been developed and it is currently understood that vibrational effects on current depend on the electron–phonon coupling as well as electronic coupling between the electrodes and molecules.[134,217] The latter can be tuned in different experimental realizations such as STM, MCBJs or three terminal devices.

STM was the first experimental platform to describe IETS at the single-molecule level, by recording the C–H stretching mode of C_2H_2 adsorbed on copper.[218] In this report, authors replaced hydrogen by its heavier isotope, deuterium, in order to confirm the origin of peaks observed in d^2I/dV^2 on the energy scale corresponding to C–H stretching mode. In this seminal paper it was already acknowledged that certain expected vibrational modes were observed while others were hindered, and the molecule–substrate coupling was suggested as a possible cause. Further understanding in this direction was achieved in an experiment in which copper phthalocyanine was electronically decoupled from the substrate, by using bare and oxidized NiAl(110).[219] In this work, vibronic features were only observed for molecules adsorbed on the oxidized substrate (ultra-thin Al_2O_3); the absence of vibrational signatures on the bare NiAl(110) surface was attributed to spectral broadening when the molecule is coupled to the metallic substrate. Another case of the absence (appearance) of expected (unexpected) vibronic modes is nitrobenzene on Cu(111), which was expected to display 39 internal modes out of which only seven were observed in the IETS spectra.[220] Both absent and additional modes in the spectra were attributed to molecular–metal coupling, which suggested that intimate details of the metal–molecule interface might be unveiled from this type of measurements. Along this line, IETS was recently used to understand the changes in a molecule–metal contact with benzendithiol (BDT) attached to gold electrodes in a STM break junction setup.[221] Two modes were identified: a 14 mV mode (due to either oscillation of BDT with respect to the gold electrodes or to gold–gold bonds in the contact) and modes between 0.1–0.2 eV (due to vibrations of the benzene ring). These modes changed with displacement of the STM tip and this was used to demonstrate that strain was applied at the molecule–electrode contact when stretching or compressing the junction.

In an attempt to perform both STM and optical spectroscopy on the same molecule, STM has been combined with tip enhanced Raman spectroscopy (TERS).[222–224] These types of experiments allow not only chemical identification of the molecules adsorbed on a surface, but also information about adsorption configuration and chemical bonding in or between molecules. In particular for copper phthalocyanine (CuPc) on Ag(111), up to eight vibrational modes were identified and assigned *via* DFT calculations.[224] Further progress in STM

and IETS includes the observation of spin splitting of individual vibronic states in neutral and charged magnesium porphines in a magnetic field of up to 9 T.[225] These types of studies may help unveiling the nature of the electron charge and spin coupling to molecular vibrations.

As a remark, STM studies of vibrational modes in molecules correspond to off-resonant tunnelling where the electron–phonon interaction is weak and thus the signature of vibrational modes is a small increase in the differential conductance, better seen as antisymmetric peaks in $d^2I/dV^2(V)$. However, an interesting regime appears in the strong metal–molecule regime, where the electrical conductance of the junctions is of the order of $G_0 = 2e^2/h$ (with e the elementary charge and h the Planck constant). In this case, vibrations are observed as dips (instead of peaks) in the $d^2I/dV^2(V)$ spectrum. This has been observed on chains of gold atoms,[226,227] hydrogen,[43,228] and water molecules.[229] The reader is referred to ref. 217 and 230 for a comprehensive discussion.

Other techniques that offer a similar test bed to STM experiments for the study of vibrational effects in single molecules are the cross-wire tunnel junction,[231] the nanopore technique,[232] and the MCBJ.[43,228] Albeit these experiments probe SAMs rather than single molecules, progress has been made in recent years to understand if metallic electrodes are bridged by a single molecule using conductance histograms.[43,50,228,233–235] Similar to STM studies, IETS has been used in these experimental set-ups to explain changes in molecular conformation, contact geometry, and metal–molecule bonding in *e.g.* alkanedithiol molecular junctions (Fig. 21).[50]

Altogether, state-of-the-art IETS in single-molecule junctions can be used to identify the presence of molecules as well as to infer the geometry at the molecule–metal interface. Similar to optical spectroscopy, where selection rules predict the observation of certain vibrational modes, intense theoretical work is being carried out to develop such selection rules in IETS.[220,236–238]

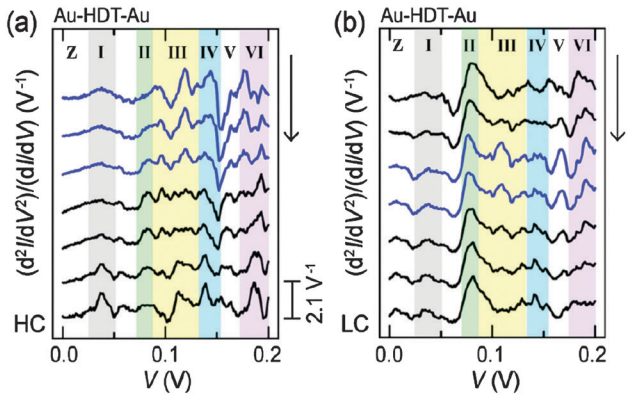

Fig. 21 IETS from a MCBJ experiment to identify hexanedithiol (HDT) conformation and geometry of contact to gold electrodes in a high conductance HC (a) and low conductance LC (b) molecular junction made.[50] The IETS spectra are measured as the metal–molecule–metal junction is stretched (arrow direction) from 0.5 Å (top) to 4.5 Å (bottom). The vibrational modes correspond to *Z*, longitudinal metal phonon; (I) Au–S stretching; (II) C–S stretching; (III) C–H rocking; (IV) C–C stretching; (V) C–H wagging; (VI) C–H scissoring. Reprinted by permission from (Y. Kim, H. Song, F. Strigl, H.-F. Pernau, T. Lee and E. Scheer, *Phys. Rev. Lett.*, 2011, **106**, 196804). Copyright (2011) by the American Physical Society.

In comparison to two terminal devices, three-terminal devices offer a new regime in electron–phonon coupling in single molecules (weak coupling). Particularly, for this case, when a gate electrode is available, vibrational effects induce peculiar features on the current transport through the junction. This is discussed in further detail in Section 4.4.

4.3. Switching

A particularly attractive type of molecular (electrical) functionality is that of a switch, where the transmolecular conductance can be changed between two or more states. The reason for this is that transistors, the core of modern computing, are ultimately operated as switches where the conductance is efficiently turned on and off by a gate electrode. Single molecule switches might thus, in principle, be the prototypical device used to replace silicon in logic and memory elements offering the *a priori* advantage of ultra-large density integration, of the order of $\sim$1 TB cm^{-2}.

Molecules that display stable isomers are good candidates to be used as the kernel in molecular switches. Changes in molecular conductance arise from changes in their geometry, since the spatial arrangement of atoms leads to changes in several physical properties including the electronic structure of the molecule and thus in its density of states. When a molecule is placed between electrodes (Fig. 22a), the current I through it as a function of the voltage V across the device can be estimated using the Landauer formalism.[239] The device conductance is $dI/dV \propto (2e^2/h)T(E_F\text{-eV})$, where e is the elementary charge, h is Planck's constant, E_F is the electrochemical potential of the contacts and $T(E_F\text{-eV})$ is related to the molecular transmission function through the density of states in the molecule. The conductance of a molecule, directly proportional to the density of states, reflects thus the internal electronic structure of the molecule and can be switched by triggering molecular rearrangements. From an engineering point of view, the challenge is to fabricate a single molecule switch where changes in conductance are significant, ideally from zero (OFF state) to infinity (ON state).

The conductance (bi-) multi-stability of a molecular switch requires molecules with (two) several stable isomers, and the transition between isomers to be controlled by external stimuli (*e.g.* light, heat, current or electric field). Fig. 22b shows the potential landscape of a bistable molecule for its ground and excited states. The reaction coordinate axis is a physical parameter such as the intramolecular bond length or the torsion angle. The two states of the switch (state 1 and state 2) correspond to the two minima in the ground state separated by an activation barrier ΔE_{act}, much larger than the thermal energy k_BT. Switching between states can be done by bringing the molecule from state 2 to an excited state then let it relax to state 1, or by driving the molecule over the potential barrier by stimuli such as heat or the electric field.

Early studies of single-molecule switches were performed in STM setups. The first example of single molecule switch based on conformation changes of molecules was carried out in phenylene ethynylene oligomers isolated in matrices of self-assembled

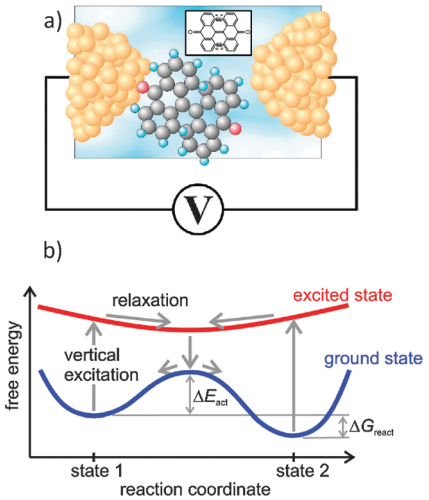

Fig. 22 Molecular switches. (a) Schematic representation of a molecular switch based on bianthrone connected to metallic electrodes. Reprinted by permission from (S. Lara-Avila, A. Danilov, V. Geskin, S. Bouzakraoui, S. Kubatkin, J. Cornil and T. Bjørnholm, *J. Phys. Chem. C*, 2010, **114**, 20686–20695). Copyright (2010) by the American Physical Society. (b) Potential energy landscape of a bistable molecular switch; bistability arises from the two local minima of molecular the ground state. On the *x* axis, a 'reaction coordinate' is physical parameter such as a distance between two atoms or a rotation angle between intramolecular bonds. Switching is realized by bringing the molecule to an excited state *via* external stimuli (*e.g.* light) or by exciting the molecule over the ground state barrier by means of heat, vibrations (*i.e.* electron–phonon coupling) or by electric-field induced barrier lowering.[239] Reprinted by permission from (van der Molen and Liljeroth. Charge transport through molecular switches. *J. Phys.: Condens. Matter*, 2010, **22**(13), 133001).

monolayers (SAM) of alkanethiolate.[29] In this work, a special protocol was used to assemble the functional molecules on an Au surface. Once the SAM is present on the Au surface, ammonium hydroxide was used to hydrolyse the acetyl group of the functional molecule, generating the thiolate or thiol that adsorbed on the Au surface at existing defect sites in the dodecane thiolate SAM. During STM imaging, the stability of the SAM contrasted with that of the phenylene ethynylene molecules, which reversibly changed the conductance state between high and low with persistence times in the range from seconds (poorly ordered SAM) to tens of hours (well ordered SAM). The origin of conductance switching was attributed to conformational changes in the molecules rather than electrostatic effects of charge transfer. This latter observation was derived from the topographic profile of the molecule, since in the high conductance state the active molecules protruded out of the SAM, while in the low conductance state their height relative to the SAM is lower.

In Section 5 we present a thorough description of how to implement molecular switches by chemical design of the molecular systems, a variety of stimuli used to trigger molecular transition and their applicability as devices. Here we highlight the importance for molecular switches, and more generally for any single-molecule device, of considering the environment for adequate modeling, design and implementation. In practice, even if the existence of two states is encoded in molecular design, the crucial operational parameters, switching voltages and the mere existence of bistability are environmentally sensitive. Strong coupling to metallic contacts or electrostatic interaction with the substrate might be detrimental for the operation of single molecule switches. An example of the environment effect on the electronic structure of the molecule is the case of bianthrone on aluminum oxide substrates connected to silver electrodes.[240] Bianthrone is a sterically hindered compound that exists in the form of two nonplanar isomers, and the transition can be triggered by light or heat (Fig. 22a). In ref. 240, a single bianthrone switch revealed persistent switching of the electric conductance at low temperatures, which was associated with molecular isomerization events from spectroscopic d*I*/d*V* measurements. Based on the statistics of switching events, authors were able to measure the activation energy of the process to be of the order of 35–90 meV. This value was an order of magnitude lower to that measured for free bianthrone ($\Delta E_{act} \sim 0.9$ eV) and the explanation for this is that, when placed in contact with silver and on high permittivity dielectric, one of the bianthrone isomers acquires negative charge that shifts molecular geometry (due to image forces in the substrate) which in turns lowers the transition barrier. This result showed that the impact of the environment on the performance of single molecules devices, and in particular, the profound changes induced in the energy landscape of the molecular kernel by highly polarizable substrates and metallic electrodes.

Single-molecule photoswitches are other examples where it has been shown that coupling to electrodes can modify or even suppress bistability. In this type of devices, if the molecule is strongly coupled to metallic contacts, the photo-excited electron and hole may escape the molecule before triggering the transition between isomers. One route to prevent this is to decouple the molecular switch from the metal as it was demonstrated in a single molecule photoswitch with the dihydroazulene (DHA) and vinylheptafulvene (VHF) isomers.[241,242] Despite the inherent bistability of this molecule, authors in ref. 241 observed reversible light-triggered conductance switching only three times when the molecule is strongly coupled to metallic electrodes. In a follow-up work by the same group, authors showed an enhanced performance of the DHA/VHF switch in which the weak coupling to electrodes was ensured by incorporating $-SCH_3$ end groups into the molecule.[242] The result was that conductance through both DHA (high resistivity) and VHF (low resistivity) (Fig. 23a) could be systematically reversed, achieving a high conductance state (ON) by light, and the reverse (OFF) by heat and electric field (Fig. 23b).

4.4. Coulomb blockade

Compared to measurements of transport in a two-terminal configuration, studies of transport in molecules in a three terminal configuration offer significantly more information about the molecular system. In addition to source and drain electrodes, a third (gate) electrode is capacitively coupled to the molecule, allowing tuning of the energy level spectrum of the molecule with respect to the probing source and drain electrodes (Fig. 24). That is, the gate can tune the internal energy levels of

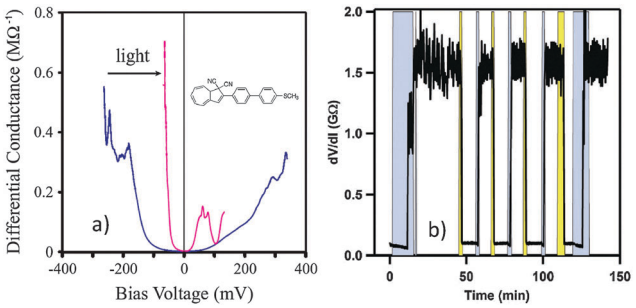

Fig. 23 Single molecule photo switch measurements. (a) The effect of shining light on molecular junction which incorporates dihydroazulene (DHA)/vinylheptafulvene (VHF) (inset) weakly coupled to electrodes leads to a reduced transport gap (zero-current area) observed in the d*I*/d*V*(*V*) plot. (b) A series of ON–OFF switching events in the same device. The highlighted background indicates the time intervals when the sample was illuminated with light (yellow) or the bias voltage was increased to 80 mV (blue) to reset the switch. The differential resistance d*V*/d*I* was taken at the bias voltage *V* = 25 mV for both ON (VHF) and OFF (DHA) states. Taken with permission of authors of ref. 242 S. L. Broman, *et al.* Dihydroazulene Photoswitch operating in Sequential Tunneling Regime: Synthesis and Single-Molecule Junction Studies. *Adv. Funct. Mater.*, 2012.

the molecule (redox or charge states) to be in resonance with the Fermi level in the leads. If the coupling between metallic electrodes and the molecules is weak, electrons tunnel one by one in and out of the molecular "island" (or quantum dot, QD) due to electrostatic repulsion when the molecule is occupied by one electron, that is, due to Coulomb blockade. These types of devices are called (molecular) single electron transistors (SET's), and the sequential tunnelling of electrons on and off the island reveals itself as steps in the *IV* curve of the SET whenever the resonant condition is met.[243] Solid-state SETs have been extensively studied for decades and a classic review of single electron transistors can be found in ref. 244.

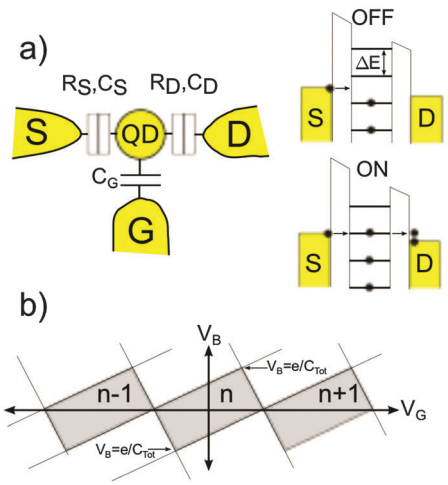

Fig. 24 Electron transport in quantum dots (QD) (three-terminal configuration). (a) In addition to source and grain electrodes, a three-terminal measurement incorporates a third electrode capacitively coupled to the quantum dot (molecule), allowing tuning of its energy level spectrum with respect to source and drain electrodes. (b) Stability diagram of a quantum dot in the coulomb blockade regime shows the charge state of the dot *n*.

Conditions to observe single-electron tunnelling are (1) thermal energy must be below the charging energy $k_BT < e^2/C$ (with k_B the Boltzmann constant, T temperature and C the self-capacitance of the island) and (2) the (tunnelling) resistance between source/drain electrodes and the island should be greater than the resistance quantum $R_T > h/2e^2$. Smaller islands (small self capacitance) lead to greater charging energies, potentially enabling observation of single electron tunnelling at room temperature. The conductivity of a single electron transistor (SET) as a function of source–drain bias as well as gate electrode potential is typically displayed in a so-called stability diagram (Fig. 24), where the differential conductance of the SET is colour coded and the greyed rhomboids (also called Coulomb diamonds) represent charging states of the dot.

Sufficiently small islands can be fabricated using state-of-the-art lithography (*e.g.* e-beam lithography).[245] A practical disadvantage of these top-down fabricated devices is the challenge to make several of them with the exact same geometry. The lack of reproducibility on the island dimensions translates into substantial changes in the stability diagram, making large-scale integration very difficult. In this sense, SETs fabricated with semiconducting nanoparticles[246] and carbon nanotubes[247] offer better reproducibility. The use of molecules as QDs to make SETs offers several advantages. One of them is their small size (a single to a few nm), which leads to a very small self-capacitance and therefore large charging energies, enabling potential room temperature operation. Furthermore, molar amounts of identical molecules can be chemically synthesized; in principle, intra molecular tunnel barriers can be defined during chemical synthesis in order to improve reproducibility even further.[137] The chemical aspect of molecular synthesis is well developed, but the fabrication of stable nano-contacts remains a large challenge. In practice, molecular SETs are studied at low temperatures to ensure stability of the molecule–metal junction.

The first demonstration of a molecular SET involved C_{60} coupled to gold electrodes created by electro migration.[54] The gate electrode is the underlying oxidized, degenerately doped, silicon substrate. This study showed evidence for transport through a single molecule by coulomb blockade with a 150 mV gap. Additionally, two vibrational modes were observed: 33 mV due to internal vibration of C_{60} and a 5 mV mode corresponding to motion of the entire C_{60} molecule in the van der Waals potential of the gold electrodes.

Kubatkin *et al.* reported a single electron transistor with a thiol end-capped oligophenylene vinylene, OPV5, and gold contacts (Fig. 25a).[19] The device was fabricated using the angle evaporation technique in which the nanogap formation and molecule deposition by sublimation are performed in the same UHV cycle, ensuring a very clean and well-characterized system. Though the precise geometry of the junction is not well known in this experiment, weak metal molecule coupling is revealed by the observed coulomb blockade which displays eight diamonds in the stability diagram corresponding to eight different charging states of the molecule. A significant result is that the spectroscopic HOMO–LUMO gap of OPV5 has been observed to

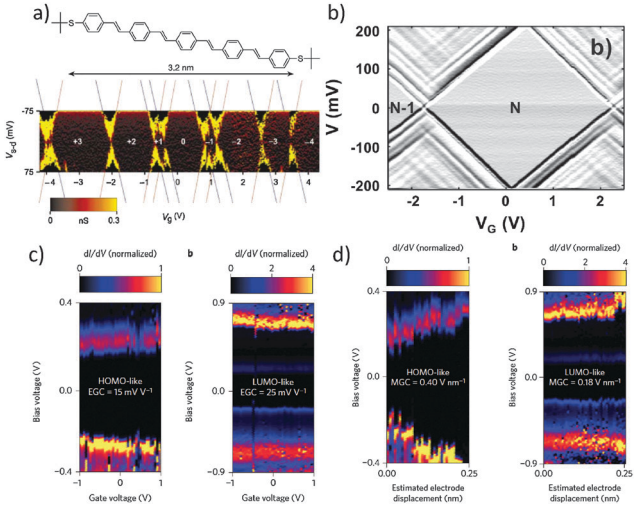

Fig. 25 Renormalization of addition energies in molecules on solid-state devices. (a, b) Stability diagram of OPV5 from two independent experiments revealed a decrease of addition energies of the molecule due to image charges (from $\Delta E_{HOMO-LUMO} \sim 2.5$ eV to $\Delta E_{HOMO-LUMO} \sim 0.2$ eV).[19,70] (b) Shows (color coded) the numerically calculated second derivative, which serves to highlight the fine structure of the excitations showing as lines running parallel to coulomb diamonds. Reprinted by permission from *Nature*, copyright (2003).[19] Reprinted by permission from John Wiley and Sons, copyright (2007).[70] The evolution of HOMO-like and LUMO like levels in thiol terminated zinc porphyrin in gateable-MCBJ experiment under electrostatic (c) and geometric control (d) confirmed renormalization effects due electrostatic environment. Under geometric control the measured renormalization of the HOMO-like level was remarkably large (0.40 V nm^{-1}). Reprinted by permission from *Nat. Nanotechnol.*, copyright (2013).[41]

be an order of magnitude lower than that in a vacuum. This renormalization was explained to be a consequence of the electrostatic environment of the molecule, which substantially modifies its electronic structure. Image charges generated by the charges in the molecule on metallic contacts and dielectric effects are postulated to be the origin of this effect.[19] Importantly, the surprisingly large renormalization of OPV5 was confirmed in an independent experiment where contacts were prepared by electromigration.[248,249] Additionally, vibronic effects were clearly observable and they manifest as lines running parallel to coulomb diamonds (Fig. 25b). Following these experimental results, more complete theoretical modelling of charging effects on the molecular electronic spectrum has been made possible.[70,240,249,250] The effect of the solid-state environment on molecules is presented in a thorough review.[251]

Recently, the effect of image charges has been confirmed in a porphyrin-type molecule using electrically gateable break junctions (Fig. 25c and d).[41,252] In this set-up, the position of the occupied and unoccupied molecular energy levels can be followed *in situ* under simultaneous mechanical and electrostatic control of the device. When increasing the electrode separation (to reduce image charge effects) an increase of the transport gap and level shifts as high as several hundreds of meV (0.40 V nm^{-1} for the HOMO-like orbital) were observed. Analysis of this large gap renormalization based on density functional theory confirms and clarifies the important role of image-charge effects due to the electrostatic environment in single-molecule junctions. The large changes in electronic properties due to minute changes in geometry explain the lack of reproducibility in numerous single-molecule experiments, and suggest the need for both electrostatic and geometric control of the molecular junction to achieve reproducible *IV* characteristics of single-molecule junctions.

Coulomb blockade effects are thus not only a curious phenomenon in single-molecule transistors, but also a very powerful tool to unveil fine details of electron transport in these nanoscopic systems.

4.5. Thermoelectric power in single-molecule junctions

When two metals bridged by a molecule experience a gradient of temperature across the molecular junction, a potential difference ΔV between the cold and the hot electrodes can be induced. Analogously to macroscopic thermoelectric effects, this potential difference results from the thermal equilibration of the free charge carriers. A fundamental difference in the single-molecule thermoelectric effect is related to the large mismatch between the discrete vibrational states of the molecules and the metallic electrodes, which considerably reduces the thermal conductivity across the molecular junction.[248] Furthermore, the discrete electronic-energy states of the molecular systems allow transport across single energy levels that cannot be easily achieved with continuous energy bands present in bulk materials. In single-molecule junctions the thermoelectric figure of merit, describing the efficiency of the thermoelectric process, can be written as:

$$ZT = \frac{S^2 G_e T}{G_{th}}$$

where S is the thermoelectric power, T is the absolute temperature, and G_e and G_{th} are the electronic and the thermal conductance, respectively. G_e and G_{th} depend on the properties of the molecules and of the materials constituting the electrodes. The ideal junction for thermopower generation would have a high electronic conductance and a low thermal exchange between the hot and cold thermodynamic reservoirs, leading to the maximum ZT value. In this sense, the relative position of the Fermi level of the electrode with respect to the HOMO and LUMO of the molecule determines the electronic transport properties across the molecular junction,[253,254] while the overlap of the vibrational states of the metal substrate and the molecule is responsible for the thermal conductance through phonon/molecular vibration conversion. The combination of these two opposite processes will determine the efficiency of thermopower generation in the molecular junction. Murphy *et al.* predicted that high ZT values can be achieved for weakly coupled molecular orbitals if their energies were of the order of $k_B T$ away from the Fermi energy of the electrodes.[255]

In recent years, there has been significant interest in both theoretical and experimental studies of single-molecule thermoelectric effects.[256] The major reason for this interest is the ability of molecular thermopower devices to generate work from heat without any moving parts. This feature gives a considerable

advantage with respect to thermodynamic machines relying on the conversion of thermal energy into motion. Furthermore, the miniaturization level that can be achieved with single-molecule devices is beyond any power-generation technology available today. Therefore the development of thermopower devices based on molecular systems will represent a fundamental technological breakthrough for the future design of nanomachines and nanoactuators.

Experimentally, low-dimensional nanostructures, such as bidimensional arrays, have been investigated to improve ZT values with respect to bulk materials.[257–265] Chen and Kanatzidis *et al.* have confirmed that quantum well superlattices are promising materials that allow independent control of the thermal conductivity through increased phonon scattering rates at the interfaces.[257,266] Tsutsui *et al.* reported direct assessment of electrical heating in a metallic nanocontact, and found asymmetric electrical heating effects in symmetric single-atom contacts.[267]

In addition, the effect of molecular length on ZT has been investigated, leading to the fundamental understanding of thermoelectric properties of single-molecule devices.[268–276] These studies indicate that an increase of molecular length results in an enhancement of the thermopower generation, but at the cost of a considerable decrease in electronic conductance. Therefore very long molecules may not be a good choice for the design of single-molecule thermoelectric devices. Ke *et al.* suggested a similar effect using density functional theory calculations.[277] In this case the increase of molecular length induces an enhancement of thermopower generation, but the decay of conductance causes an overall decreasing contribution to ZT.

As an outlook, many efforts on single-molecule thermopower focus on improving the thermoelectric conversion efficiency by *e.g.* tuning of the Fermi level of the electrodes, chemical doping, and functional-group substitution in conductive organic molecules.[265,269,278,279] Examples in this direction include that by Yee *et al.* who showed how n-type single fullerene molecules placed between metal electrodes could generate high thermopower values[265] and that of Baheti *et al. who* reported that ZT could be increased by tuning the HOMO level of the molecules by modifying the molecular structure with donor or acceptor substituents.[279]

4.6. Spintronics

Using the spin degree of freedom for information processing is widespread in consumer electronics, such as the use of the giant magnetoresistance (GMR) effect in magnetic hard-drives. The main component of a magnetic read head is a spin valve, a sandwich of magnetic–nonmagnetic–magnetic materials, which displays a significant change in resistance depending on the polarization of the magnetic materials. The resistance value can go from high to low by changing from parallel to antiparallel magnetization (Fig. 26a).

Molecular spin-based devices could lead to the ultimate integration level in magnetic memories or spin transistors with high speed and ultra low power consumption.[280,281] Additionally, being of quantum mechanical nature, manipulation and read out of the spin degree-of-freedom can lead to hardware for quantum computing applications with long coherence times in organic molecules due to the low spin orbit coupling in such systems.

Spin-electron coupling was manifested already in early studies of single-molecule transport,[53] such as the observation of Kondo resonances in single-molecule transistors. In metallic systems, the Kondo effect refers to the increase in resistance at low temperatures due to scattering of conduction electrons with magnetic impurities.[283] In the context of transport through single molecules, intermediate coupling between a metal and magnetic molecule results in a multi-peaked transmission spectrum (Fig. 26b). If the ground state of the molecule is spin 1/2 (unpaired electron), screening of the spin by conduction electrons occurs and manifests as an enhanced conductance at zero bias (Fig. 26). In seminal experiments by Park *et al.*[53] and Liang *et al.*[56] using devices fabricated by electromigration, it was observed that the Kondo resonance disappeared if the coupling to the magnetic molecule is decreased,[53] or by changing the charge in the molecule to an even number of electrons (*i.e.* $S = 0$).

In recent years, single (magnetic) molecule devices have been used as "toy" models to understand quantum phase transition through Kondo resonances. Understanding electron correlations at the molecular scale could serve as a starting point for explaining behaviour of significantly more complex, strongly correlated materials (*e.g.* high temperature superconductors). In this direction, quantum phase transition between singlet and triplet states was studied in C_{60}–gold junctions fabricated by electromigration. By using the gate electrode it was possible to promote a transition from $S = 0$ (even charge sate) to $S = 1/2$ (odd charge state).[284] Kondo resonance was used as a way to read out the phase transition. In MCBJ experiments, it was found that phase transitions can also be observed by breaking the symmetry of the molecule upon stretching.[285] In this experiment it was observed that the Kondo resonance splits into two peaks upon stretching individual cobalt complexes

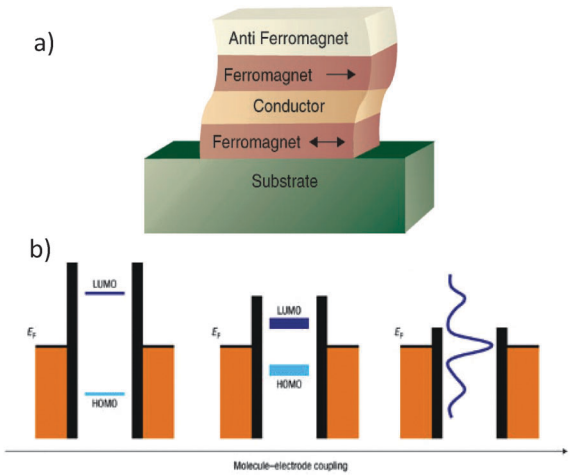

Fig. 26 Spin valve geometry (a)[281] (reprinted by permission by *Science*, copyright (2001)) and formation of Kondo resonance in quantum dots in the intermediate coupling regime (b). Reprinted by permission from *Nat. Mater.*, copyright (2008).[282]

having spin $S = 1$. The explanation is that the degeneracy of the $S = 1$ triplet ground state is broken and the $S_z = 0$ state will be lowered by a zero-field splitting energy D below the $S_z = \pm T_1$ states. Inelastic tunnelling at energies $V = TD/e$ leads to double peak resonance. In another experiment with MCBJs, the Kondo anomaly was used to detect a bias driven transition between a pseudo-singlet and a pseudo-triplet state in a cobalt complex.[286] Experimentally, these states were assigned to the absence and occurrence of a Kondo-like resonance, respectively.

In practice, careful control experiments must be designed when interpreting these types of experiments, since Kondo effects can be observed in bare gold break junctions.[287] Kondo resonances were found in 30% of the devices just after electromigration of gold, which was suggested to be caused by atomic-scale metallic grains formed during electromigration. In this sense, STM experiments have been crucial for providing insight into the nature of the Kondo effect at molecule/metal interfaces, since they allow the direct observation of the molecule and might, in principle, be less prone to artefacts.

STM experiments have shown that Kondo effects could be suppressed in a molecule by changing its conformation, since conformational changes lead to a different (enhanced or decreased) interaction of the molecule with electrons on the copper surface.[288] This was the case for TBrPP–Co (TBrPP = 5,10,15,20-tetrakis(4-bromophenyl)porphyrin). This molecule consists of a porphyrin unit with a cobalt (Co) atom caged at the center and four bromophenyl groups at the end parts. With TBrPP–Co deposited on a Cu(111) surface, a large voltage applied to the tip of the STM induced conformational changes in the molecule and switched the Kondo resonance on and off. It was also shown through Kondo resonances that the molecule metal coupling depends strongly on the adsorption site and configuration of the molecule on the metal.[289] Another interesting finding of STM experiments is that magnetism and superconductivity can coexist within manganese-phthalocyanine (MnPc) adsorbed on Pb(111) and compete to influence the ground state of a localized magnetic moment.[290]

Non-magnetic molecules are also relevant for molecular spintronics, especially when combined with ferromagnetic contacts into a spin-valve configuration. A 60% change in magnetoresistance has been reported in an STM experiment using (non-magnetic) hydrogen phthalocyanine contacted by a ferromagnetic tip of a scanning tunnelling microscope. This large magnetoresistance was explained to be the consequence of spin-dependent hybridization of molecular and electrode orbitals.[290] A similar explanation was postulated in the large magnetoresistance (80%) observed in a single C_{60} molecule transistor contacted with nickel using the electromigration technique.[291] An even larger value of magnetoresistance was reported for single-walled carbon nanotubes contacted with non-magnetic electrodes, coupled through supramolecular interactions to $TbPc_2$ single-molecule magnets.[292] In this molecule, a terbium atom is sandwiched between two phthalocyanine molecules, and the localized magnetic moments lead to magnetoresistance ratios up to 300% at temperatures less than 1 K.

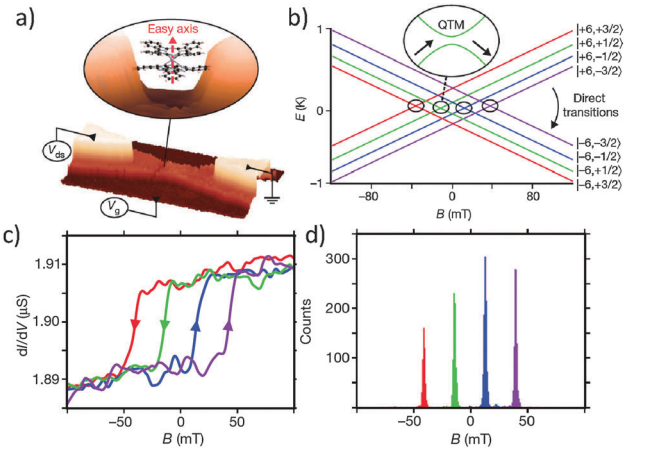

Fig. 27 (a) Geometry of the molecular spin transistor with bis(phthalocyaninato)terbium(III) (TbPc2) made by the electromigration technique. (b) Zeeman diagram presenting the energy E of the two ground states as a function of the magnetic field. (c) Abrupt jumps in the differential conductance plot as a function of the magnetic field (arrows indicate the field-sweep direction) are attributed to the switching of the Tb^{3+} magnetic moment. (d) Histogram of the switching field obtained for 11 000 field sweeps showing four preferential field values that are assigned to Quantum Tunnelling of Magnetization events. Reprinted by permission from *Nature*, copyright (2012).[294]

An interesting direction in the field of molecular spintronics is quantum informatics. In particular, the $TbPc_2$ system (Fig. 27a and b) has been widely investigated in recent years and it has been shown that it is possible to manipulate and read-out the quantum state of the Tb ion nuclear spin.[293–295] For the bis(phthalocyaninato) terbium(III) molecule, the Pc ligands form a molecular quantum dot and the anisotropic magnetic moment of the Tb^{3+} ion is coupled to the electron path only indirectly (by ferromagnetic exchange interaction). In the presence of a magnetic field, the current through the Pc ligands was used to read-out the reversal of the electronic magnetic moment carried by the Tb^{3+} ion.[295] Switching of the Tb^{3+} magnetic moment was observed as jumps in the differential conductance, which was used to extract spin relaxation times in the order of seconds (Fig. 27c and d). This work has been extended recently and authors were able to detect up to four different nuclear spin states of the Tb^{3+} ion with high fidelity (better than 69%). Another possibility to read the spin state of this molecule is to use high-Q nanomechanical resonators, which opens up a route for enabling coherent spin manipulation and quantum entanglement.[296]

4.7. Quantum interference (QI)

In view of electronic components and in analogy with semiconductor technology, one long-standing dream is to develop a single-molecule switch with a very high ON/OFF ratio operating at room temperature. One proposal to achieve this vision is to exploit quantum mechanical interference within the molecule so that the electron pathway from the source to the drain is effectively broken.[297]

Quantum interference effects have been studied in phase-coherent mesoscopic systems for decades. The classic example is an Aharonov–Bohm (AB) ring (Fig. 28, inset), where an electron wave coming from the left contact (source) splits, follows path A and B and can interfere on its way to the right contact (drain).[298] The interference pattern can go from constructive to destructive by applying a magnetic field through the ring, because the electron waves travelling through A will accumulate a different phase than those travelling through B. Overall, interference leads to oscillations in the electrical resistance as a function of the externally applied magnetic field B, with period $\Delta B = h/(eA)$, h is Planck's constant, e is the elementary charge and A is the area of the ring. In these types of experiments, quantum interference is present as long as the phase-coherence length of the electron wave is comparable to the dimensions of the ring. Inelastic scattering leads to phase-randomization and thus to the suppression of quantum mechanical effects.

In the context of molecules, benzene can be thought as the ultimate miniaturization of an AB ring. However, in order to observe AB oscillations the magnetic field required is impracticably high ($B = \Phi_0/A \sim 10$ kT). Nonetheless, interference effects can play a more subtle role in the electronic conduction through molecules by changing the intra-molecular current paths, which in turn affects profoundly the electron transmission through the molecule.

Quantum interference effects on intramolecular currents have been a matter of intense theoretical study for over a decade. Since the first proposal to use destructive interference within a molecular device to switch its conductance on and off,[297] theoretical efforts have been devoted to understand how interference effects play a role as antiresonances (decreased transmission) in the electron transmission spectrum.[299,300] Further studies have discussed the impact of electrical contacts on disturbing interference effects and it was anticipated that strong π–σ hybridization could suppress the effect of quantum interference on small molecules such as benzene, but play a less important role in larger molecules.[301]

In general, from a theoretical point of view, there is consensus that quantum interference effects on molecules modify the transmission spectrum,[302] leading to a reduction in electron transmission. Transmission can be restored by breaking the translational symmetry of the molecule,[303] and as a test-bed, acyclic cross-conjugated molecules and linearly conjugated counterparts have been suggested.[199] Beyond modifications of the transmission spectrum, quantum interference has been found to affect intra-molecular electron transfer paths, and in some instances current can flow mainly through-space rather than through molecular bonds.[304] These findings can have very important practical implications in the design of molecules suitable for single-electron devices, since they allow predicting if substituents will disrupt intramolecular current flows and overall transmission through the molecule.

In analogy with mesoscopic experiments, where phase-breaking inelastic scattering leads to suppression of quantum interference, it was suggested that electron phonon coupling in molecules (vibrational effects) can quench quantum interference effects.[306] For molecules where QI create antiresonances in the transmission spectrum, it was predicted that molecular vibrations (inelastic scattering) should destroy QI effects and thus cause an increase in molecular conductance. Stimulated by this theoretical prediction, Ballman *et al.* presented a study of interference effects in linear and cross conjugated molecules,[305] and it was indeed demonstrated an enhancement of molecular conductance with increasing temperature (Fig. 29). The authors discussed that if current in the molecules is carried by energetically quasi-degenerate electronic states, then the current plateaus observed in the *IV* characteristics due to resonant tunnelling are sensitive only to vibrational excitation

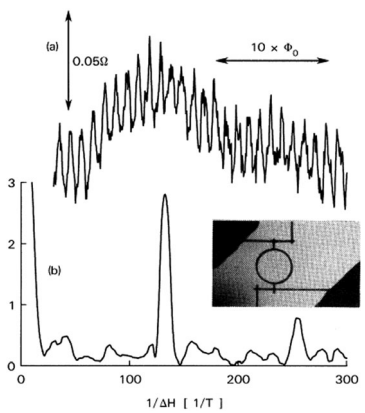

Fig. 28 (a) Magnetoresistance of an Aharonov–Bohm ring measured at T = 0,01 K. (b) Fourier power spectrum in arbitrary units showing resistance peaks at (inverse) magnetic field $1/\Delta H$ corresponding to h/e ($1/\Delta H$ = 131 T^{-1}) and $h/2e$ ($1/\Delta H$ = 260 T^{-1}). The peak at $h/2e$ is a higher order mesoscopic effect. Inset showed a photograph of the larger ring. Reprinted by permission from *Phys. Rev. Lett.* Copyright (1985) by the American Physical Society.[298]

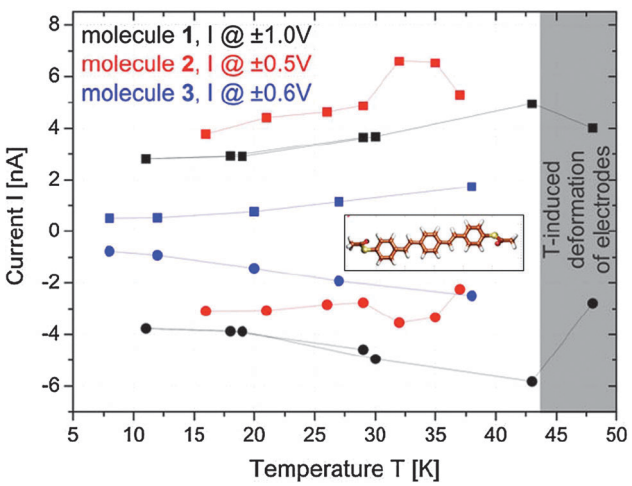

Fig. 29 A signature of decoherence due to molecular vibrations is signalled by the *increase* in molecular conductance as temperature is increased, in MCBJ experiments with cross conjugated molecular wires.[305] Reprinted by permission from *Phys. Rev. Lett.* Copyright (2012) by the American Physical Society.

and no other effects, such as thermal broadening of electronic levels. Experimentally, it is complicated to perform temperature dependence measurements on nanogaps, because the small dimensions lead to thermal structural instabilities in the molecular junction. To rule out these effects, the authors presented an experiment using a pair of gold electrodes without molecules. The temperature range of measurements of the bare nanogap conductance was limited by instabilities at $T > 22$ K, and it could be only monitored at low bias (0.2 V). In the presence of a molecule, the junction becomes more stable, and the range of temperatures can be extended up to 40 K and 1.0 V.

Experiments to confirm the theoretical predictions that interference effects modify the transmission spectra (conductance) through single molecules have recently been performed.[197,307–310] These experiments involve conductance measurements on molecules that have been designed and synthesized with or without substituents to enable or avoid QI effects. In a room temperature AFM experiment,[307] Aradhya *et al.* showed that thiol end-capped *para*-stilbene and its *meta*-(symmetry-broken) counter part display indeed significantly different conductance.[307] Only *para*-stilbene showed a measurable current while the *meta*-stilbene, expected to display low transmission due to interference effects, showed a conductance two orders of magnitude smaller. Another conducting AFM experiment by Guédon *et al.* showed evidence for transmission anti-resonance in a multi-molecular junction of linear and cross conjugated molecules, in which a conductance two orders of magnitude lower compared to that of the linearly conjugated molecule was measured.[197] As expected, the cross-conjugated molecule showed a dip in the differential conductance close to zero-bias (anti-resonance). Quantum interference effects were also suggested as the cause for suppressed conductance in a single *meta*-coupled benzene ring compared to *para*-coupled benzene.[308] Similarly, low-bias conductance through a single *meta*-OPV3 molecule is one order of magnitude smaller than through a *para*-OPV3.[309]

In summary, the vision of demonstrating a high performance QI molecular switch is still to be materialized. Nonetheless, studies of QI effects in molecules have contributed to our understanding of electronic transmission through single-molecule devices. This knowledge can be eventually used to assist the design and synthesis of molecules where substituents added to the molecular structure enhance the operation of single-molecule devices based on physical phenomena other than QI.

5. Molecular switches

In view of future applications, one of the most promising functionalities of a single-molecule device is that of a bi- or multi-stable element (*i.e.* switch). After all, the core of digital electronics, the silicon-based transistor, is a switch in which its electrical conductance can be turned on and off (with very high ON/OFF ratio) by an additional electrode (*i.e.* gate). Molecular switches might find application in ultra-low power, high-density molecular memories and multi-valued logic processors.

Molecular switches have been widely studied in solution, but the study of single molecules at the surface increases the complexity of the systems and the associated experimental challenges, considering that the local environment of the molecule at the surface is drastically different in bulk solution. In the following section we review some of the molecular switches that have been employed in molecular electronic devices, including photochromic and electrochemical switches.

5.1. Photochromic molecular switches: using light to trigger electronic properties of molecules

Molecular photoswitches are molecular systems in which the excited state can undergo reversible photoisomerization, leading to a new high-energy isomer state that cannot decay spontaneously through electronic transitions to the ground state.[311–314] For the high-energy isomer, several characteristics, such as absorption and fluorescence properties, refractive index, crystal structure, hydrophobicity, magnetic properties, and electric conductivity may differ from that of the precursor in the ground state.[315–342]

The increased interest in molecular photo-switches rises from the complementary field of organic electronics. The impressive improvement of electron mobility in organic conducting materials has suggested the possibility of using photo-switches to build single-molecule electronic transistors, able to perform logical operations and data storage in very small volumes.[343,344]

During recent years, several examples of photochromic molecular electronic switches have been demonstrated on the single-molecule level.[345–352] Sensitive experimental techniques, such as fluorescence spectroscopy and SERS, can provide information on photochromic transitions at the single-molecule level, and the potential of single-molecule electronic switches in applications such as ultra-high density optical memory units has been demonstrated.[317,353,354] Also, photo-switching of electrical transport properties based on photochromic transitions has been proposed as a fundamental concept for future design of molecular electronic circuits,[355] organic light-emitting devices,[356,357] and molecular machines.[313,358–360]

The first observation of this phenomenon can be attributed to Tsujioka and Irie, who demonstrated switching of the electrical current in solid film devices by photoisomerization of diarylethene derivatives.[361] This pioneering work, originally based on micrometer length scale measurements of multiple molecules, established the basis for the subsequent development of single-molecule photo-switches based on photochromic transitions. Specifically for this molecular system, since the ionization potentials of the two states of diarylethene are similar, the difference in electrical conductivity between different isomers can be attributed to the change in mobility of charge carriers across the molecule.[362] He *et al.* studied the electronic changes caused by light-induced isomerization of a photochromic molecule between an open state (that absorbs in the UV to become closed) and a closed state (that absorbs in the visible to become open).[363]

The switching of diarylethene conductivity upon photoisomerization has also been probed at the single-molecule

level.[364] The change in conductivity between the two photo-isomers is dependent on the molecular structure, and can reach more than two orders of magnitude. In the case of diarylethene molecules, the huge difference can be attributed to the considerable change in molecular geometry between the two isomers. This change is accompanied by the rearrangement of covalent bonds. The reproducibility in the switching molecules promotes or disrupts the conjugation of π-electrons across the molecule, bridging the probing electrodes. Exploiting these particular properties, the electric conductivity of different photo-isomers of single diarylethene molecules has been studied, and experimental results were comparable to theoretical calculations.[363,365–370] In these experiments, when the high-energy isomer is deactivated by irradiation with a specific wavelength, the molecules lose their π-conjugation and become isolators (OFF state). In the OFF state, the resistance is three orders of magnitude higher, and therefore the photo-isomerization of the molecule induces a jump in resistance that can be directly attributed to the change in the conformation of the switching molecule. Following this concept, the current switching in different diarylethene molecules has been demonstrated to be reversible.[365] Recently, single-molecule switches, based on the photo-isomerization of dihydroazulene (DHA) to vinylheptafulvene (VHF), have been developed (Fig. 30).[241,242] The reproducibility and robustness of this molecule in single molecule transport measurements has been demonstrated by more than 20 "ON–OFF" cycles. By analysing the experimental conductance data, the authors of this report concluded that electric transport through both DHA (high resistivity) and VHF (low resistivity) isomers occurs by sequential tunnelling.

In addition to the experimental study of molecular switches, theoretical simulations are very useful for the interpretation and design of single-molecule electronic switches. The electrical transport properties across diarylperfluorocyclopentene nanowire have been theoretically investigated using density functional theory and Green's function method.[367,369]

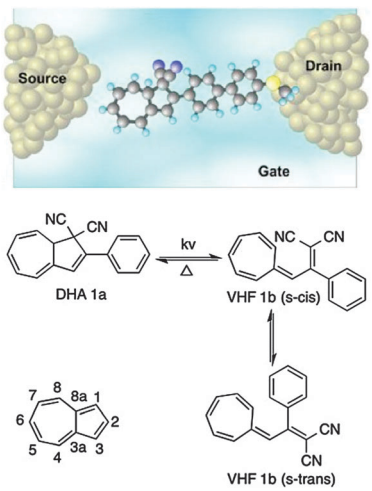

Fig. 30 Dihydroazulene (DHA 1a)/vinylheptafulvene (VHF 1b) photo-/thermoswitch. A schematic representation of the sample geometry of a molecule anchored to one electrode in a silver nanogap. Reprinted by permission from John Wiley and Sons, copyright (2012).[242]

The affinity of thiol-groups for noble metal surfaces has been exploited to build photo-switchable devices incorporating metal nanoparticles.[371] The conductance of the two photo-isomers of diarylethene bridging Au nanoparticle networks has been studied using sulfur-based anchoring groups. The diarylethene derivatives hold thiophenol units at each end, allowing the interaction with the surface of metal nanoparticles.[371] These thiophenol moieties act as the junction, creating a conducting pathway between two metal electrodes, and hence allowing the charge carriers transport between two electrodes connected to a macroscopic power source. By measuring the conductance with alternate UV and visible light irradiation, the photo-isomerization process can be triggered and the conductivity altered by a factor of 5.[371] The integration of the device with the electrodes was facilitated by the use of metal nanoparticles as the probing units. A similar approach has been used to investigate the transport properties in two-dimensional lattices of gold nanoparticles connected with dithiol–diarylethenes molecules.[372] The gold nanoparticles were self-assembled in hexagonally ordered monolayers, and considering geometrical constraints, each interparticle junction could only hold a single or at most a few molecular bridges. This device showed a reversible photo-induced switching of the transport properties that was reproducible up to eight ON–OFF cycles.

Other types of self-assembly strategies to combine the components of single-molecule electronic devices have also been explored. Hydrophobic complexes of conjugated molecules with cyclodextrins have been used to assemble water-soluble molecular wires, able to build single-molecule junctions between metal nanoparticles.[374] Scherman *et al.* have proposed an approach that combines supramolecular chemistry with nanoparticle self-assembly to develop a photoinduced molecular switch.[373] The selective photoisomerism or photodimerization of diaminostilbene molecules can be monitored *in situ* within gold nanoparticle gaps, confined by a cucurbit[*n*]uril molecular cavity, and the size of this cavity can be tuned by choosing appropriate molecules (Fig. 31). This conceptual framework might be extended to several molecular systems and applications, and constitute a considerable advancement in the field, since it might be a way to control the local environment of the single molecules and therefore improve reproducibility in the performance of devices. Another interesting example of single-molecule electroluminescence measurements has been reported by Mayor *et al.*, using carbon nanotube tips bridged by a rod-like molecule.[375]

5.2. Electrochemically driven molecular switches

Electrochemical switching is another way to modify single-molecule systems.[376–379] The integration of organic molecules containing redox centres into complex assemblies remains challenging,[380,381] but the functional behaviour of these systems[208,382] and the ability to display resonant electron tunneling that can be reversibly controlled by the redox state of the molecule[383,384] offer exciting opportunities. The principle behind this kind of devices is based on the change in transport properties of different oxidation states of conjugated molecules.[380] When aromaticity is compromised by the

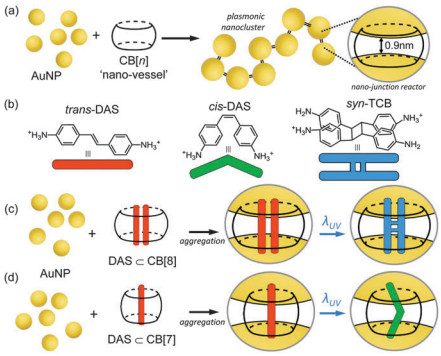

Fig. 31 (a) AuNPs (d = 60 nm) self-assemble into dendritic nanoclusters with fixed 0.9 nm interparticle separations by the action of the rigid sub-nm CB[n] linker. (b) Following UV irradiation in solution, *trans*-DAS predominantly undergoes photoisomerization into *cis*-DAS with photodimerization a minor pathway of which *syn*-TCB is a particular product. (c) When complexed within CB[8], the photoreaction of DAS is templated to yield almost exclusively *syn*-TCB, which can be measured *in situ* within the interparticle junction of the plasmonic cluster. (d) The complexation of a single DAS within the narrower CB[7] results in a templated photoisomerization reaction to *cis*-DAS. Reprinted with permission from R. W. Taylor, R. J. Coulston, F. Biedermann, S. Mahajan, J. J. Baumberg and O. A. Scherman, *Nano Lett.*, 2013, **13**, 5985–5990. Copyright 2013 American Chemical Society.[373]

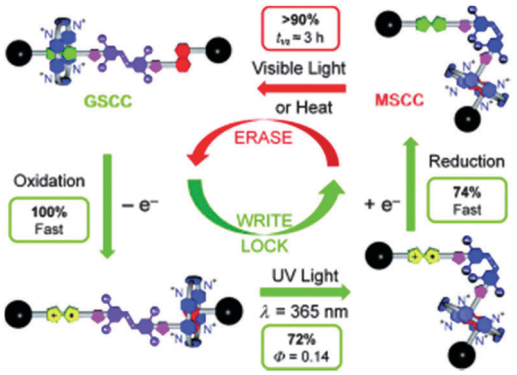

Fig. 32 Chemically and photochemically triggered memory switching cycle of the [2]rotaxane 1^{4+}. The lifetime of the MSCC can be controlled by isomerization of the TMeAB unit from its *trans* to *cis* configuration. Reprinted by permission from John Wiley and Sons, copyright (2012).[391]

incorporation or release of an electron during a redox process, the electric conductivity of the molecules changes considerably, allowing the control of the tunnelling current through the electrochemical potentials. Furthermore, some molecular systems are able to display more than one oxidation state that can be selectively reached by tuning the environmental conditions of the device. Electrochemical control of single-molecule electronic devices has been developed in the solid state *via* so-called three-terminal devices. In the liquid state, it is also possible to control the electrochemical environment, by using source and drain electrodes immersed into the solution and connected to a bipotentiostat.[173,385–388] The ability to combine electrochemistry with scanning tunnelling spectroscopy (STS) allows the investigation of electron transport through individual molecules.

Cryogenic STM has been used to control the formation of covalent bonds between conductive molecules and metal surfaces.[389] The switching between the bonded and the non-bonded state has been associated with different electric charges, and it is accompanied by a considerable change in the tunnelling current, allowing the use of these kinds of devices as molecular switches. Tao *et al.* recently reported electrochemical gating of single anthraquinone-based switches bridging two Au electrodes by using the STM break-junction technique.[390]

M. Venturi studied a photoinduced memory effect in a redox controllable bistable mechanical molecular switch in the form of a bistable [2]rotaxane.[391] The [2]rotaxane-based device can be operated as a bistable memory element under kinetic control (Fig. 32). The data can be written on the rotaxane by an oxidation stimulus, and locked by UV light irradiation. After the writing process, the oxidized species can be reduced back to the original form without losing the written data for a remarkably long time, compared to most thermodynamically controlled molecular switches. The data remain stored for hours at room temperature until the thermally activated opening of the azobenzene gate occurs spontaneously. Light irradiation not only locks the data previously recorded by oxidation, but also protects the nonoxidized rotaxanes from accidental writing. These characteristics confirm that these kinds of molecular switches could find technological applications in the future. However, in order to compete with established data storage devices, longer lifetime of the written information should be achieved.[391,392]

Rigaut *et al.* have developed molecular transport junctions that are orthogonally modulated by optical and electrochemical stimuli.[393] The molecules are placed on chemically fabricated nanogaps and display a reversible switching behaviour. These systems are able to perform basic logic operations associated with a modification of the transport properties across the electrodes. The electrochemically induced reciprocal transformations of DNA molecules adsorbed onto gold electrodes in the presence of Pb^{2+} have been used to develop molecular logic gates.[394] This work opens up new perspectives for the design of electrochemical logic devices that might be integrated into microprocessors or electronic chips.

Single molecule transport experiments have been combined with transient electrochemistry ensemble methods to investigate the correlation between molecular conductance and electron transfer rate-constants from coordinated metal centers to electrodes.[395] This kind of multi-technique approach revealed that the evaluation of electronic coupling could lead different results, depending on the experimental set up used. Therefore, the understanding of intrinsic properties at the single molecule level requires the combination of complementary experimental and theoretical approaches. Non-conjugated redox-active molecules have also been used as switches for molecular-junction conductance experiments. Liao *et al.* have inserted dithiolated tetrathiafulvalene derivatives (TTFdT) in two-dimensional nanoparticle arrays, building interlinked networks of molecular junctions.[396] Upon oxidation of the TTFdT unit the conductance of the networks increased by one order of magnitude. The system was proven to be redox-reversible, demonstrating

switching of the transport properties across the linker molecules. This specific example was based on ensemble measurement, but one can foresee the use of this kind of redox switches in single molecule experiments. Other redox active switching units, such as pyrrolo-tetrathiafulvalene, viologen, and anthraquinone have been successfully used to switch the transport properties across non-conjugated single-molecule junctions.[379,388] In some of the examples described above, the electrochemical switching of the single-molecule junctions is achieved by STM break-junction methods, demonstrating the versatility of this technique.[379,388,395]

5.3. Nanomechanical molecular switches

Mechanical forces can be also used to control the conductance switching of single-molecule junctions. The possibility to build artificial single-molecule mechanical devices has been theoretically explored.[397] However, the implementation of these systems under lab conditions still faces several challenges, which could be a major research interest in the coming years. One of the first experimental examples of a single-molecule mechanical device was introduced in 2002 by Gaub *et al.*[360] They investigated polymeric azobenzenes, which have two photo-isomers, *cis* and *trans*, with bond angles changing by 120 degrees upon isomerization. This system was able to optically lengthen and contract across the polymer backbone against an external force applied with an AFM tip, delivering measurable mechanical work.

The integration of single-molecule pulling techniques with molecular electronics has contributed to develop applications for mechanically controlled electronic devices and to improve the set of tools for studying the states of single molecules, highlighting the relevance between conformation and properties of molecules.[398–405] Tao *et al.* recently found that the conductance of individual 1,4-benzenedithiol molecules bridging two gold electrodes could be increased by more than one order of magnitude when the molecules are stretched.[221] Intramolecular reversible translocations have also been used as a proof of principle for the cyclic action of molecular machines.[406] Hihath *et al.* reported mechanically controlled molecular orbital alignment in single-molecule junctions.[221] The electromechanical properties of a 1,4′-benzenedithiol molecular junction change as the junction is stretched and compressed. It was also found that the conductance increases by more than one order of magnitude during stretching, decreasing again as the junction is compressed.

Martin *et al.* developed a gate based on tunable single-atom switches.[407] The electrostatic attraction of the source–drain electrodes leads to a deflection and rotation of the electrode tips and a change in electrode separation, which results in the reversible break and formation of a single-atom contact. Their work indicated that the details of switching depend sensitively on the nanoscale morphology and geometry of the electrode tips. The work of Kawai *et al.* further demonstrated the geometrical dependence of mechanically controlled single-molecule switches.[408]

Additionally, theoretical studies suggested a novel type of electronic switching effect, driven by the geometrical reconstruction of nanoscale graphene-based junctions.[409] The results

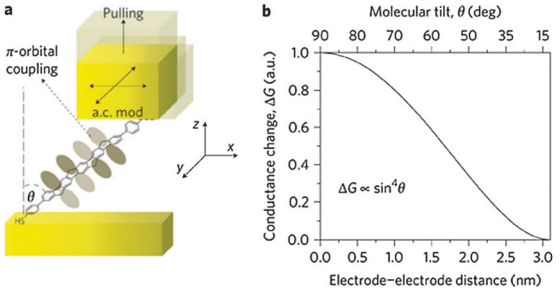

Fig. 33 (a) Schematic of lateral coupling experiment. As the two electrodes are separated or modulated within the horizontal plane, the angle θ decreases and the conductance G falls; (b) Change in conductance, ΔG, *versus* electrode–electrode distance (bottom x-axis) and θ (top x-axis). Reprinted by permission from Nature Nanotechnology (I. Diez-Perez, J. Hihath, T. Hines, Z.-S. Wang, G. Zhou, K. Mullen and N. Tao, *Nat. Nanotechnol.*, 2011, **6**, 226–231), Copyright (2011).[413]

suggested that it is possible to design modern logical switching devices or mechanophore sensors, monitored by mechanical strain and structural rearrangements. Bokes *et al.* investigated the conductance of dithioazobenzene-based optomechanical switches theoretically.[410] They demonstrated that the transport properties of different conformers were broadly similar. Venkataraman *et al.* also reported the reversible binary switching in a single-molecule contact geometry.[162] The single-molecule junction 4,4′-bipyridine–gold can be controllably switched between two conductance states by mechanical manipulation of the electrode separation. Ralph *et al.* reported a single-molecule switch with pyridine-terminated dithienylethene with conducting closed configuration and nonconducting open configuration.[411] The pyridine groups were used to link the molecules to gold electrodes to achieve relatively well-defined molecular contacts and stable conductance.

Ratner *et al.* analysed the relationship between force-extension and molecular switch behaviour, by pulling the molecules with an AFM tip.[412] Using molecular dynamics to simulate the conducting AFM tip manipulating a molecule bound to a surface, they were able to illustrate some of the fundamental structure–function relationships in this molecular switch, mapping the dominant interactions in the molecule, mediating charge transport throughout the pulling simulation. Using a similar technique, Chi *et al.* directly measured the coordinative bonding strength of single molecules.[30]

The geometry of electrode–molecule bonds can influence the transport properties at the single-molecule level, especially in conjugated systems with lateral coupling of π orbitals (Fig. 33).[413]

6. Conclusions and outlook

Single-molecule electronics seeks to incorporate single molecule components as functional elements in electronic devices. In recent years, we have seen an improved understanding in many aspects of single molecule electronics, including molecular design, molecule/contact interface engineering and the integration of this knowledge into more reproducible measurements.

In combination with the evolution of experimental techniques to address single molecules, techniques for data collection and analysis have enabled the study and further understanding of electron transport through single molecules across different experimental realizations.[159] As a result, discrepancies among several single-molecule experiments have been clarified and fundamentally new molecular devices with not-foreseen functionality have emerged.[413]

In particular for the molecule/electrode interface, one of the long-standing challenges in single-molecule electronics is controlling the precise geometry at the molecule–metal contacts, which can dominate the performance of single-molecule devices. In this direction, a variety of systematic studies, with variations in both electrode materials and in functional groups in the molecular system, have been reported. These studies have led to a more detailed understanding of a number of anchoring systems, among others: sulfur–gold bonds, amine- and phosphine-based anchors, as well as the development of new systems with multiple surface attachment sites, such as C_{60}, that are expected to be less prone to small variations in local microstructure at the interface and therefore should lead to more robust and reproducible systems.[51,170,171] Another direction is the use of 2D materials as the electrode material for contacting single molecules. The impressive evolution of 2D materials, and the recent demonstration that it is possible to contact these electrodes with molecules,[96,138] is an area of research where we foresee new breakthroughs to occur.

While the experimental methods and setups developed to probe single molecule conductivity have improved during recent years, especially in terms of faster throughput, as well as the introduction of more complex devices (*e.g.* gateable break junctions[41,252]), experimental techniques to fabricate identical single-molecule devices in a reproducible way are still sought. Furthermore, a remaining challenge is to develop ways to fabricate multiple single molecule devices in a parallel way. One way to achieve this could be by improved resolution and smaller feature sizes offered by today's state of the art nanofabrication techniques.[414,415] Another approach might be to bridge the length scale between the single molecules and the nanofabricated systems by the use of combinations of advanced self-assembly techniques with nanofabricated templates.[7] The versatility offered by the extensive repertoire of chemical synthesis might be the key to materializing large-scale single-molecule electronics.

In view of applications, our view is that two-terminal devices such as wires, rectifiers and multivalued logic single-molecule devices can be expected to emerge as the most feasible route towards molecular devices. In comparison, three-terminal molecular devices offer a complete experimental platform to perform studies of electronics at the single molecular level that could pave the road for improved understanding and increased complexity in future single-molecule devices. With the combined ingenuity and creativity possessed by researchers in this field worldwide, we are at this stage optimistic towards the future development of single molecule electronics from the research laboratory to real applications.

Acknowledgements

We would like to acknowledge Prof. S. Kubatkin, Dr. A. Roffey, Mr. J. Eklöf and Mr. M. B. Ergette for careful reading of this manuscript. Financial support from the Knut and Alice Wallenberg Foundation, Chalmers Area of Advance in Materials Science and in Nanoscience and Nanotechnology, The Knut and Alice Wallenberg foundation, as well as the ERC Starting grant project SIMONE (Grant Agreement No. 337221) is acknowledged.

Notes and references

1 M. Ratner, *Nat. Nanotechnol.*, 2013, **8**, 378–381.
2 A. Aviram and M. A. Ratner, *Chem. Phys. Lett.*, 1974, **29**, 277–283.
3 L. A. Bumm, J. J. Arnold, M. T. Cygan, T. D. Dunbar, T. P. Burgin, L. Jones, D. L. Allara, J. M. Tour and P. S. Weiss, *Science*, 1996, **271**, 1705–1707.
4 H. Song, M. A. Reed and T. Lee, *Adv. Mater.*, 2011, **23**, 1583–1608.
5 R. L. McCreery and A. J. Bergren, *Adv. Mater.*, 2009, **21**, 4303–4322.
6 T. Li, W. Hu and D. Zhu, *Adv. Mater.*, 2010, **22**, 286–300.
7 T. A. Gschneidtner, Y. A. Diaz Fernandez and K. Moth-Poulsen, *J. Mater. Chem. C*, 2013, **1**, 7127–7133.
8 D. Xiang, H. Jeong, T. Lee and D. Mayer, *Adv. Mater.*, 2013, **25**, 4845–4867.
9 N. Darwish, M. N. Paddon-Row and J. J. Gooding, *Acc. Chem. Res.*, 2014, **47**, 385–395.
10 S. Guo, J. M. Artes and I. Diez-Perez, *Electrochim. Acta*, 2013, **110**, 741–753.
11 M. Kiguchi and S. Kaneko, *Phys. Chem. Chem. Phys.*, 2013, **15**, 2253–2267.
12 M. Tsutsui and M. Taniguchi, *Sensors*, 2012, **12**, 7259–7298.
13 X. Guo and C. Nuckolls, *J. Mater. Chem.*, 2009, **19**, 5470–5473.
14 H. B. Akkerman and B. de Boer, *J. Phys.: Condens. Matter*, 2008, **20**, 013001.
15 M. A. Reed, C. Zhou, C. J. Muller, T. P. Burgin and J. M. Tour, *Science*, 1997, **278**, 252–254.
16 A. F. Morpurgo, C. M. Marcus and D. B. Robinson, *Appl. Phys. Lett.*, 1999, **74**, 2084–2086.
17 H. Park, A. K. L. Lim, A. P. Alivisatos, J. Park and P. L. McEuen, *Appl. Phys. Lett.*, 1999, **75**, 301–303.
18 A. Bezryadin, C. Dekker and G. Schmid, *Appl. Phys. Lett.*, 1997, **71**, 1273–1275.
19 S. Kubatkin, A. Danilov, M. Hjort, J. Cornil, J.-L. Bredas, N. Stuhr-Hansen, P. Hedegard and T. Bjornholm, *Nature*, 2003, **425**, 698–701.
20 X. D. Cui, A. Primak, X. Zarate, J. Tomfohr, O. F. Sankey, A. L. Moore, T. A. Moore, D. Gust, G. Harris and S. M. Lindsay, *Science*, 2001, **294**, 571–574.
21 S. R. Nicewarner-Peña, R. G. Freeman, B. D. Reiss, L. He, D. J. Peña, I. D. Walton, R. Cromer, C. D. Keating and M. J. Natan, *Science*, 2001, **294**, 137–141.

22 L. Qin, S. Park, L. Huang and C. A. Mirkin, *Science*, 2005, **309**, 113–115.
23 A. Hatzor and P. S. Weiss, *Science*, 2001, **291**, 1019–1020.
24 T. Dadosh, Y. Gordin, R. Krahne, I. Khivrich, D. Mahalu, V. Frydman, J. Sperling, A. Yacoby and I. Bar-Joseph, *Nature*, 2005, **436**, 677–680.
25 C. Joachim, J. K. Gimzewski, R. R. Schlittler and C. Chavy, *Phys. Rev. Lett.*, 1995, **74**, 2102–2105.
26 J. K. Gimzewski and C. Joachim, *Science*, 1999, **283**, 1683–1688.
27 L. E. Scullion, E. Leary, S. J. Higgins and R. J. Nichols, *J. Phys.: Condens. Matter*, 2012, **24**, 164211.
28 F.-R. F. Fan, J. Yang, L. Cai, D. W. Price, S. M. Dirk, D. V. Kosynkin, Y. Yao, A. M. Rawlett, J. M. Tour and A. J. Bard, *J. Am. Chem. Soc.*, 2002, **124**, 5550–5560.
29 Z. J. Donhauser, B. A. Mantooth, K. F. Kelly, L. A. Bumm, J. D. Monnell, J. J. Stapleton, D. W. Price, A. M. Rawlett, D. L. Allara, J. M. Tour and P. S. Weiss, *Science*, 2001, **292**, 2303–2307.
30 X. Hao, N. Zhu, T. Gschneidtner, E. Ö. Jonsson, J. Zhang, K. Moth-Poulsen, H. Wang, K. S. Thygesen, K. W. Jacobsen, J. Ulstrup and Q. Chi, *Nat. Commun.*, 2013, **4**, 2121.
31 E. Wierzbinski, X. Yin, K. Werling and D. H. Waldeck, *J. Phys. Chem. B*, 2012, **117**, 4431–4441.
32 M. Frei, S. V. Aradhya, M. Koentopp, M. S. Hybertsen and L. Venkataraman, *Nano Lett.*, 2011, **11**, 1518–1523.
33 J. Frommer, *Angew. Chem.*, 1992, **104**, 1325–1357.
34 B. Xu and N. J. Tao, *Science*, 2003, **301**, 1221–1223.
35 X. Y. Xiao, B. Q. Xu and N. J. Tao, *Nano Lett.*, 2004, **4**, 267–271.
36 W. Haiss, H. van Zalinge, D. Bethell, J. Ulstrup, D. J. Schiffrin and R. J. Nichols, *Faraday Discuss.*, 2006, **131**, 253–264.
37 T. Niu and A. Li, *J. Phys. Chem. Lett.*, 2013, **4**, 4095–4102.
38 J. Moreland, J. W. Ekin, L. F. Goodrich, T. E. Capobianco, A. F. Clark, J. Kwo, M. Hong and S. H. Liou, *Phys. Rev. B: Condens. Matter Mater. Phys.*, 1987, **35**, 8856–8857.
39 C. J. Muller, J. M. van Ruitenbeek and L. J. de Jongh, *Phys. C*, 1992, **191**, 485–504.
40 C. J. Muller, B. J. Vleeming, M. A. Reed, J. J. S. Lamba, R. Hara, L. J. II and J. M. Tour, *Nanotechnology*, 1996, **7**, 409.
41 M. L. Perrin, C. J. O. Verzijl, C. A. Martin, A. J. Shaikh, R. Eelkema, H. van EschJan, J. M. van Ruitenbeek, J. M. Thijssen, H. S. J. van der Zant and D. Dulic, *Nat. Nanotechnol.*, 2013, **8**, 282–287.
42 C. Kergueris, J. P. Bourgoin, S. Palacin, D. Esteve, C. Urbina, M. Magoga and C. Joachim, *Phys. Rev. B: Condens. Matter Mater. Phys.*, 1999, **59**, 12505–12513.
43 R. H. M. Smit, Y. Noat, C. Untiedt, N. D. Lang, M. C. van Hemert and J. M. van Ruitenbeek, *Nature*, 2002, **419**, 906–909.
44 J. Reichert, R. Ochs, D. Beckmann, H. B. Weber, M. Mayor and H. v. Löhneysen, *Phys. Rev. Lett.*, 2002, **88**, 176804.
45 D. Djukic and J. M. van Ruitenbeek, *Nano Lett.*, 2006, **6**, 789–793.
46 E. Lortscher, B. Gotsmann, Y. Lee, L. Yu, C. Rettner and H. Riel, *ACS Nano*, 2012, **6**, 4931–4939.
47 M. Ruben, A. Landa, E. Loertscher, H. Riel, M. Mayor, H. Goerls, H. B. Weber, A. Arnold and F. Evers, *Small*, 2008, **4**, 2229–2235.
48 W. Hong, H. Li, S.-X. Liu, Y. Fu, J. Li, V. Kaliginedi, S. Decurtins and T. Wandlowski, *J. Am. Chem. Soc.*, 2012, **134**, 19425–19431.
49 J.-H. Tian, B. Liu, X. Li, Z.-L. Yang, B. Ren, S.-T. Wu, N. Tao and Z.-Q. Tian, *J. Am. Chem. Soc.*, 2006, **128**, 14748–14749.
50 Y. Kim, H. Song, F. Strigl, H.-F. Pernau, T. Lee and E. Scheer, *Phys. Rev. Lett.*, 2011, **106**, 196804.
51 J. Fock, J. K. Sorensen, E. Lortscher, T. Vosch, C. A. Martin, H. Riel, K. Kilsa, T. Bjornholm and H. van der Zant, *Phys. Chem. Chem. Phys.*, 2011, **13**, 14325–14332.
52 M. Galperin, A. Nitzan and M. A. Ratner, *Phys. Rev. B: Condens. Matter Mater. Phys.*, 2006, **74**, 075326.
53 J. Park, A. N. Pasupathy, J. I. Goldsmith, C. Chang, Y. Yaish, J. R. Petta, M. Rinkoski, J. P. Sethna, H. D. Abruna, P. L. McEuen and D. C. Ralph, *Nature*, 2002, **417**, 722–725.
54 H. Park, J. Park, A. K. L. Lim, E. H. Anderson, A. P. Alivisatos and P. L. McEuen, *Nature*, 2000, **407**, 57–60.
55 L. H. Yu and D. Natelson, *Nano Lett.*, 2003, **4**, 79–83.
56 W. Liang, M. P. Shores, M. Bockrath, J. R. Long and H. Park, *Nature*, 2002, **417**, 725–729.
57 H. Yu, Y. Luo, K. Beverly, J. F. Stoddart, H.-R. Tseng and J. R. Heath, *Angew. Chem., Int. Ed.*, 2003, **42**, 5706–5711.
58 H. S. J. van der Zant, Y.-V. Kervennic, M. Poot, K. O'Neill, Z. de Groot, J. M. Thijssen, H. B. Heersche, N. Stuhr-Hansen, T. Bjornholm, D. Vanmaekelbergh, C. A. van Walree and L. W. Jenneskens, *Faraday Discuss.*, 2006, **131**, 347–356.
59 D. E. Johnston, D. R. Strachan and A. T. C. Johnson, *Nano Lett.*, 2007, **7**, 2774–2777.
60 C. Tao, W. G. Cullen and E. D. Williams, *Science*, 2010, **328**, 736–740.
61 D. Stöffler, S. Fostner, P. Grütter and R. Hoffmann-Vogel, *Phys. Rev. B: Condens. Matter Mater. Phys.*, 2012, **85**, 033404.
62 S. Girod, J.-L. Bubendorff, F. Montaigne, L. Simon, D. Lacour and M. Hehn, *Nanotechnology*, 2012, **23**, 365302.
63 B. Gao, E. A. Osorio, K. B. Gaven and H. S. J. v. d. Zant, *Nanotechnology*, 2009, **20**, 415207.
64 T. Kizuka, S. Kodama and T. Matsuda, *Nanotechnology*, 2010, **21**, 495706.
65 D. R. Ward, N. K. Grady, C. S. Levin, N. J. Halas, Y. Wu, P. Nordlander and D. Natelson, *Nano Lett.*, 2007, **7**, 1396–1400.
66 D. R. Ward, N. J. Halas, J. W. Ciszek, J. M. Tour, Y. Wu, P. Nordlander and D. Natelson, *Nano Lett.*, 2008, **8**, 919–924.
67 D. R. Ward, F. Huser, F. Pauly, J. C. Cuevas and D. Natelson, *Nat. Nanotechnol.*, 2010, **5**, 732–736.
68 H. Song, Y. Kim, J. Ku, Y. H. Jang, H. Jeong and T. Lee, *Appl. Phys. Lett.*, 2009, **94**, 103110.
69 A. S. Zyazin, J. W. G. van den Berg, E. A. Osorio, H. S. J. van der Zant, N. P. Konstantinidis, M. Leijnse, M. R. Wegewijs,

F. May, W. Hofstetter, C. Danieli and A. Cornia, *Nano Lett.*, 2010, **10**, 3307–3311.
70 E. A. Osorio, K. O'Neill, N. Stuhr-Hansen, O. F. Nielsen, T. Bjørnholm and H. S. J. van der Zant, *Adv. Mater.*, 2007, **19**, 281–285.
71 Y. Naitoh, T. Ohata, R. Matsushita, E. Okawa, M. Horikawa, M. Oyama, M. Mukaida, D. F. Wang, M. Kiguchi, K. Tsukagoshi and T. Ishida, *ACS Appl. Mater. Interfaces*, 2013, **5**, 12869–12875.
72 D. Natelson, Y. Li and J. B. Herzog, *Phys. Chem. Chem. Phys.*, 2013, **15**, 5262–5275.
73 M. Rahimi and A. Troisi, *Phys. Rev. B: Condens. Matter Mater. Phys.*, 2009, **79**, 113413.
74 H. Song, Y. Kim, H. Jeong, M. A. Reed and T. Lee, *J. Phys. Chem. C*, 2010, **114**, 20431–20435.
75 F. Prins, A. J. Shaikh, J. H. van Esch, R. Eelkema and H. S. J. van der Zant, *Phys. Chem. Chem. Phys.*, 2011, **13**, 14297–14301.
76 T. Jain, Q. Tang, T. Bjørnholm and K. Nørgaard, *Acc. Chem. Res.*, 2013, **47**, 2–11.
77 Y. D. Fernandez, L. Sun, T. Gschneidtner and K. Moth-Poulsen, *APL Mater.*, 2014, **2**, 010702.
78 I. Amlani, A. M. Rawlett, L. A. Nagahara and R. K. Tsui, *Appl. Phys. Lett.*, 2002, **80**, 2761–2763.
79 J.-S. Na, J. Ayres, K. L. Chandra, C. Chu, C. B. Gorman and G. N. Parsons, *Nanotechnology*, 2007, **18**, 035203.
80 T. Jain, F. Westerlund, E. Johnson, K. Moth-Poulsen and T. Bjørnholm, *ACS Nano*, 2009, **3**, 828–834.
81 J. P. Hermes, F. Sander, T. Peterle, C. Cioffi, P. Ringler, T. Pfohl and M. Mayor, *Small*, 2011, **7**, 920–929.
82 A. Guttman, D. Mahalu, J. Sperling, E. Cohen-Hoshen and I. Bar-Joseph, *Appl. Phys. Lett.*, 2011, **99**, 063113.
83 S. Karmakar, S. Kumar, P. Marzo, E. Primiceri, R. Di Corato, R. Rinaldi, P. G. Cozzi, A. P. Bramanti and G. Maruccio, *Nanoscale*, 2012, **4**, 2311–2316.
84 S. Kober, G. Gotesman and R. Naaman, *J. Phys. Chem. Lett.*, 2013, **4**, 2041–2045.
85 K. Du, C. R. Knutson, E. Glogowski, K. D. McCarthy, R. Shenhar, V. M. Rotello, M. T. Tuominen, T. Emrick, T. P. Russell and A. D. Dinsmore, *Small*, 2009, **5**, 1974–1977.
86 F. Yaghmaie, J. Fleck, A. Gusman and R. Prohaska, *Microelectron. Eng.*, 2010, **87**, 2629–2632.
87 T. Jain, S. Lara-Avila, Y.-V. Kervennic, K. Moth-Poulsen, K. Nørgaard, S. Kubatkin and T. Bjørnholm, *ACS Nano*, 2012, **6**, 3861–3867.
88 Y. Cui, M. T. Björk, J. A. Liddle, C. Sönnichsen, B. Boussert and A. P. Alivisatos, *Nano Lett.*, 2004, **4**, 1093–1098.
89 C. Kuemin, L. Nowack, L. Bozano, N. D. Spencer and H. Wolf, *Adv. Funct. Mater.*, 2012, **22**, 702–708.
90 A. Rey, G. Billardon, E. Lortscher, K. Moth-Poulsen, N. Stuhr-Hansen, H. Wolf, T. Bjornholm, A. Stemmer and H. Riel, *Nanoscale*, 2013, **5**, 8680–8688.
91 S. Gómez-Graña, F. Hubert, F. Testard, A. Guerrero-Martínez, I. Grillo, L. M. Liz-Marzán and O. Spalla, *Langmuir*, 2011, **28**, 1453–1459.
92 X. Guo, J. P. Small, J. E. Klare, Y. Wang, M. S. Purewal, I. W. Tam, B. H. Hong, R. Caldwell, L. Huang, S. O'Brien, J. Yan, R. Breslow, S. J. Wind, J. Hone, P. Kim and C. Nuckolls, *Science*, 2006, **311**, 356–359.
93 J. Lefebvre, M. Radosavljević and A. T. Johnson, *Appl. Phys. Lett.*, 2000, **76**, 3828–3830.
94 E. P. De Poortere, H. L. Stormer, L. M. Huang, S. J. Wind, S. O'Brien, M. Huang and J. Hone, *Appl. Phys. Lett.*, 2006, **88**, 143124.
95 D. Wei, Y. Liu, L. Cao, Y. Wang, H. Zhang and G. Yu, *Nano Lett.*, 2008, **8**, 1625–1630.
96 F. Prins, A. Barreiro, J. W. Ruitenberg, J. S. Seldenthuis, N. Aliaga-Alcalde, L. M. K. Vandersypen and H. S. J. van der Zant, *Nano Lett.*, 2011, **11**, 4607–4611.
97 Y. Cao, S. Dong, S. Liu, L. He, L. Gan, X. Yu, M. L. Steigerwald, X. Wu, Z. Liu and X. Guo, *Angew. Chem., Int. Ed.*, 2012, **51**, 12228–12232.
98 L. Jiang, J. Gao, E. Wang, H. Li, Z. Wang, W. Hu and L. Jiang, *Adv. Mater.*, 2008, **20**, 2735–2740.
99 A. Ongaro, F. Griffin, L. Nagle, D. Iacopino, R. Eritja and D. Fitzmaurice, *Adv. Mater.*, 2004, **16**, 1799–1803.
100 C. R. Martin and L. A. Baker, *Science*, 2005, **309**, 67–68.
101 S. Liu, J. B. H. Tok and Z. Bao, *Nano Lett.*, 2005, **5**, 1071–1076.
102 X. Chen, S. Yeganeh, L. Qin, S. Li, C. Xue, A. B. Braunschweig, G. C. Schatz, M. A. Ratner and C. A. Mirkin, *Nano Lett.*, 2009, **9**, 3974–3979.
103 M. J. Banholzer, L. Qin, J. E. Millstone, K. D. Osberg and C. A. Mirkin, *Nat. Protoc.*, 2009, **4**, 838–848.
104 K. D. Osberg, A. L. Schmucker, A. J. Senesi and C. A. Mirkin, *Nano Lett.*, 2011, **11**, 820–824.
105 K. D. Osberg, M. Rycenga, N. Harris, A. L. Schmucker, M. R. Langille, G. C. Schatz and C. A. Mirkin, *Nano Lett.*, 2012, **12**, 3828–3832.
106 C. A. Mirkin, R. L. Letsinger, R. C. Mucic and J. J. Storhoff, *Nature*, 1996, **382**, 607–609.
107 J. Zheng, P. E. Constantinou, C. Micheel, A. P. Alivisatos, R. A. Kiehl and N. C. Seeman, *Nano Lett.*, 2006, **6**, 1502–1504.
108 J. J. Storhoff and C. A. Mirkin, *Chem. Rev.*, 1999, **99**, 1849–1862.
109 E. Dujardin, L.-B. Hsin, C. R. C. Wang and S. Mann, *Chem. Commun.*, 2001, 1264–1265, DOI: 10.039/B102319P.
110 S. Y. Park, A. K. R. Lytton-Jean, B. Lee, S. Weigand, G. C. Schatz and C. A. Mirkin, *Nature*, 2008, **451**, 553–556.
111 H. Yao, C. Yi, C.-H. Tzang, J. Zhu and M. Yang, *Nanotechnology*, 2007, **18**, 015102.
112 M. M. Maye, M. T. Kumara, D. Nykypanchuk, W. B. Sherman and O. Gang, *Nat. Nanotechnol.*, 2010, **5**, 116–120.
113 M. P. Busson, B. Rolly, B. Stout, N. Bonod, E. Larquet, A. Polman and S. Bidault, *Nano Lett.*, 2011, **11**, 5060–5065.
114 G. P. Acuna, M. Bucher, I. H. Stein, C. Steinhauer, A. Kuzyk, P. Holzmeister, R. Schreiber, A. Moroz, F. D. Stefani, T. Liedl, F. C. Simmel and P. Tinnefeld, *ACS Nano*, 2012, **6**, 3189–3195.

115 C. Chi, F. Vargas-Lara, A. V. Tkachenko, F. W. Starr and O. Gang, *ACS Nano*, 2012, **6**, 6793–6802.
116 X. Lan, Z. Chen, B.-J. Liu, B. Ren, J. Henzie and Q. Wang, *Small*, 2013, **9**, 2308–2315.
117 F. Vargas Lara and F. W. Starr, *Soft Matter*, 2011, **7**, 2085–2093.
118 M.-P. Valignat, O. Theodoly, J. C. Crocker, W. B. Russel and P. M. Chaikin, *Proc. Natl. Acad. Sci. U. S. A.*, 2005, **102**, 4225–4229.
119 L. Lermusiaux, A. Sereda, B. Portier, E. Larquet and S. Bidault, *ACS Nano*, 2012, **6**, 10992–10998.
120 D.-K. Lim, K.-S. Jeon, J.-H. Hwang, H. Kim, S. Kwon, Y. D. Suh and J.-M. Nam, *Nat. Nanotechnol.*, 2011, **6**, 452–460.
121 A. Y. Kasumov, M. Kociak, S. Guéron, B. Reulet, V. T. Volkov, D. V. Klinov and H. Bouchiat, *Science*, 2001, **291**, 280–282.
122 D. Porath, A. Bezryadin, S. de Vries and C. Dekker, *Nature*, 2000, **403**, 635–638.
123 X. Guo, A. A. Gorodetsky, J. Hone, J. K. Barton and C. Nuckolls, *Nat. Nanotechnol.*, 2008, **3**, 163–167.
124 J. M. Krans, C. J. Muller, I. K. Yanson, T. C. M. Govaert, R. Hesper and J. M. van Ruitenbeek, *Phys. Rev. B: Condens. Matter Mater. Phys.*, 1993, **48**, 14721–14724.
125 X. Li, J. He, J. Hihath, B. Xu, S. M. Lindsay and N. Tao, *J. Am. Chem. Soc.*, 2006, **128**, 2135–2141.
126 Y. S. Park, A. C. Whalley, M. Kamenetska, M. L. Steigerwald, M. S. Hybertsen, C. Nuckolls and L. Venkataraman, *J. Am. Chem. Soc.*, 2007, **129**, 15768–15769.
127 M. Kamenetska, M. Koentopp, A. C. Whalley, Y. S. Park, M. L. Steigerwald, C. Nuckolls, M. S. Hybertsen and L. Venkataraman, *Phys. Rev. Lett.*, 2009, **102**, 126803.
128 C. R. Arroyo, E. Leary, A. Castellanos-Gomez, G. Rubio-Bollinger, M. T. Gonzalez and N. Agrait, *J. Am. Chem. Soc.*, 2011, **133**, 14313–14319.
129 M. T. Gonzalez, A. Diaz, E. Leary, R. Garcia, M. A. Herranz, G. Rubio-Bollinger, N. Martin and N. Agrait, *J. Am. Chem. Soc.*, 2013, **135**, 5420–5426.
130 H. Häkkinen, *Nat. Chem.*, 2012, **4**, 443–455.
131 L. Venkataraman, J. E. Klare, I. W. Tam, C. Nuckolls, M. S. Hybertsen and M. L. Steigerwald, *Nano Lett.*, 2006, **6**, 458–462.
132 M. S. Hybertsen, L. Venkataraman, J. E. Klare, A. C. Whalley, M. L. Steigerwald and C. Nuckolls, *J. Phys.: Condens. Matter*, 2008, **20**, 374115.
133 A. Mishchenko, L. A. Zotti, D. Vonlanthen, M. Bürkle, F. Pauly, J. C. Cuevas, M. Mayor and T. Wandlowski, *J. Am. Chem. Soc.*, 2010, **133**, 184–187.
134 L. A. Zotti, T. Kirchner, J.-C. Cuevas, F. Pauly, T. Huhn, E. Scheer and A. Erbe, *Small*, 2010, **6**, 1529–1535.
135 F. Chen, X. Li, J. Hihath, Z. Huang and N. Tao, *J. Am. Chem. Soc.*, 2006, **128**, 15874–15881.
136 C. Jia and X. Guo, *Chem. Soc. Rev.*, 2013, **42**, 5642–5660.
137 A. Danilov, S. Kubatkin, S. Kafanov, P. Hedegard, N. Stuhr-Hansen, K. Moth-Poulsen and T. Bjornholm, *Nano Lett.*, 2008, **8**, 1–5.
138 Y. Cao, S. Dong, S. Liu, Z. Liu and X. Guo, *Angew. Chem., Int. Ed.*, 2013, **52**, 3906–3910.
139 X.-Y. Zhou, Z.-L. Peng, Y.-Y. Sun, L.-N. Wang, Z.-J. Niu and X.-S. Zhou, *Nanotechnology*, 2013, **24**, 465204.
140 M. Kamenetska, S. Y. Quek, A. C. Whalley, M. L. Steigerwald, H. J. Choi, S. G. Louie, C. Nuckolls, M. S. Hybertsen, J. B. Neaton and L. Venkataraman, *J. Am. Chem. Soc.*, 2010, **132**, 6817–6821.
141 S. V. Aradhya and L. Venkataraman, *Nat. Nanotechnol.*, 2013, **8**, 399–410.
142 L. Venkataraman, J. E. Klare, C. Nuckolls, M. S. Hybertsen and M. L. Steigerwald, *Nature*, 2006, **442**, 904–907.
143 E. A. Osorio, K. Moth-Poulsen, H. S. J. van der Zant, J. Paaske, P. Hedegard, K. Flensberg, J. Bendix and T. Bjoernholm, *Nano Lett.*, 2010, **10**, 105–110.
144 J. C. Love, L. A. Estroff, J. K. Kriebel, R. G. Nuzzo and G. M. Whitesides, *Chem. Rev.*, 2005, **105**, 1103–1170.
145 A. Ulman, *Chem. Rev.*, 1996, **96**, 1533–1554.
146 C. Li, I. Pobelov, T. Wandlowski, A. Bagrets, A. Arnold and F. Evers, *J. Am. Chem. Soc.*, 2007, **130**, 318–326.
147 S. K. Yee, J. Sun, P. Darancet, T. D. Tilley, A. Majumdar, J. B. Neaton and R. A. Segalman, *ACS Nano*, 2011, **5**, 9256–9263.
148 R. S. Klausen, J. R. Widawsky, T. A. Su, H. Li, Q. Chen, M. L. Steigerwald, L. Venkataraman and C. Nuckolls, *Chem. Sci.*, 2014, **5**, 1561–1564.
149 S. Yasuda, S. Yoshida, J. Sasaki, Y. Okutsu, T. Nakamura, A. Taninaka, O. Takeuchi and H. Shigekawa, *J. Am. Chem. Soc.*, 2006, **128**, 7746–7747.
150 B. Kim, J. M. Beebe, Y. Jun, X. Y. Zhu and C. D. Frisbie, *J. Am. Chem. Soc.*, 2006, **128**, 4970–4971.
151 B. Xu, X. Xiao and N. J. Tao, *J. Am. Chem. Soc.*, 2003, **125**, 16164–16165.
152 C. A. Martin, D. Ding, J. K. Sørensen, T. Bjørnholm, J. M. van Ruitenbeek and H. S. J. van der Zant, *J. Am. Chem. Soc.*, 2008, **130**, 13198–13199.
153 E. Leary, M. T. González, C. van der Pol, M. R. Bryce, S. Filippone, N. Martín, G. Rubio-Bollinger and N. s. Agraït, *Nano Lett.*, 2011, **11**, 2236–2241.
154 E. Lörtscher, V. Geskin, B. Gotsmann, J. Fock, J. K. Sørensen, T. Bjørnholm, J. Cornil, H. S. J. van der Zant and H. Riel, *Small*, 2013, **9**, 332.
155 W. Chen, J. R. Widawsky, H. Vázquez, S. T. Schneebeli, M. S. Hybertsen, R. Breslow and L. Venkataraman, *J. Am. Chem. Soc.*, 2011, **133**, 17160–17163.
156 W.-k. Paik, S. Han, W. Shin and Y. Kim, *Langmuir*, 2003, **19**, 4211–4216.
157 E. Lortscher, C. J. Cho, M. Mayor, M. Tschudy, C. Rettner and H. Riel, *ChemPhysChem*, 2011, **12**, 1677–1682.
158 W. Hong, D. Z. Manrique, P. Moreno-García, M. Gulcur, A. Mishchenko, C. J. Lambert, M. R. Bryce and T. Wandlowski, *J. Am. Chem. Soc.*, 2011, **134**, 2292–2304.
159 J. Hihath and N. Tao, *Semicond. Sci. Technol.*, 2014, **29**, 054007.
160 F. Pauly, J. K. Viljas, J. C. Cuevas and G. Schön, *Phys. Rev. B: Condens. Matter Mater. Phys.*, 2008, **77**, 155312.

161 D. R. Jones and A. Troisi, *J. Phys. Chem. C*, 2007, **111**, 14567–14573.
162 S. Y. Quek, M. Kamenetska, M. L. Steigerwald, H. J. Choi, S. G. Louie, M. S. Hybertsen, J. B. Neaton and L. Venkataraman, *Nat. Nanotechnol.*, 2009, **4**, 230–234.
163 A. Bagrets, A. Arnold and F. Evers, *J. Am. Chem. Soc.*, 2008, **130**, 9013–9018.
164 S. Guo, J. Hihath, I. Díez-Pérez and N. Tao, *J. Am. Chem. Soc.*, 2011, **133**, 19189–19197.
165 P. Chinwangso, A. C. Jamison and T. R. Lee, *Acc. Chem. Res.*, 2011, **44**, 511–519.
166 X. Chen, A. B. Braunschweig, M. J. Wiester, S. Yeganeh, M. A. Ratner and C. A. Mirkin, *Angew. Chem., Int. Ed.*, 2009, **48**, 5178–5181.
167 J. P. Hermes, F. Sander, U. Fluch, T. Peterle, D. Thompson, R. Urbani, T. Pfohl and M. Mayor, *J. Am. Chem. Soc.*, 2012, **134**, 14674–14677.
168 Z. L. Cheng, R. Skouta, H. Vazquez, J. R. Widawsky, S. Schneebeli, W. Chen, M. S. Hybertsen, R. Breslow and L. Venkataraman, *Nat. Nanotechnol.*, 2011, **6**, 353–357.
169 E. Lortscher, *Nat. Nanotechnol.*, 2013, **8**, 381–384.
170 C. Rogero, J. I. Pascual, J. Gómez-Herrero and A. M. Baró, *J. Chem. Phys.*, 2002, **116**, 832–836.
171 E. Lörtscher, V. Geskin, B. Gotsmann, J. Fock, J. K. Sørensen, T. Bjørnholm, J. Cornil, H. S. J. van der Zant and H. Riel, *Small*, 2013, **9**, 209–214.
172 T. Böhler, A. Edtbauer and E. Scheer, *Phys. Rev. B: Condens. Matter Mater. Phys.*, 2007, **76**, 125432.
173 T. Hines, I. Diez-Perez, H. Nakamura, T. Shimazaki, Y. Asai and N. Tao, *J. Am. Chem. Soc.*, 2013, **135**, 3319–3322.
174 L. Luo, S. H. Choi and C. D. Frisbie, *Chem. Mater.*, 2011, **23**, 631–645.
175 W. Hu, J. Jiang, H. Nakashima, Y. Luo, Y. Kashimura, K.-Q. Chen, Z. Shuai, K. Furukawa, W. Lu, Y. Liu, D. Zhu and K. Torimitsu, *Phys. Rev. Lett.*, 2006, **96**, 027801.
176 V. Kaliginedi, P. Moreno-García, H. Valkenier, W. Hong, V. M. García-Suárez, P. Buiter, J. L. H. Otten, J. C. Hummelen, C. J. Lambert and T. Wandlowski, *J. Am. Chem. Soc.*, 2012, **134**, 5262–5275.
177 R. Huber, M. T. González, S. Wu, M. Langer, S. Grunder, V. Horhoiu, M. Mayor, M. R. Bryce, C. Wang, R. Jitchati, C. Schönenberger and M. Calame, *J. Am. Chem. Soc.*, 2007, **130**, 1080–1084.
178 S. H. Choi, B. Kim and C. D. Frisbie, *Science*, 2008, **320**, 1482–1486.
179 A. E. Nel, L. Madler, D. Velegol, T. Xia, E. M. V. Hoek, P. Somasundaran, F. Klaessig, V. Castranova and M. Thompson, *Nat. Mater.*, 2009, **8**, 543–557.
180 S. H. Choi, C. Risko, M. C. R. Delgado, B. Kim, J.-L. Brédas and C. D. Frisbie, *J. Am. Chem. Soc.*, 2010, **132**, 4358–4368.
181 L. Luo and C. D. Frisbie, *J. Am. Chem. Soc.*, 2010, **132**, 8854–8855.
182 B. Q. Xu, X. L. Li, X. Y. Xiao, H. Sakaguchi and N. J. Tao, *Nano Lett.*, 2005, **5**, 1491–1495.
183 P. Moreno-García, M. Gulcur, D. Z. Manrique, T. Pope, W. Hong, V. Kaliginedi, C. Huang, A. S. Batsanov, M. R. Bryce, C. Lambert and T. Wandlowski, *J. Am. Chem. Soc.*, 2013, **135**, 12228–12240.
184 X. Zhao, C. Huang, M. Gulcur, A. S. Batsanov, M. Baghernejad, W. Hong, M. R. Bryce and T. Wandlowski, *Chem. Mater.*, 2013, **25**, 4340–4347.
185 S.-Y. Jang, P. Reddy, A. Majumdar and R. A. Segalman, *Nano Lett.*, 2006, **6**, 2362–2367.
186 Z. Li, I. Pobelov, B. Han, T. Wandlowski, A. Błaszczyk and M. Mayor, *Nanotechnology*, 2007, **18**, 044018.
187 N. Tuccitto, V. Ferri, M. Cavazzini, S. Quici, G. Zhavnerko, A. Licciardello and M. A. Rampi, *Nat. Mater.*, 2009, **8**, 41–46.
188 S. Rigaut, *Dalton Trans.*, 2013, **42**, 15859–15863.
189 S. Ho Choi, B. Kim and C. D. Frisbie, *Science*, 2008, **320**, 1482–1486.
190 H. Valkenier, C. M. Guédon, T. Markussen, K. S. Thygesen, S. J. van der Molen and J. C. Hummelen, *Phys. Chem. Chem. Phys.*, 2014, **16**, 653–662.
191 Q. Lu, K. Liu, H. Zhang, Z. Du, X. Wang and F. Wang, *ACS Nano*, 2009, **3**, 3861–3868.
192 L. Cui, B. Liu, D. Vonlanthen, M. Mayor, Y. Fu, J.-F. Li and T. Wandlowski, *J. Am. Chem. Soc.*, 2011, **133**, 7332–7335.
193 C. A. van Walree, V. E. M. Kaats-Richters, S. J. Veen, B. Wieczorek, J. H. van der Wiel and B. C. van der Wiel, *Eur. J. Org. Chem.*, 2004, 3046–3056.
194 A. B. Ricks, G. C. Solomon, M. T. Colvin, A. M. Scott, K. Chen, M. A. Ratner and M. R. Wasielewski, *J. Am. Chem. Soc.*, 2010, **132**, 15427–15434.
195 M. Zarea, D. Powell, N. Renaud, M. R. Wasielewski and M. A. Ratner, *J. Phys. Chem. B*, 2013, **117**, 1010–1020.
196 J. P. Bergfield, G. C. Solomon, C. A. Stafford and M. A. Ratner, *Nano Lett.*, 2011, **11**, 2759–2764.
197 C. M. Guédon, H. Valkenier, T. Markussen, K. S. Thygesen, J. C. Hummelen and S. J. van der Molen, *Nat. Nanotechnol.*, 2012, **7**, 305–309.
198 D. Fracasso, H. Valkenier, J. C. Hummelen, G. C. Solomon and R. C. Chiechi, *J. Am. Chem. Soc.*, 2011, **133**, 9556–9563.
199 G. C. Solomon, D. Q. Andrews, R. H. Goldsmith, T. Hansen, M. R. Wasielewski, R. P. Van Duyne and M. A. Ratner, *J. Am. Chem. Soc.*, 2008, **130**, 17301–17308.
200 N. P. Guisinger, M. E. Greene, R. Basu, A. S. Baluch and M. C. Hersam, *Nano Lett.*, 2003, **4**, 55–59.
201 A. Sen and C.-C. Kaun, *ACS Nano*, 2010, **4**, 6404–6408.
202 Y. Cho, W. Y. Kim and K. S. Kim, *J. Phys. Chem. A*, 2009, **113**, 4100–4104.
203 A. Aviram, C. Joachim and M. Pomerantz, *Chem. Phys. Lett.*, 1988, **146**, 490–495.
204 M. Pomerantz, A. Aviram, R. A. McCorkle, L. Li and A. G. Schrott, *Science*, 1992, **255**, 1115–1118.
205 G. J. Ashwell, W. D. Tyrrell and A. J. Whittam, *J. Am. Chem. Soc.*, 2004, **126**, 7102–7110.
206 I. Diez-Perez, J. Hihath, Y. Lee, L. Yu, L. Adamska, M. A. Kozhushner, I. I. Oleynik and N. Tao, *Nat. Chem.*, 2009, **1**, 635–641.
207 J. M. van Ruitenbeek, A. Alvarez, I. Pineyro, C. Grahmann, P. Joyez, M. H. Devoret, D. Esteve and C. Urbina, *Rev. Sci. Instrum.*, 1996, **67**, 108–111.

208 J. Chen, M. A. Reed, A. M. Rawlett and J. M. Tour, *Science*, 1999, **286**, 1550–1552.
209 M. Elbing, R. Ochs, M. Koentopp, M. Fischer, C. von Hänisch, F. Weigend, F. Evers, H. B. Weber and M. Mayor, *Proc. Natl. Acad. Sci. U. S. A.*, 2005, **102**, 8815–8820.
210 S. E. Kubatkin, A. V. Danilov, A. L. Bogdanov, H. Olin and T. Claeson, *Appl. Phys. Lett.*, 1998, **73**, 3604–3606.
211 A. V. Danilov, P. Hedegård, D. S. Golubev, T. Bjørnholm and S. E. Kubatkin, *Nano Lett.*, 2008, **8**, 2393–2398.
212 X. Lu, M. Grobis, K. H. Khoo, S. G. Louie and M. F. Crommie, *Phys. Rev. Lett.*, 2003, **90**, 096802.
213 X. Lu, M. Grobis, K. H. Khoo, S. G. Louie and M. F. Crommie, *Phys. Rev. B: Condens. Matter Mater. Phys.*, 2004, **70**, 115418.
214 M. A. Reed, *Mater. Today*, 2008, **11**, 46–50.
215 R. C. Jaklevic and J. Lambe, *Phys. Rev. Lett.*, 1966, **17**, 1139–1140.
216 *Tunneling Spectroscopy: Capabilities, Applications, and New Techniques*, ed. P. K. Hansma, Plenum Press, 1982.
217 C. Schirm, M. Matt, F. Pauly, J. C. Cuevas, P. Nielaba and E. Scheer, *Nat. Nanotechnol.*, 2013, **8**, 645–648.
218 B. C. Stipe, M. A. Rezaei and W. Ho, *Phys. Rev. Lett.*, 1998, **81**, 1263–1266.
219 X. H. Qiu, G. V. Nazin and W. Ho, *Phys. Rev. Lett.*, 2004, **92**, 206102.
220 K. Morgenstern, *J. Phys.: Condens. Matter*, 2011, **23**, 484007.
221 C. Bruot, J. Hihath and N. Tao, *Nat. Nanotechnol.*, 2012, **7**, 35–40.
222 J. Steidtner and B. Pettinger, *Rev. Sci. Instrum.*, 2007, **78**, 103104.
223 J. Steidtner and B. Pettinger, *Phys. Rev. Lett.*, 2008, **100**, 236101.
224 N. Jiang, E. T. Foley, J. M. Klingsporn, M. D. Sonntag, N. A. Valley, J. A. Dieringer, T. Seideman, G. C. Schatz, M. C. Hersam and R. P. Van Duyne, *Nano Lett.*, 2012, **12**, 5061–5067.
225 U. Ham and W. Ho, *Phys. Rev. Lett.*, 2012, **108**, 106803.
226 N. Agrait, C. Untiedt, G. Rubio-Bollinger and S. Vieira, *Phys. Rev. Lett.*, 2002, **88**, 216803.
227 C. Untiedt, G. Rubio Bollinger, S. Vieira and N. Agraït, *Phys. Rev. B: Condens. Matter Mater. Phys.*, 2000, **62**, 9962–9965.
228 D. Djukic, K. S. Thygesen, C. Untiedt, R. H. M. Smit, K. W. Jacobsen and J. M. van Ruitenbeek, *Phys. Rev. B: Condens. Matter Mater. Phys.*, 2005, **71**, 161402.
229 O. Tal, M. Krieger, B. Leerink and J. M. van Ruitenbeek, *Phys. Rev. Lett.*, 2008, **100**, 196804.
230 E. Scheer, P. Konrad, C. Bacca, A. Mayer-Gindner, H. von Lohneysen, M. Hafner and J. C. Cuevas, *Phys. Rev. B: Condens. Matter Mater. Phys.*, 2006, **74**, 205430.
231 J. G. Kushmerick, J. Lazorcik, C. H. Patterson, R. Shashidhar, D. S. Seferos and G. C. Bazan, *Nano Lett.*, 2004, **4**, 639–642.
232 W. Wang, T. Lee, I. Kretzschmar and M. A. Reed, *Nano Lett.*, 2004, **4**, 643–646.
233 J. Hihath, C. Bruot, H. Nakamura, Y. Asai, I. Díez-Pérez, Y. Lee, L. Yu and N. Tao, *ACS Nano*, 2011, **5**, 8331–8339.
234 Y. Kim, T. J. Hellmuth, M. Bürkle, F. Pauly and E. Scheer, *ACS Nano*, 2011, **5**, 4104–4111.
235 Y. Kim, A. Garcia-Lekue, D. Sysoiev, T. Frederiksen, U. Groth and E. Scheer, *Phys. Rev. Lett.*, 2012, **109**, 226801.
236 A. Troisi and M. A. Ratner, *J. Chem. Phys.*, 2006, **125**, 214709.
237 J. M. Beebe, H. J. Moore, T. R. Lee and J. G. Kushmerick, *Nano Lett.*, 2007, **7**, 1364–1368.
238 S. R. Burema and M.-L. Bocquet, *J. Phys. Chem. Lett.*, 2012, **3**, 3007–3011.
239 S. J. v. d. Molen and P. Liljeroth, *J. Phys.: Condens. Matter*, 2010, **22**, 133001.
240 S. Lara-Avila, A. Danilov, V. Geskin, S. Bouzakraoui, S. Kubatkin, J. Cornil and T. Bjornholm, *J. Phys. Chem. C*, 2010, **114**, 20686–20695.
241 S. Lara-Avila, A. V. Danilov, S. E. Kubatkin, S. L. Broman, C. R. Parker and M. B. Nielsen, *J. Phys. Chem. C*, 2011, **115**, 18372–18377.
242 S. L. Broman, S. Lara-Avila, C. L. Thisted, A. D. Bond, S. Kubatkin, A. Danilov and M. B. Nielsen, *Adv. Funct. Mater.*, 2012, **22**, 4249–4258.
243 T. A. Fulton and G. J. Dolan, *Phys. Rev. Lett.*, 1987, **59**, 109–112.
244 M. Kastner, *Rev. Mod. Phys.*, 1992, **64**, 849.
245 D. C. Ralph, C. T. Black and M. Tinkham, *Phys. Rev. Lett.*, 1997, **78**, 4087–4090.
246 D. L. Klein, R. Roth, A. K. L. Lim, A. P. Alivisatos and P. L. McEuen, *Nature*, 1997, **389**, 699–701.
247 S. J. Tans, M. H. Devoret, R. J. A. Groeneveld and C. Dekker, *Nature*, 1998, **394**, 761–764.
248 R. Y. Wang, R. A. Segalman and A. Majumdar, *Appl. Phys. Lett.*, 2006, **89**, 173113.
249 P. Hedegård and T. Bjørnholm, *Chem. Phys.*, 2005, **319**, 350–359.
250 K. Kaasbjerg and K. Flensberg, *Nano Lett.*, 2008, **8**, 3809–3814.
251 K. Moth-Poulsen and T. Bjornholm, *Nat. Nanotechnol.*, 2009, **4**, 551–556.
252 A. R. Champagne, A. N. Pasupathy and D. C. Ralph, *Nano Lett.*, 2005, **5**, 305–308.
253 J. P. Bergfield, M. A. Solis and C. A. Stafford, *ACS Nano*, 2010, **4**, 5314–5320.
254 C. M. Finch, V. M. Garcia-Suarez and C. J. Lambert, *Phys. Rev. B: Condens. Matter Mater. Phys.*, 2009, **79**, 033405.
255 P. Murphy, S. Mukerjee and J. Moore, *Phys. Rev. B: Condens. Matter Mater. Phys.*, 2008, **78**, 161406.
256 P. Reddy, S.-Y. Jang, R. A. Segalman and A. Majumdar, *Science*, 2007, **315**, 1568–1571.
257 C. J. Vineis, A. Shakouri, A. Majumdar and M. G. Kanatzidis, *Adv. Mater.*, 2010, **22**, 3970–3980.
258 L. D. Hicks and M. S. Dresselhaus, *Phys. Rev. B: Condens. Matter Mater. Phys.*, 1993, **47**, 12727–12731.
259 T. C. Harman, P. J. Taylor, M. P. Walsh and B. E. LaForge, *Science*, 2002, **297**, 2229–2232.
260 V. M. Garcia-Suarez, R. Ferradas and J. Ferrer, *Phys. Rev. B: Condens. Matter Mater. Phys.*, 2013, **88**, 235417.

261 S. Hershfield, K. A. Muttalib and B. J. Nartowt, *Phys. Rev. B: Condens. Matter Mater. Phys.*, 2013, **88**, 085426.
262 W. Lee, K. Kim, W. Jeong, L. A. Zotti, F. Pauly, J. C. Cuevas and P. Reddy, *Nature*, 2013, **498**, 209–212.
263 Y. Wang, J. Liu, J. Zhou and R. Yang, *J. Phys. Chem. C*, 2013, **117**, 24716–24725.
264 Z.-H. Wu, H.-Q. Xie and Y.-B. Zhai, *Appl. Phys. Lett.*, 2013, **103**, 243901.
265 S. K. Yee, J. A. Malen, A. Majumdar and R. A. Segalman, *Nano Lett.*, 2011, **11**, 4089–4094.
266 G. Chen, *Phys. Rev. B: Condens. Matter Mater. Phys.*, 1998, **57**, 14958–14973.
267 M. Tsutsui, T. Kawai and M. Taniguchi, *Sci. Rep.*, 2012, **2**, 1–11.
268 J. A. Malen, P. Doak, K. Baheti, T. D. Tilley, R. A. Segalman and A. Majumdar, *Nano Lett.*, 2009, **9**, 1164–1169.
269 J. A. Malen, P. Doak, K. Baheti, T. D. Tilley, A. Majumdar and R. A. Segalman, *Nano Lett.*, 2009, **9**, 3406–3412.
270 Y. Asai, *J. Phys.: Condens. Matter*, 2013, **25**, 155305.
271 Z. Golsanamlou, S. Izadi Vishkayi, M. Bagheri Tagani and H. Rahimpour Soleimani, *Chem. Phys. Lett.*, 2014, **594**, 51–57.
272 O. Karlstrom, M. Strange and G. C. Solomon, *J. Chem. Phys.*, 2014, **140**, 044315.
273 F. Pauly, J. K. Viljas and J. C. Cuevas, *Phys. Rev. B: Condens. Matter Mater. Phys.*, 2008, **78**, 035315.
274 A. Tan, J. Balachandran, B. D. Dunietz, S.-Y. Jang, V. Gavini and P. Reddy, *Appl. Phys. Lett.*, 2012, **101**, 243107.
275 A. Tan, J. Balachandran, S. Sadat, V. Gavini, B. D. Dunietz, S.-Y. Jang and P. Reddy, *J. Am. Chem. Soc.*, 2011, **133**, 8838–8841.
276 J. R. Widawsky, W. Chen, H. Vazquez, T. Kim, R. Breslow, M. S. Hybertsen and L. Venkataraman, *Nano Lett.*, 2013, **13**, 2889–2894.
277 S.-H. Ke, W. Yang, S. Curtarolo and H. U. Baranger, *Nano Lett.*, 2009, **9**, 1011–1014.
278 W. Liang, A. I. Hochbaum, M. Fardy, O. Rabin, M. Zhang and P. Yang, *Nano Lett.*, 2009, **9**, 1689–1693.
279 K. Baheti, J. A. Malen, P. Doak, P. Reddy, S.-Y. Jang, T. D. Tilley, A. Majumdar and R. A. Segalman, *Nano Lett.*, 2008, **8**, 715–719.
280 S. Datta and B. Das, *Appl. Phys. Lett.*, 1990, **56**, 665–667.
281 S. A. Wolf, D. D. Awschalom, R. A. Buhrman, J. M. Daughton, S. von Molnar, M. L. Roukes, A. Y. Chtchelkanova and D. M. Treger, *Science*, 2001, **294**, 1488–1495.
282 L. Bogani and W. Wernsdorfer, *Nat. Mater.*, 2008, **7**, 179–186.
283 J. Kondo, *Prog. Theor. Phys.*, 1964, **32**, 37–49.
284 N. Roch, S. Florens, V. Bouchiat, W. Wernsdorfer and F. Balestro, *Nature*, 2008, **453**, 633–637.
285 J. J. Parks, A. R. Champagne, T. A. Costi, W. W. Shum, A. N. Pasupathy, E. Neuscamman, S. Flores-Torres, P. S. Cornaglia, A. A. Aligia, C. A. Balseiro, G. K.-L. Chan, H. D. Abruña and D. C. Ralph, *Science*, 2010, **328**, 1370–1373.
286 S. Wagner, F. Kisslinger, S. Ballmann, F. Schramm, R. Chandrasekar, T. Bodenstein, O. Fuhr, D. Secker, K. Fink, M. Ruben and H. B. Weber, *Nat. Nanotechnol.*, 2013, **8**, 575–579.
287 A. A. Houck, J. Labaziewicz, E. K. Chan, J. A. Folk and I. L. Chuang, *Nano Lett.*, 2005, **5**, 1685–1688.
288 V. Iancu, A. Deshpande and S.-W. Hla, *Nano Lett.*, 2006, **6**, 820–823.
289 M. J. Calderón, B. Koiller and S. Das Sarma, *Phys. Rev. B: Condens. Matter Mater. Phys.*, 2007, **75**, 125311.
290 K. J. Franke, G. Schulze and J. I. Pascual, *Science*, 2011, **332**, 940–944.
291 K. Yoshida, I. Hamada, S. Sakata, A. Umeno, M. Tsukada and K. Hirakawa, *Nano Lett.*, 2013, **13**, 481–485.
292 M. Urdampilleta, S. Klyatskaya, J. P. Cleuziou, M. Ruben and W. Wernsdorfer, *Nat. Mater.*, 2011, **10**, 502–506.
293 S. Xu, G. Podoprygorina, V. Boehmer, Z. Ding, P. Rooney, C. Rangan and S. Mittler, *Org. Biomol. Chem.*, 2007, **5**, 558–568.
294 R. Vincent, S. Klyatskaya, M. Ruben, W. Wernsdorfer and F. Balestro, *Nature*, 2012, **488**, 357–360.
295 S. Thiele, R. Vincent, M. Holzmann, S. Klyatskaya, M. Ruben, F. Balestro and W. Wernsdorfer, *Phys. Rev. Lett.*, 2013, **111**, 037203.
296 M. Ganzhorn, S. Klyatskaya, M. Ruben and W. Wernsdorfer, *Nat. Nanotechnol.*, 2013, **8**, 165–169.
297 R. Baer and D. Neuhauser, *J. Am. Chem. Soc.*, 2002, **124**, 4200–4201.
298 R. A. Webb, S. Washburn, C. P. Umbach and R. B. Laibowitz, *Phys. Rev. Lett.*, 1985, **54**, 2696.
299 K. Walczak, *Cent. Eur. J. Chem.*, 2004, **2**, 524–533.
300 D. Walter, D. Neuhauser and R. Baer, *Chem. Phys.*, 2004, **299**, 139–145.
301 S.-H. Ke, W. Yang and H. U. Baranger, *Nano Lett.*, 2008, **8**, 3257–3261.
302 G. C. Solomon, D. Q. Andrews, T. Hansen, R. H. Goldsmith, M. R. Wasielewski, R. P. Van Duyne and M. A. Ratner, *J. Chem. Phys.*, 2008, **129**, 054701.
303 J. Rincón, K. Hallberg, A. A. Aligia and S. Ramasesha, *Phys. Rev. Lett.*, 2009, **103**, 266807.
304 G. C. Solomon, C. Herrmann, T. Hansen, V. Mujica and M. A. Ratner, *Nat. Chem.*, 2010, **2**, 223–228.
305 S. Ballmann, R. Haertle, P. B. Coto, M. Elbing, M. Mayor, M. R. Bryce, M. Thoss and H. B. Weber, *Phys. Rev. Lett.*, 2012, **109**, 056801.
306 R. Haertle, M. Butzin, O. Rubio-Pons and M. Thoss, *Phys. Rev. Lett.*, 2011, **107**, 046802.
307 S. V. Aradhya, J. S. Meisner, M. Krikorian, S. Ahn, R. Parameswaran, M. L. Steigerwald, C. Nuckolls and L. Venkataraman, *Nano Lett.*, 2012, **12**, 1643–1647.
308 C. R. Arroyo, S. Tarkuc, R. Frisenda, J. S. Seldenthuis, C. H. M. Woerde, R. Eelkema, F. C. Grozema and H. S. J. van der Zant, *Angew. Chem., Int. Ed.*, 2013, **52**, 3152–3155.
309 C. R. Arroyo, R. Frisenda, K. Moth-Poulsen, J. S. Seldenthuis, T. Bjørnholm and H. S. van der Zant, *Nanoscale Res. Lett.*, 2013, **8**, 234.
310 C. Nef, P. L. T. M. Frederix, J. Brunner, C. Schonenberger and M. Calame, *Nanotechnology*, 2012, **23**, 365201.
311 M. Irie, *Chem. Rev.*, 2000, **100**, 1685–1716.
312 *Studies in Organic Chemistry 40: Photochromism: Molecules and Systems*, ed. H. Duerr and H. Bouas-Laurent, Elsevier, 1990.

313 *Molecular Switches*, ed. B. L. Feringa, Wiley-VCH, 2001.
314 *Organic Photochromic and Thermochromic Compounds*, ed. J. C. Crano and R. J. Guglielmetti, Plenum, vol. 1: Main Photochromic Families, 1999.
315 N. Tanifuji, K. Matsuda and M. Irie, *Org. Lett.*, 2005, **7**, 3777–3780.
316 P. Gutlich, Y. Garcia and T. Woike, *Coord. Chem. Rev.*, 2001, **219–221**, 839–879.
317 M. Irie, T. Fukaminato, T. Sasaki, N. Tamai and T. Kawai, *Nature*, 2002, **420**, 759–760.
318 T. Fukaminato, T. Sasaki, T. Kawai, N. Tamai and M. Irie, *J. Am. Chem. Soc.*, 2004, **126**, 14843–14849.
319 P. A. Liddell, G. Kodis, A. L. Moore, T. A. Moore and D. Gust, *J. Am. Chem. Soc.*, 2002, **124**, 7668–7669.
320 K. Uchida, N. Izumi, S. Sukata, Y. Kojima, S. Nakamura and M. Irie, *Angew. Chem., Int. Ed.*, 2006, **45**, 6470–6473.
321 T. B. Norsten and N. R. Branda, *J. Am. Chem. Soc.*, 2001, **123**, 1784–1785.
322 M. Irie, S. Kobatake and M. Horichi, *Science*, 2001, **291**, 1769–1772.
323 H. Cho and E. Kim, *Macromolecules*, 2002, **35**, 8684–8687.
324 N. Tanifuji, M. Irie and K. Matsuda, *J. Am. Chem. Soc.*, 2005, **127**, 13344–13353.
325 T. A. Golovkova, D. V. Kozlov and D. C. Neckers, *J. Org. Chem.*, 2005, **70**, 5545–5549.
326 K. Matsuda and M. Irie, *Chem. – Eur. J.*, 2001, **7**, 3466–3473.
327 V. W.-W. Yam, C.-C. Ko and N. Zhu, *J. Am. Chem. Soc.*, 2004, **126**, 12734–12735.
328 G. M. Tsivgoulis and J.-M. Lehn, *Angew. Chem., Int. Ed. Engl.*, 1995, **34**, 1119–1122.
329 N. P. M. Huch and B. L. Feringa, *J. Chem. Soc., Chem. Commun.*, 1995, 1095–1096.
330 T. J. Wigglesworth, D. Sud, T. B. Norsten, V. S. Lekhi and N. R. Branda, *J. Am. Chem. Soc.*, 2005, **127**, 7272–7273.
331 P. Dedecker, C. Flors, J.-i. Hotta, H. Uji-i and J. Hofkens, *Angew. Chem., Int. Ed.*, 2007, **46**, 8330–8332.
332 T. Fukaminato, *J. Photochem. Photobiol., C*, 2011, **12**, 177–208.
333 J. W. Shaevitz, *Nat. Methods*, 2008, **5**, 471–472.
334 M. Sauer, *Proc. Natl. Acad. Sci. U. S. A.*, 2005, **102**, 9433–9434.
335 C. Geisler, A. Schoenle, C. von Middendorff, H. Bock, C. Eggeling, A. Egner and S. W. Hell, *Appl. Phys. A: Mater. Sci. Process.*, 2007, **88**, 223–226.
336 T. Yamaguchi, K. Uchida and M. Irie, *J. Am. Chem. Soc.*, 1997, **119**, 6066–6071.
337 M. Heilemann, P. Dedecker, J. Hofkens and M. Sauer, *Laser Photonics Rev.*, 2009, **3**, 180–202.
338 J. Vogelsang, C. Steinhauer, C. Forthmann, I. H. Stein, B. Person-Skegro, T. Cordes and P. Tinnefeld, *ChemPhysChem*, 2010, **11**, 2475–2490.
339 T. Tsujioka and M. Irie, *J. Photochem. Photobiol., C*, 2010, **11**, 1–14.
340 A. Bianchi, E. Delgado-Pinar, E. Garcia-Espana, C. Giorgi and F. Pina, *Coord. Chem. Rev.*, 2014, **260**, 156–215.
341 J. Zhou, G. Du and J. Chen, *Curr. Opin. Biotechnol.*, 2014, **25**, 17–23.
342 C. Yun, J. You, J. Kim, J. Huh and E. Kim, *J. Photochem. Photobiol., C*, 2009, **10**, 111–129.
343 J. Hwang, M. Pototschnig, R. Lettow, G. Zumofen, A. Renn, S. Gotzinger and V. Sandoghdar, *Nature*, 2009, **460**, 76–80.
344 H. Song, Y. Kim, Y. H. Jang, H. Jeong, M. A. Reed and T. Lee, *Nature*, 2009, **462**, 1039–1043.
345 T. Fukaminato, *J. Photochem. Photobiol., C*, 2011, **12**, 177–208.
346 C. Jia, J. Wang, C. Yao, Y. Cao, Y. Zhong, Z. Liu, Z. Liu and X. Guo, *Angew. Chem., Int. Ed.*, 2013, **52**, 8666–8670.
347 Y. Kim, T. J. Hellmuth, D. Sysoiev, F. Pauly, T. Pietsch, J. Wolf, A. Erbe, T. Huhn, U. Groth, U. E. Steiner and E. Scheer, *Nano Lett.*, 2012, **12**, 3736–3742.
348 P. Liljeroth, *Nat. Nanotechnol.*, 2012, **7**, 5–6.
349 A. Perrier, F. Maurel and D. Jacquemin, *Acc. Chem. Res.*, 2012, **45**, 1173–1182.
350 E. G. Petrov, V. O. Leonov and V. Snitsarev, *J. Chem. Phys.*, 2013, **138**, 184709.
351 C. Sciascia, R. Castagna, M. Dekermenjian, R. Martel, A. R. Srimath Kandada, F. Di Fonzo, A. Bianco, C. Bertarelli, M. Meneghetti and G. Lanzani, *J. Phys. Chem. C*, 2012, **116**, 19483–19489.
352 D. Kim, H. Jeong, H. Lee, W.-T. Hwang, J. Wolf, E. Scheer, T. Huhn, H. Jeong and T. Lee, *Adv. Mater.*, 2014, **26**, 3968–3973.
353 T. Tsujioka, Y. Hamada, K. Shibata, A. Taniguchi and T. Fuyuki, *Appl. Phys. Lett.*, 2001, **78**, 2282–2284.
354 T. Tsujioka and M. Irie, *J. Opt. Soc. Am. B*, 2002, **19**, 297–303.
355 Y. Kim and E. Kim, *Macromol. Res.*, 2006, **14**, 584–587.
356 P. Zacharias, M. C. Gather, A. Koehnen, N. Rehmann and K. Meerholz, *Angew. Chem., Int. Ed.*, 2009, **48**, 4038–4041.
357 Z. Zhang, X. Liu, Z. Li, Z. Chen, F. Zhao, F. Zhang and C.-H. Tung, *Adv. Funct. Mater.*, 2008, **18**, 302–307.
358 Optical sensors and switches, *Molecular and Supramolecular Photochemistry*, ed. V. Ramamurthy and K. S. Schanze, Marcel Dekker, Inc., New York, 2001.
359 N. Koumura, R. W. J. Zijlstra, R. A. van Delden, N. Harada and B. L. Feringa, *Nature*, 1999, **401**, 152–155.
360 T. Hugel, N. B. Holland, A. Cattani, L. Moroder, M. Seitz and H. E. Gaub, *Science*, 2002, **296**, 1103–1106.
361 T. Tsujioka and M. Irie, *J. Photochem. Photobiol., C*, 2010, **11**, 1–14.
362 K. Matsuda and M. Irie, *Polyhedron*, 2005, **24**, 2477–2483.
363 J. He, F. Chen, P. A. Liddell, J. Andreasson, S. D. Straight, D. Gust, T. A. Moore, A. L. Moore, J. Li, O. F. Sankey and S. M. Lindsay, *Nanotechnology*, 2005, **16**, 695–702.
364 A. Aviram, M. Ratner, Proceedings of a Conference on Molecular Electronics: Science and Technology, 14–18 December 1997, in Humacao, Puerto Rico. [In: *Ann. N. Y. Acad. Sci.*, 1998; 852], New York Academy of Sciences, 1998.
365 A. C. Whalley, M. L. Steigerwald, X. Guo and C. Nuckolls, *J. Am. Chem. Soc.*, 2007, **129**, 12590–12591.
366 M. Taniguchi, Y. Nojima, K. Yokota, J. Terao, K. Sato, N. Kambe and T. Kawai, *J. Am. Chem. Soc.*, 2006, **128**, 15062–15063.
367 A. Staykov, D. Nozaki and K. Yoshizawa, *J. Phys. Chem. C*, 2007, **111**, 3517–3521.

368 J. Huang, Q. Li, H. Ren, H. Su, Q. W. Shi and J. Yang, *J. Chem. Phys.*, 2007, **127**, 094705.
369 M. Kondo, T. Tada and K. Yoshizawa, *Chem. Phys. Lett.*, 2005, **412**, 55–59.
370 N. Katsonis, T. Kudernac, M. Walko, S. J. van der Molen, B. J. van Wees and B. L. Feringa, *Adv. Mater.*, 2006, **18**, 1397–1400.
371 M. Ikeda, N. Tanifuji, H. Yamaguchi, M. Irie and K. Matsuda, *Chem. Commun.*, 2007, 1355–1357.
372 S. J. van der Molen, J. Liao, T. Kudernac, J. S. Agustsson, L. Bernard, M. Calame, B. J. van Wees, B. L. Feringa and C. Schonenberger, *Nano Lett.*, 2009, **9**, 76–80.
373 R. W. Taylor, R. J. Coulston, F. Biedermann, S. Mahajan, J. J. Baumberg and O. A. Scherman, *Nano Lett.*, 2013, **13**, 5985–5990.
374 A. B. Petersen, E. Thyrhaug, T. Jain, K. Kilsaa, M. Bols, K. Moth-Poulsen, N. Harrit and T. Bjørnholm, *J. Phys. Chem. B*, 2010, **114**, 11771–11777.
375 C. W. Marquardt, S. Grunder, A. Blaszczyk, S. Dehm, F. Hennrich, H. v. Lohneysen, M. Mayor and R. Krupke, *Nat. Nanotechnol.*, 2010, **5**, 863–867.
376 A. Peters and N. R. Branda, *J. Am. Chem. Soc.*, 2003, **125**, 3404–3405.
377 T. Saika, M. Irie and T. Shimidzu, *J. Chem. Soc., Chem. Commun.*, 1994, 2123–2124.
378 A. Peters and N. R. Branda, *Chem. Commun.*, 2003, 954–955.
379 N. Darwish, I. Diez-Perez, P. Da Silva, N. Tao, J. J. Gooding and M. N. Paddon-Row, *Angew. Chem., Int. Ed.*, 2012, **51**, 3203–3206.
380 D. I. Gittins, D. Bethell, D. J. Schiffrin and R. J. Nichols, *Nature*, 2000, **408**, 67–69.
381 Y.-Y. Sun, Z.-L. Peng, R. Hou, J.-H. Liang, J.-F. Zheng, X.-Y. Zhou, X.-S. Zhou, S. Jin, Z.-J. Niu and B.-W. Mao, *Phys. Chem. Chem. Phys.*, 2014, **16**, 2260–2267.
382 D. L. Feldheim and C. D. Keating, *Chem. Soc. Rev.*, 1998, **27**, 1–12.
383 N. J. Tao, *Phys. Rev. Lett.*, 1996, **76**, 4066–4069.
384 W. Han, E. N. Durantini, T. A. Moore, A. L. Moore, D. Gust, P. Rez, G. Leatherman, G. R. Seely, N. Tao and S. M. Lindsay, *J. Phys. Chem. B*, 1997, **101**, 10719–10725.
385 N. J. Kay, S. J. Higgins, J. O. Jeppesen, E. Leary, J. Lycoops, J. Ulstrup and R. J. Nichols, *J. Am. Chem. Soc.*, 2012, **134**, 16817–16826.
386 C. Li, A. Mishchenko, Z. Li, I. Pobelov, T. Wandlowski, X. Q. Li, F. Wurthner, A. Bagrets and F. Evers, *J. Phys.: Condens. Matter*, 2008, **20**, 374122.
387 S. Tsoi, I. Griva, S. A. Trammell, A. S. Blum, J. M. Schnur and N. Lebedev, *ACS Nano*, 2008, **2**, 1289–1295.
388 E. Leary, S. J. Higgins, H. van Zalinge, W. Haiss, R. J. Nichols, S. Nygaard, J. O. Jeppesen and J. Ulstrup, *J. Am. Chem. Soc.*, 2008, **130**, 12204–12205.
389 F. Mohn, J. Repp, L. Gross, G. Meyer, M. S. Dyer and M. Persson, *Phys. Rev. Lett.*, 2010, **105**, 266102.
390 N. Darwish, I. Diez-Perez, S. Guo, N. Tao, J. J. Gooding and M. N. Paddon-Row, *J. Phys. Chem. C*, 2012, **116**, 21093–21097.
391 T. Avellini, H. Li, A. Coskun, G. Barin, A. Trabolsi, A. N. Basuray, S. K. Dey, A. Credi, S. Silvi, J. F. Stoddart and M. Venturi, *Angew. Chem., Int. Ed.*, 2012, **51**, 1611–1615.
392 A. B. Gaspar, V. Ksenofontov, M. Seredyuk and P. Guetlich, *Coord. Chem. Rev.*, 2005, **249**, 2661–2676.
393 F. Meng, Y.-M. Hervault, Q. Shao, B. Hu, L. Norel, S. Rigaut and X. Chen, *Nat. Commun.*, 2014, **5**, 3023.
394 W. Zhai, C. Du and X. Li, *Chem. Commun.*, 2014, **50**, 2093–2095.
395 X.-S. Zhou, L. Liu, P. Fortgang, A.-S. Lefevre, A. Serra-Muns, N. Raouafi, C. Amatore, B.-W. Mao, E. Maisonhaute and B. Schöllhorn, *J. Am. Chem. Soc.*, 2011, **133**, 7509–7516.
396 J. Liao, J. S. Agustsson, S. Wu, C. Schönenberger, M. Calame, Y. Leroux, M. Mayor, O. Jeannin, Y.-F. Ran, S.-X. Liu and S. Decurtins, *Nano Lett.*, 2010, **10**, 759–764.
397 J. S. Seldenthuis, F. Prins, J. M. Thijssen and H. S. J. van der Zant, *ACS Nano*, 2010, **4**, 6681–6686.
398 M. Rief, M. Gautel, F. Oesterhelt, J. M. Fernandez and H. E. Gaub, *Science*, 1997, **276**, 1109–1112.
399 J. Liphardt, B. Onoa, S. B. Smith, I. Tinoco and C. Bustamante, *Science*, 2001, **292**, 733–737.
400 A. F. Oberhauser, P. K. Hansma, M. Carrion-Vazquez and J. M. Fernandez, *Proc. Natl. Acad. Sci. U. S. A.*, 2001, **98**, 468–472.
401 C. Joachim, J. K. Gimzewski and A. Aviram, *Nature*, 2000, **408**, 541–548.
402 A. Nitzan and M. A. Ratner, *Science*, 2003, **300**, 1384–1389.
403 C. Joachim and M. A. Ratner, *Proc. Natl. Acad. Sci. U. S. A.*, 2005, **102**, 8801–8808.
404 M. Galperin, M. A. Ratner, A. Nitzan and A. Troisi, *Science*, 2008, **319**, 1056–1060.
405 F. Chen and N. J. Tao, *Acc. Chem. Res.*, 2009, **42**, 429–438.
406 L. Fabbrizzi, F. Gatti, P. Pallavicini and E. Zambarbieri, *Chem. – Eur. J.*, 1999, **5**, 682–690.
407 C. A. Martin, R. H. M. Smit, H. S. J. van der Zant and J. M. van Ruitenbeek, *Nano Lett.*, 2009, **9**, 2940–2945.
408 M. Taniguchi, M. Tsutsui, K. Yokota and T. Kawai, *Chem. Sci.*, 2010, **1**, 247–253.
409 T. Kawai, M. Poetschke, Y. Miyamoto, C. G. Rocha, S. Roche and G. Cuniberti, *Phys. Rev. B: Condens. Matter Mater. Phys.*, 2011, **83**, 241405.
410 M. Zemanová Diešková, I. Štich and P. Bokes, *Phys. Rev. B: Condens. Matter Mater. Phys.*, 2013, **87**, 245418.
411 E. S. Tam, J. J. Parks, W. W. Shum, Y.-W. Zhong, M. E. B. Santiago-Berríos, X. Zheng, W. Yang, G. K. L. Chan, H. D. Abruña and D. C. Ralph, *ACS Nano*, 2011, **5**, 5115–5123.
412 I. Franco, C. B. George, G. C. Solomon, G. C. Schatz and M. A. Ratner, *J. Am. Chem. Soc.*, 2011, **133**, 2242–2249.
413 I. Diez-Perez, J. Hihath, T. Hines, Z.-S. Wang, G. Zhou, K. Mullen and N. Tao, *Nat. Nanotechnol.*, 2011, **6**, 226–231.
414 M. Manheller, S. Trellenkamp, R. Waser and S. Karthaeuser, *Nanotechnology*, 2012, **23**, 125302.
415 Y. Wu, W. Hong, T. Akiyama, S. Gautsch, V. Kolivoska, T. Wandlowski and N. F. de Rooij, *Nanotechnology*, 2013, **24**, 235302.